DETERMINATION AND MITIGATION OF PRECIPITATION EFFECTS ON PORTAL MONITOR GAMMA BACKGROUND LEVELS

A Thesis

by

STEPHEN MICHAEL REVIS

Submitted to the Office of Graduate Studies of
Texas A&M University
in partial fulfillment of the requirements for the degree of

MASTER OF SCIENCE

May 2012

Major Subject: Nuclear Engineering

DETERMINATION AND MITIGATION OF PRECIPITATION EFFECTS ON PORTAL MONITOR GAMMA BACKGROUND LEVELS

A Thesis

by

STEPHEN MICHAEL REVIS

Submitted to the Office of Graduate Studies of
Texas A&M University
in partial fulfillment of the requirements for the degree of

MASTER OF SCIENCE

Approved by:

Chair of Committee,	William S. Charlton
Committee Members,	Craig M. Marianno
	Yu Ding
Head of Department,	Raymond J. Juzaitis

May 2012

Major Subject: Nuclear Engineering

ABSTRACT

Determination and Mitigation of Precipitation Effects on Portal Monitor Gamma Background Levels. (May 2012)

Stephen Michael Revis, B.S., University of Wisconsin-Madison

Chair of Advisory Committee: Dr. William S. Charlton

The purpose of this project is to establish a correlation between precipitation and background gamma radiation levels at radiation portal monitors (RPM) deployed at various ports worldwide, and to devise a mechanism by which the effects of these precipitation-induced background fluctuations could be mitigated. The task of detecting special nuclear materials (SNM) by passive gamma spectroscopy is very difficult due to the low signal-to-noise ratio observed in an uncontrolled environment. Due to their low activities and the low energies of their characteristic gamma rays, the signals from many types of SNM can easily be obscured by background radiation. While this can be somewhat mitigated by taking regular background radiation measurements, even this cannot resolve the issue if background levels change suddenly and dramatically. Furthermore, any increase in background count rate will increase the statistical uncertainty of the count rate measurement, and thus decrease the minimum quantity of SNM that can be reliably detected. Existing research suggests that the advent of precipitation is the culprit behind many such large and sudden increases in background radiation. The correlation between precipitation and background levels was explored by in-situ testing on a full-scale portal monitor at Oak Ridge National Laboratory, and by comparing previously recorded background radiation and weather data from portal monitors located at ports worldwide. The first was utilized to determine the frequency and magnitude at which precipitation introduces background activity, and the second was used to quantify the effects of various quantities and types of

precipitation in various parts of the world. Once this analysis was complete, various methods of mitigating these changes in background radiation were developed based on the collected data.

Precipitation was found to be the most common culprit for rapid increases in background count rate, and was attributable to 85.6% of all such events. Based on extensive simulation via the Origen-ARP and MCNP software, a response function for the portal monitor was developed, and an algorithm designed to predict the contribution of the precipitation to the background count rate was developed. This algorithm was able to attenuate the contribution of precipitation to the background count rate by an average of 45% with very minimal over-correction. Such an algorithm could be utilized to adjust the alarm levels of the RPM to better allow it to compensate for the rise and fall in background count rate due to precipitation.

Additionally, the relative contribution of precipitation which landed at various distances from the portal monitor to the increase in background count rate was measured via simulation. This simulation demonstrated that 37.2% of all background counts were due to the radon daughters which landed within a 2.76 m radius from the center of the portal monitor. This radius encompasses the area between the two portals. Based on this, several designs for shielding were simulated, the most successful of which was a concrete structure that was able to attenuate 71.3% of the background radiation caused by a given precipitation event at a materials cost of approximately $6,000 per RPM. This method is recommended as the primary means of mitigating this issue.

To Walter Charles Revis 1957-2011

ACKNOWLEDGMENTS

First and foremost, I'd like to thank Dr. Alexander Solodov for his friendship and guidance throughout not only this undertaking but also the last several years of my life. He was responsible for mentoring me throughout my three internships at Oak Ridge National Laboratory, introducing me to the Nuclear Security Science and Policy Institute program at Texas A&M University and obtaining much of the resources and funding for this very research. Truly, he was a member of my committe in all but name, and would have been an actual member but for various clerical issues. I'd also like to thank the chair of my committee, Dr. William Charlton, for his invaluable mentorship and unwavering support throughout the considerable adversity I've faced during my post-graduate career. I'd like to thank Dr. Marianno for his constant enthusiasm for my work and Dr. Ding for taking the time to familiarize himself with this subject matter. I'd also like to thank my parents, Walter and Jennifer Revis, for their tireless, nurturing support and encouragement throughout my life and my college career. Last but certainly not least, I'd like to thank Ann Morris of the University of Wisconsin-Madison for giving me a second look and helping me avoid squandering my remaining undergraduate years.

TABLE OF CONTENTS

CHAPTER Page

CHAPTER Page

LIST OF TABLES

LIST OF FIGURES

FIGURE Page

FIGURE Page

CHAPTER I

INTRODUCTION AND LITERATURE REVIEW

A. Introduction

The acquisition of a nuclear weapon or special nuclear material (SNM) by a terrorist group or other non-state entity represents one of the gravest possible scenarios in the field of nuclear nonproliferation. Unlike a state, such an organization would be highly likely to use a nuclear weapon almost immediately upon acquisition [1]. Furthermore, such a group would likely attempt to transport such a device to its target using the target state's own transportation infrastructure, thus bypassing traditional military defenses. Locating then depriving such an adversary of their nuclear weapon or SNM represents the only realistic possibility of eliminating such a threat should it arise.

While safeguards and physical protection measures taken at nuclear facilities certainly represent the first line of defense against nuclear proliferation, these alone are not sufficient to fully address the threat posed by non-state actors. Between 1993 and 2004, the IAEA has documented 662 confirmed cases of nuclear smuggling, 16 of which involved SNM [2]. Their data suggests that this trafficking is motivated, at least in part, by a perceived black market demand for these items.

Although the amounts of SNM stolen in the above cases were far less than one significant quantity [3], or the approximate minimum amount needed to construct a nuclear weapon, bolder attempts to steal greater amounts have been made. The attack on the Pelindaba Nuclear Facility in 2007, in which the perpetrators penetrated

---

This thesis follows the style of Nuclear Instruments and Methods in Physics Research A.

multiple layers of security undetected and nearly gained access to over 25 significant quantities of highly enriched uranium [4, 5], is a striking example of this.

Even if all the existing gaps in first line nuclear security were somehow closed, a complicit state could intentionally give a nuclear device to a non-state actor to execute an attack. This is a particularly likely delivery method for a rogue state which lacks highly developed aircraft and missile technologies.

Thus, it is necessary to implement a second line of defense designed to interdict nuclear materials as they are passed through the world's transportation infrastructure. The National Nuclear Security Administration's (NNSA) Second Line of Defense (SLD) Initiative and its daughter project, the Megaports Initiative, represent concerted efforts to do just that. The Megaports Initiative seeks to install radiation portal monitors (RPM) to monitor cargo containers at major seaports worldwide [6].

The radiation portal monitors used in the Megaports initiative consist of two columns containing detectors spaced 5.39 m apart, as seen in Fig. 1. Each of these columns contains two ^{3}He neutron detector units and two Polyvinyl Toluene (PVT) plastic scintillator gamma ray detection units. The ^{3}He detector units consist of two ^{3}He tubes encased in a white polyethylene moderator, while the PVT detector units consist of a single, large rectangular prism of PVT, which is covered in black plastic to prevent ordinary visible light from affecting the detector. In Fig. 2, the PVT detector unit can be seen on the lower left-hand side of the column, while the ^{3}He detector unit can be seen on the lower right-hand side. Part of the identical, upper pair of detectors can be seen as well.

Fig. 1. Wide angle view of the RPM at Oak Ridge National Laboratory.

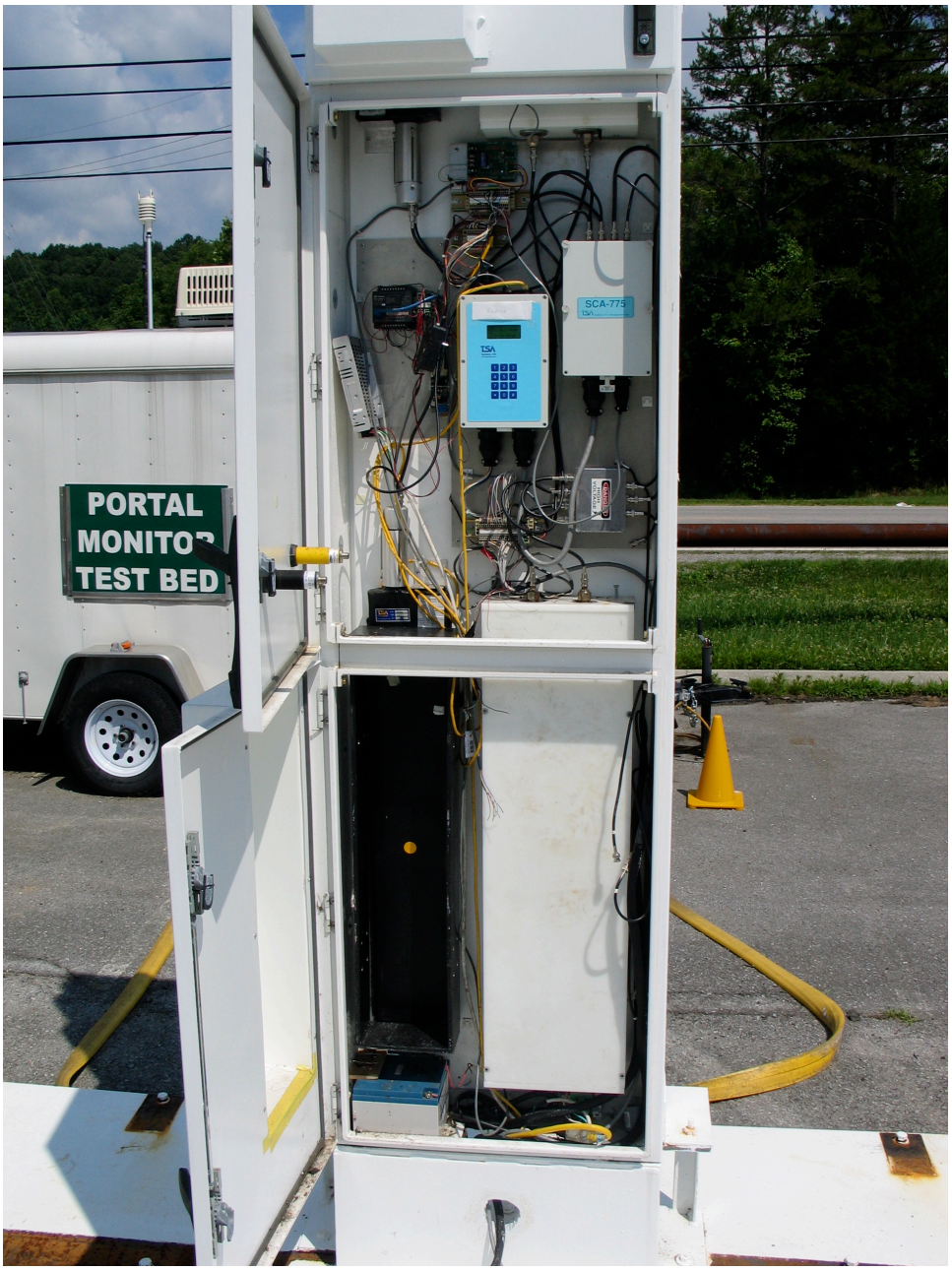

Fig. 2. Image of the detectors inside the lower part of one of the columns of the RPM. This column was on the left-hand side in Fig. 1.

Due to their design, the performance of these RPMs can be dramatically impacted by fluctuations in background radiation levels caused by changes in weather.

This is due to the use of PVT as a scintillator for gamma-ray detection. While PVT is relatively inexpensive and can be formed into large and highly efficient detectors, it has very poor energy resolution, meaning that it is not generally possible to determine the energy of a detected gamma ray with any certainty. This makes it effectively impossible to determine what isotope emitted said radiation or distinguish different sources of gamma radiation from one another with a PVT detector. Far from being a mistake, this was a conscious and intelligent design choice. While it is possible to use other materials which have far greater energy resolution, merely upgrading to the next least costly one available would increase the cost of the detector by a factor of 22.5, if enough of this material was used to achieve the same efficiency. Sacrificing efficiency may not be acceptable in this application, as a significantly less efficient detector would be unlikely to detect the presence of special nuclear materials in many cases.

Due to their lack of energy resolution, these PVT scintillators cannot directly distinguish naturally occurring background radiation from the weak radiation emitted from SNM or other radioactive materials. To compensate for background radiation, the RPMs automatically sense when they are unoccupied, and count the background radiation during this period. When a vehicle subsequently occupies the RPM, the background count rate is subtracted from the count rate detected while the vehicle passes through. This yields an estimate of the count rate due to the vehicle's presence and thus permits the calculation of the rate of radiation emission by the vehicle's contents. This system, however, has a fundamental shortcoming in that the level of background radiation, or background activity, must not change significantly during the duration of the two counts in order to yield accurate results. Were such a variation to occur, the RPMs could give off false alarms, or worse yet, could fail to alarm when a threat passes through. Fortunately, no such concerns exist for the ^{3}He neutron

detectors, as no common natural phenomenona or man-made goods emit neutrons in any significant quantity, much less at a rapidly fluctuating rate.

Unfortunately, such rapid variations in background activity can and do occur. Existing research indicates that certain weather events, particularly precipitation, are a major cause of these variations. Mitigating these effects is paramount to ensuring that the portal monitors achieve the highest possible probability of detection, and the least number of false alarms.

B. Literature Review

The question as specified above is to first determine what, if any meteorological parameters affect the level of background activity, then to determine a means of mitigating this effect. While the effects of most meteorological parameters on background activity are largely unstudied, precipitation has been identified as a culprit in previous research. Nevertheless, it is not possible to conclusively discount potential contributions by other meteorological parameters without giving them at least a cursory analysis.

Precipitation is thought to cause a prompt increase in ground-level background activity by transporting ^{222}Rn daughters present in the atmosphere to the earth's surface. The atmospheric radon is itself unaffected, as radon is a noble gas and thus not chemically reactive, whereas its daughters such as ^{218}Po, ^{214}Pb and ^{214}Bi tend to bind with atmospheric moisture and thus can be present in concentrations as high as several Bq cm^{-3} [7]. The resulting increase in background count rate is larger than that caused by the diffusion of radon across pressure or temperature gradients by orders of magnitude. Additionally, this increase occurs almost instantaneously upon the advent of precipitation, whereas the aforementioned diffusion effect is far more

gradual [8]. Furthermore, this effect is thought to be extremely non-uniform in terms of both its magnitude at different sites, and its magnitude from event to event at a given site. The path the clouds causing the precipitation take during their formation is thought to be the source of this variation [9].

While precipitation is the only parameter that has been identified as causing a substantial effect in existing research, the possibility of a correlation between other meteorological parameters and background activity still exists, and bears investigating. Furthermore, all existing studies characterizing the background activity increases caused by precipitation only characterize the effects from a pure science perspective, and do not provide sufficient information to characterize the practical effects and detriments that such background activity increases might inflict on any specific detector system.

In terms of the negative effect that rapid background fluctuations can have on the effectiveness of RPMs, studies have found that abrupt fluctuations in the level of naturally occurring radioactive materials (NORM) can cause false negatives and false positives.

False negatives are caused when a rapid decrease in background count rate cancels out enough of the increase in count rate caused by a radiation source passing through the RPM to lower the resulting total count rate below the alarm threshold. This is possible because the RPM estimates the background count rate from counts taken several seconds prior to a given vehicle passing through, and thus cannot compensate for large, rapid fluctuations that occur just before or after the instant the vehicle enters the RPM. This can be clearly seen in Fig. 3, where the green dashed line represents the RPM's alarm threshold, the black line represents the count rate resulting from a normal level of background radiation, the blue line represents the count rate resulting from a depressed level of background radiation, and the red spikes represent the

contribution of a radiation source passing through the RPM to the count rate in each scenario. Note that the radiation source causes a count rate above the alarm threshold when the "no-vehicle" background is present, but does not cause the portal monitor's count rate to reach its alarm threshold in the depressed background scenario.

False positives can occur when a rapid background count rate increase occurs just before or while the vehicle occupies the RPM [10]. This can be clearly seen in Fig. 3, where the pink line represents the count rate resulting from an elevated background count rate level, the green dashed line represents the RPM's alarm threshold, and the black line represents the count rate resulting from a normal level of background radiation. Note that the background radiation alone is sufficient to cause the portal monitor to alarm in this case.

Although the NORM in this study did not emit the same spectrum of gamma radiation as the precipitation-based sources to be investigated in this proposed work do, it is perfectly reasonable to expect identical results, as the RPMs in both studies have no ability to distinguish different sources of radiation from one another.

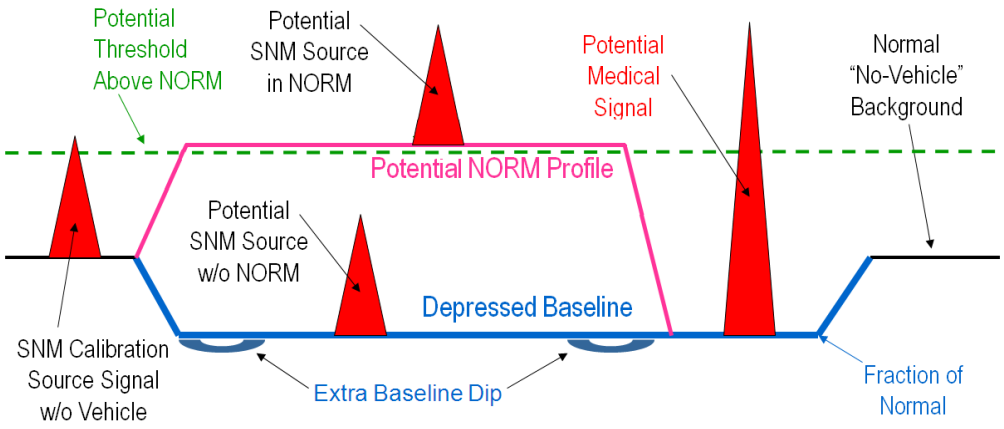

Fig. 3. Effects of fluctuations in NORM on RPM Performance [10].

Several solutions to the problem of distinguishing background radiation, or other harmless sources of NORM from man-made sources and SNM have been previously proposed, but none have been successful in this particular application for various reasons.

One method proposed to discriminate NORM and background radiation was to replace the PVT plastic scintillators with a material capable of better energy resolutions such as Sodium Iodide (NaI). While this could indeed solve the problem, it would also increase the cost per scintillator by a factor of 22.5 [11], if it were designed to yield the same intrinsic efficiency as achieved by the current PVT-based RPMs.

Lastly, dividing the counts recorded by the PVT scintillators into energy windows, or very large energy bins [12], has been proposed as a solution to the issue of differentiating NORM from SNM. While this seemed to be effective for the few individually studied terrestrial sources of NORM, it is doubtful that this would succeed when applied to the radiation generated by precipitation. This is due to the fact that this method hinges on the assumption that the newly added NORM would generate radiation that is spectrally similar to existing background, something which is not true of the background radiation generated by precipitation events.

CHAPTER II

PROBLEM

A. Introduction

The issue of determining and mitigating the effects of weather on radiation portal monitors is a complex one, and demands the application of very recent scientific research. The gamma-ray emissions and radon decay product content of precipitation are very recently explored phenomena. Little of the existing research on the topic is more than 6 years old and there are relatively few total publications. Nevertheless, there is certainly sufficient existing work to create a reasonable suspicion that the aforementioned issue exists and may very well be a critical one in terms of keeping radiation portal monitors operating effectively.

B. Theory

1. Introduction

Several previous studies have attributed the fluctuations in background radiation at portal monitors to the transport of atmospheric radon daughters to the surface during precipitation. This is due to the fact that unlike radon itself, radon's short-lived daughters, such as ^{214}Pb and ^{214}Bi, are much more likely to interact with atmospheric water since they are not noble gases [9]. Due to this effect, the advent of precipitation tends to transport these elements from the atmosphere to the surface. Furthermore, as their half-lives are on the order of tens of minutes, the period of increased activity correlates with the period of precipitation very well. However, these studies also suggest that the exact amount of activity deposited is determined by a large number of complex variables, such as the time of year, the amount of time the clouds causing

the precipitation have spent over land or sea and the amount of time that the precipitation event lasts [7]. Lastly, these studies tend to show good results over a relatively short time period, during which long-term problems such as gain stabilization are not a significant issue. Several other vectors of radon transport, such as diffusion out of surrounding surfaces, exist [8], but their contribution has been found to be insignificant compared to that of precipitation based transport.

2. Meteorological Aspects

Although the correlation between precipitation and increased background radiation is easily observable in many cases [9], the magnitude of the effect can be very difficult to quantify and predict. The National Nuclear Security Administration (NNSA) Second Line of Defense (SLD) radiation portal monitors are located at various major ports around the world, as seen in Appendix A. These portal monitors each experience radically different environmental conditions and weather patterns. This makes existing research focused on predicting the radionuclide content of precipitation based on observation of weather patterns difficult to apply, and necessitates a more robust approach to the problem.

This is compounded by the fact that the quantity of radioactive nuclides transported to the area adjacent to the portal monitor, and thus the increase in background activity, can vary by the intensity of precipitation, source of the clouds causing the precipitation and various other factors [7, 9]. To further complicate matters, weather data from the NOAA and other conventional sources tends to be recorded relatively infrequently, at a rate of once per hour for sites outside the United States [13]. This makes the timescale on which these effects occur difficult to accurately determine. Lastly, the weather stations and portal monitors being observed are not always co-located, introducing a potential lead or lag time between the detection of precipi-

tation at the weather station and the detection of increased background radiation at the portal monitor. In order to resolve these issues and accurately quantify the effects of precipitation on background radiation fluctuations at each individual site, a novel method of data analysis needed to be developed, or better data needed to be collected.

Furthermore, while precipitation is certainly the most prominent and well-studied source of weather-related background radiation, there still is some potential that other meteorological factors could have a significant effect. This demanded at least a cursory study of other meteorological variables to determine if any of them was strongly correlated with background radiation increases. Should this be the case, it could be necessary to take the presence of these newly discovered factors into account as well.

3. Common Misconceptions

It is a well known fact that many terrestrial sources of radon gas exist. Uranium or thorium bearing soils and rocks contain and can emanate radon rapidly under certain conditions, such as decreased atmospheric pressure [8]. However, these sources of radon contribute only negligibly if at all to the above effects.

A brief comparison of the dynamics of terrestrial radon to the changes in background count rate observed during precipitation demonstrate unequivocally that terrestrial radon cannot be the cause of said phenomena. First and foremost, the observed effects do not match the half-lives of any abundant isotope of terrestrial radon. ^{222}Rn, which is a ^{238}U decay product, has a half-life of 3.8 days, which is far longer than the 4 hour timeframe during which background radiation due to precipitation is observable, as seen in Fig. 4. ^{220}Rn, which is a thorium decay product, has a half-life of only a few seconds, and thus would have a much shorter-lived effect. In fact ^{220}Rn

is unlikely to diffuse to the surface before decaying into one of its non-gaseous daughter products. Furthermore, all abundant isotopes of radon undergo alpha decay and do not emit gammas, meaning that their emissions cannot be detected by the RPM.

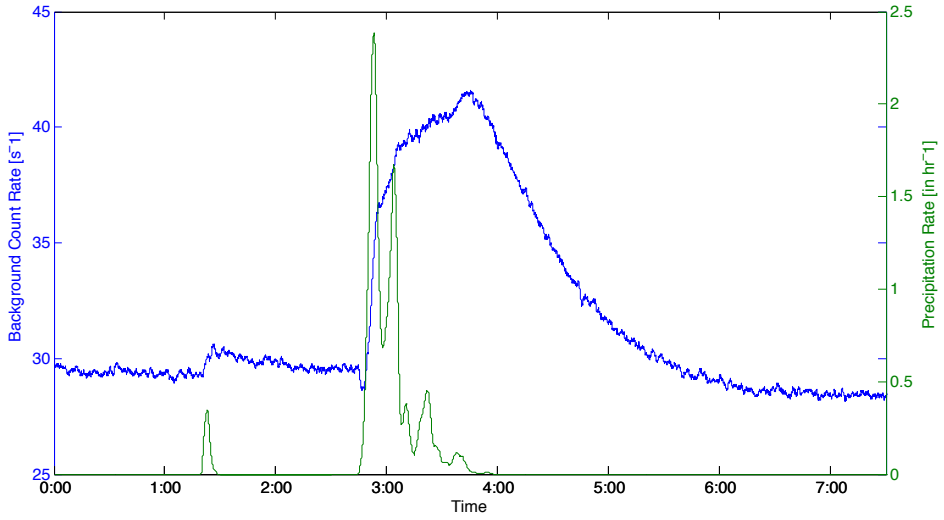

Fig. 4. Effects of a precipitation event on background count rate.

Although the daughter products of ^{222}Rn do emit gammas, these daughters can only be produced as quickly as the ^{222}Rn decays. Since these daughters have a half-life on the order of minutes, their decay occurs almost instantaneously relative to that of the ^{222}Rn itself. As a result, the decay rate of the ^{222}Rn is the limiting factor of both the population and activity of said daughter isotopes. This means that although the daughters have a much shorter half-life, their observed half-life at equilibrium will be nearly identical to that of ^{222}Rn.

The above is not a limiting factor in the case of atmospheric radon, as the daughters are scavenged by moisture, and transported to the surface in quantity during precipitation. This allows a massive, non-equilibrium quantity of daughters to rapidly accumulate, which would be impossible to achieve with diffusion alone.

4. Radiation Transport and Detection Aspects

The RPMs used in the SLD initiative are designed so that their alarm level is set at some number of standard deviations above the measured background level, as seen in Fig. 5. This number of standard deviations is referred to as the alarm threshold [14]. While this method is certainly advantageous in terms of avoiding false alarms in an environment with a fluctuating level of background activity, it also causes the RPMs to lose a significant amount of sensitivity should the background activity increase, as seen in Fig. 6. This also makes the portal monitors vulnerable to spoofing by any deliberate or inadvertent action that might increase the measured background activity.

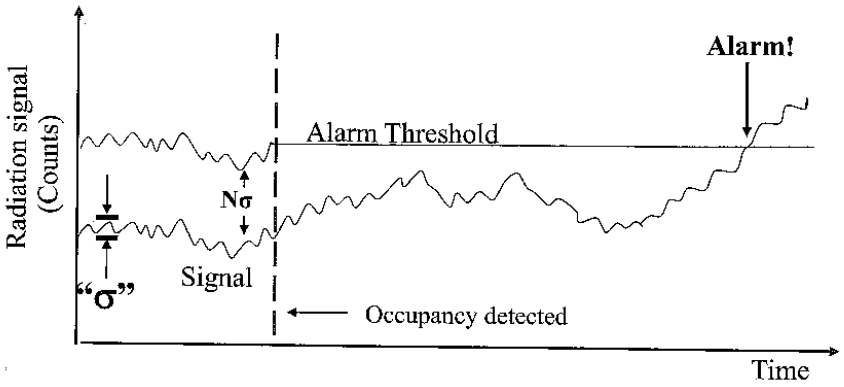

Fig. 5. Mechanism by which alarm level is determined [14].

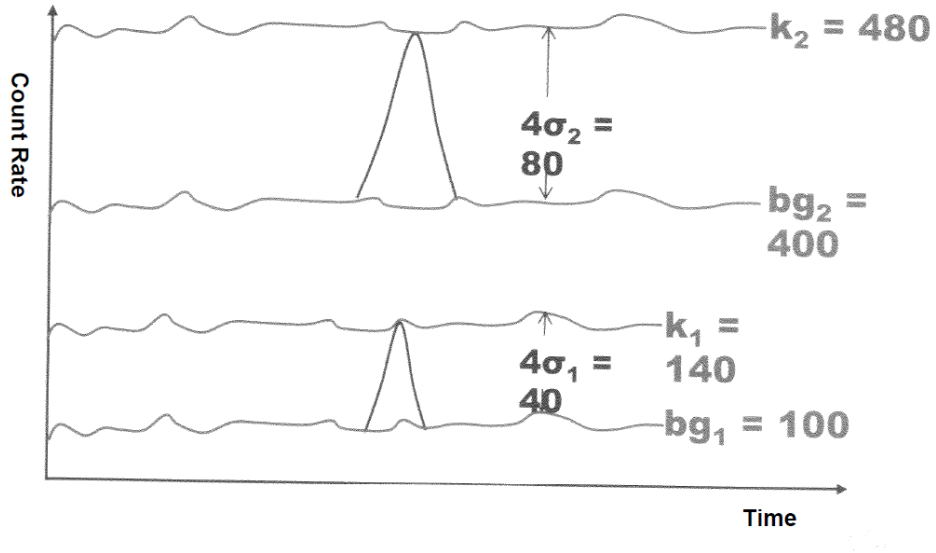

Fig. 6. Dependence of RPM sensitivity on background count rate. Note that bg is the background count rate [14].

The above issues are due to the fact that the standard deviation of a single measurement, assuming a Poisson distribution, is calculated as follows [15]:

$$\begin{aligned} s^2 &\cong \sigma^2 \\ &= \bar{x} \\ &\cong x \\ \sqrt{s^2} \cong \sigma &= \sqrt{x} \end{aligned} \tag{2.1}$$

where

s^2 is the sample variance

$\bar{x}$ is the sample mean

x is the sample measurement

σ is the standard deviation

Fig. 7 demonstrates the consequences of this phenomenon for alarm thresholds of σ to 5σ. Alarm thresholds are usually set to around 4σ depending on local conditions. Note that the actual alarm level is equal to the alarm threshold plus the background count rate.

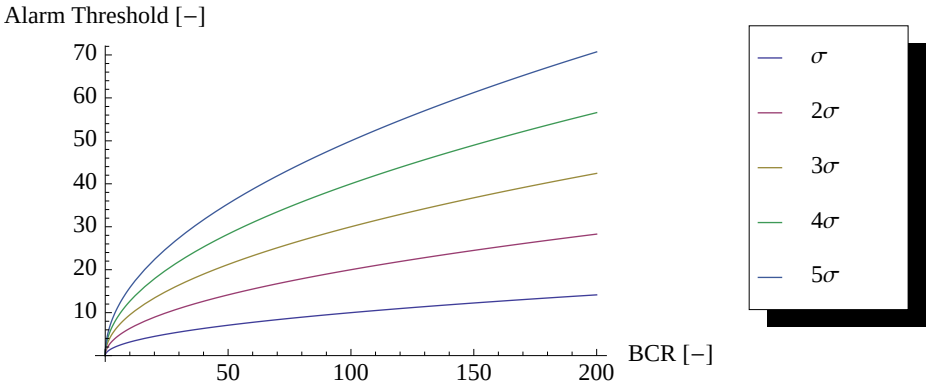

Fig. 7. Effect of increasing background count rate on various alarm threshold settings.

Obviously, a high background count rate would have disastrous consequences in terms of sensitivity and therefore the minimum quantity of nuclear or radioactive material that the portal monitor is able to detect. Thus, some means of mitigating this effect must be developed to ensure that the RPM can remain effective under those conditions.

One obvious solution to this problem would be to simply attempt to differentiate and discriminate the radiation caused by precipitation. This would be a trivial task in most cases, as the radioactive isotopes transported to the surface by rain and their gamma ray energies are well known.

Unfortunately, this cannot be accomplished when using a PVT plastic scintillator. According to a major manufacturer, PVT based radiation detectors have a full width at half max (FWHM) thirty times greater than an equivalent sodium iodide

(NaI) detector at 662 keV [16]. The relationship between FWHM and the standard deviation of the measured energy is given by the following equation [15]:

$$\text{FWHM} = 2\sqrt{2\ln(2)}\sigma \approx 2.35482\sigma \tag{2.2}$$

where σ is the standard deviation of the energy measurement.

This means that the energies recorded by the PVT detector will have a standard deviation about 13 times greater than those of the NaI detector. This is beyond unacceptable in terms of performance, as NaI is itself already considered to be the one of the lowest resolution scintillator materials practically usable for isotope identification via gamma spectroscopy. Furthermore, all deployed RPMs are, understandably, designed only to record count rate within a single, pre-selected energy range as opposed to a full spectrum. Thus, no information about the spectrum of the incoming radiation can be derived from the data. Therefore, in order to directly eliminate the radiation from the radon decay products transported to the surface by precipitation from the ordinary background, an additional detector of some sort with better resolution must be added to the system.

Since the above solution is obviously impossible to accomplish while analyzing historical data, a method had to be developed which was able to determine how weather impacted the count rate at the portal monitor using gross counts and weather data alone.

C. Conclusion

In conclusion, a methodology capable of determining how weather impacts the background count rate of SLD portal monitors must be developed. This methodology must accomplish this task using only using gross gamma ray count rate and weather

data.

Should the above results of the above methodology indicate that there is indeed a serious issue, some means of mitigating these effects must be developed. This method must not be excessively costly, and must be feasible for deployment in nations with widely varying degrees of locally available technology and infrastructure. As the portal monitors themselves cost approximately $55,000 [17], only solutions whose cost is less than or equal to this figure will be considered.

CHAPTER III

PROCEDURE

A. Initial Analysis

The procedure for accomplishing the above objectives began with determining whether a statistically significant correlation between various meteorological parameters, including precipitation, and increased background counts at the aforementioned portal monitors existed. To accomplish this, historical background count rate data was obtained from the portal monitors and compared to historical weather data. This data was gathered from the National Oceanic and Atmospheric Administration's (NOAA) Climate Data Online database, which consists of 22 different meteorological parameters, including type and intensity of precipitation, recorded once per hour [13]. This database was chosen due the fact that it is was the most complete collection of worldwide weather data available at no cost to academia.

B. Inverse Model

Once the potential worldwide sources of this increased background count rate were identified, an algorithm was created to determine the frequency of incidence and severity of this effect. This algorithm was designed to automatically determine which background count rate changes were likely to have been caused by the meteorological event(s) of interest, based on the characteristic pattern(s) of background activity known to be caused by these events. This algorithm was designed to be capable of functioning without any weather data to assist it; the weather data merely served to verify its performance.

This algorithm's effectiveness was then tested against data gathered from a por-

tal monitor test bed and weather station at Oak Ridge National Laboratory (ORNL). This step allowed the algorithm's performance against smaller timescale effects to be determined, as the weather station's sample rate was on the order of one sample per second, unlike conventional weather data sources which only record data a few times per hour at the most. The sample rate of its radiation detectors was also boosted to around one sample per second, unlike the conventional SLD RPMs which only record background count rates 4.5 times per hour on average for archival purposes. Furthermore, the weather station and portal monitor were co-located, as shown in Fig. 8, eliminating any potential variations that could result from time delays between the two.

Fig. 8. The portal monitor and weather station at ORNL.

C. Forward Model

Once an inverse model of sufficient accuracy to determine the cause of the increased background count rate with reasonable certainty was developed, a forward model was created to predict and mitigate the effects of this phenomenon. This forward model was designed so that it could be implemented with only data that can be obtained at a reasonable cost at any SLD site, or via equipment that could be added to any SLD site at a reasonable cost relative to that of the portal monitors themselves. The effectiveness of this algorithm will also be tested against data gathered from the aforementioned portal monitor test bed.

D. Shielding

The use of shielding to suppress the observed fluctuations in background count rate was also be explored. Various shields were designed to attenuate the background gamma radiation, and in some cases to prevent the source of the radiation from coming into close proximity to the detectors. These shields were designed to be as cost-effective as possible.

CHAPTER IV

INVERSE AND FORWARD MODEL RESULTS

A. Initial Analysis

Initial studies as to whether a statistically significant correlation between other meteorological parameters and the background count rate observed by RPMs existed yielded no cases in which such a correlation actually existed. At each of the four sites analyzed, distributions resulting from this analysis were completely random and further inquiry was not considered necessary. Multivariable relationships were even studied for certain cases that seemed logically promising, such as pressure and temperature, but none yielded a statistically significant correlation. Sample data from this analysis can be seen in Table I and Fig. 9. Due to the quantity of data points and the fact that the rate of precipitation had a Pearson product-moment correlation coefficient coefficient of 0.4, an absolute value of 0.3 or more was considered to be significant. Please note that the average gamma count rate is tabulated over the period from 0.5 hours before to 2 hours after the weather data point in question, for reasons that will be explained later in this chapter.

Although some correlation was initially found to exist between the rate of precipitation and the portal monitor count rates, this correlation was far weaker than previous studies suggested. However, after observing several plots of the rate of precipitation and the RPM count rate vs. time, it became clear that the expected increase in count rate was significantly leading or lagging the advent of precipitation at every site analyzed.

Table I. Correlation coefficient of background count rate with selected meteorological parameters measured at Haifa, Israel

Parameter	Correlation Coefficient Vs. Avg. Gamma Count Rate [s^{-1}]
Wind Direction [Degrees]	-0.07514
Wind Speed [mph]	0.033021
Gust Velocity [mph]	-0.10115
Cloud Ceiling [feet/100]	0.195681
Sky Cover [-]	-0.23829
Visibility [Miles]	0.027377
Temperature [Degrees F]	0.208181
Dew Point [Degrees F]	0.004513

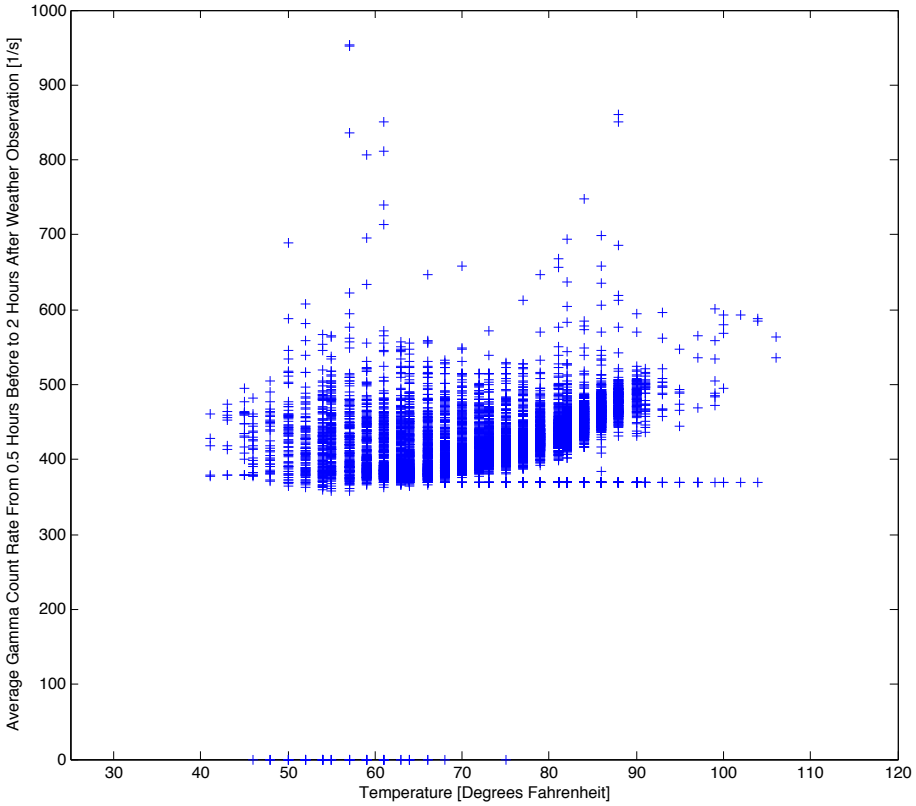

Fig. 9. Plot of temperature vs. average gamma count rate measured at Haifa, Israel.

At the relatively low sample rates involved, no noticeable lag between the two should have occurred, aside from, perhaps, a small offset due to the fact that the weather data was sampled once per hour, whereas the RPM count rate was sampled around 4.5 times per hour. However, the observed lag was significantly greater, often on the order of multiple hours. Worse yet, the observed lead or lag time was highly inconsistent and varied significantly from event to event.

This time difference between the detection of a precipitation event by a given NOAA weather station and the detection of increased background radiation by the associated SLD portal monitor was hypothesized to be caused by the distance between the weather stations and portal monitors. Due to this, it would be highly unlikely

for any weather station-portal monitor pair to record the start or end of a given precipitation event simultaneously. This also explained the random element in the variation, as a given storm could approach from many different directions at many different velocities, each of which would cause a different time offset.

Adding a constant time correction factor, determined iteratively for each site, mitigated this issue sufficiently to allow the development of the algorithm to proceed. However, this alone could not eliminate the issue entirely, as the storm's speed of movement and direction of travel varies between individual precipitation events.

B. Inverse Model

1. Development of Algorithm

To combat the issues with analyzing the historical data, the algorithm was designed to average the count rate data from some amount of time before to some amount of time after a given weather data point. It would then determine whether the mean value of that range was sufficiently greater in magnitude than the average of the values immediately before and after the range by a predetermined lower-level discriminator factor, then that weather data point would be flagged as having a precipitation event, as seen in the following equation:

$$a = \begin{cases} 1 & \text{if } \dfrac{\sum_{i=j}^{k} C_i}{k-j} \geq \dfrac{\sum_{i=j-r}^{j} C_i * L}{r} \text{ and } \dfrac{\sum_{i=j}^{k} C_i}{k-j} \geq \dfrac{\sum_{i=k}^{k+r} C_i * L}{r} \\ 0 & \text{if } \dfrac{\sum_{i=j}^{k} C_i}{k-j} < \dfrac{\sum_{i=j-r}^{j} C_i * L}{r} \text{ or } \dfrac{\sum_{i=j}^{k} C_i}{k-j} < \dfrac{\sum_{i=k}^{k+r} C_i * L}{r} \end{cases} \tag{4.1}$$

where

a represents the logic variable whose value is unity if the algorithm indicates that a

background count rate increase due to rain has occurred and otherwise is zero.
j represents the data point at which the count rate data range of interest begins.
k represents the data point at which the count rate data range of interest ends.
C represents the value of the count rate data point.
L represents the lower level discriminator's value. Note that $L > 1$.
r represents the number of data points before or after the data range of interest used to compute the average value of the range before or after the data.

This structure was particularly advantageous, as the lower-level discriminator's (LLD) value varied with long-term changes in the overall background count rate, as opposed to being fixed at an arbitrary value. This made the algorithm immune to a myriad of problems that would normally be encountered with a fixed LLD value. Gain drifts and gradual variations in other sources of the natural background count rate had no significant negative effects. It was hypothesized that the algorithm should fail only very rarely, so long as abrupt changes in background count rate do not occur with great frequency.

2. Findings from Historical NOAA Data

The algorithm was used with historical NOAA data to show that precipitation correlated with background count rate increases. Determining the exact values of the above coefficients for Eq. 4.1 would prove to be very difficult using the historical data alone due to its low resolution in the time domain. Only crude estimates could be attempted. These crude estimates could produce inaccurate results. However, for the purpose of analyzing this correlation, it should be sufficient.

The algorithm clearly indicated that a statistically significant proportion of precipitation events were correlated with unusually large, rapid increases in background

count rate. The results from a subset of this analysis is shown in Table II. These results are based on optimized time shift and LLD values; whatever combination of values produced the best results was used. The first column gives the location of the site analyzed, the second column gives the optimized time shift value, the third column gives the optimized LLD value and the last column gives the percentage of precipitation events correctly identified by the algorithm.

Furthermore, such increases rarely occurred when precipitation was not present. The particular sites analyzed were chosen based on the availability of sufficient NOAA precipitation data coinciding with the available background count rate data. Note that for all historical data, r was set to 5, as described in Equation 4.1. This meant that the area of interest had to be greater than the LLD value multiplied by the average of the background count rate for a period of approximately of 1.11 hours before and 1.11 hours after the period of interest.

Table II. Performance of algorithm on data from selected SLD sites.

Site [–]	Time Shift [hours]	LLD [–]	Correctly Identified [%]
Haifa, Israel	-2	1.025	23.4
Busan, Republic of Korea	2.5	1.0075	15.15
Veracruz, Mexico	4.75	1.025	13.82
		Average	17.46

Although the algorithm indicated that precipitation was indeed having a significant effect on the RPMs, even this was tenuous at best. The algorithm clearly needed significant improvements in order to produce results that could be relied on with confidence. To make these improvements, better data with a higher resolution in the time domain was needed.

3. Findings from ORNL Portal Monitor and Weather Station Data

Regardless of the efforts made to improve its performance, the forward model algorithm consistently suffered an excessively high failure rate when run against the historical RPM data. It was hypothesized that this was due to either:

1: The variations in time between the detection of a weather event by the weather station and the portal monitor receiving an elevated background count rate being too random to be compensated for by the algorithm's various features

2: The relatively low resolution of the data in the time domain.

To test this hypothesis, more precise data was gathered from a portal monitor and weather station at ORNL. This apparatus had three distinct advantages. First and foremost, the radiation portal monitor and weather station were co-located, being literally mere feet away from each other. This would eliminate practically all lead or lag between the weather station's detection of a weather event and the portal monitor's detection of its resulting effect on background count rate. Secondly, the apparatus at ORNL sampled both weather and radiation data at a much greater rate, on the order of once per second. This would eliminate any potential errors caused by the relative imprecision of the historical data. Lastly, the rate of precipitation was recorded quantitatively instead of qualitatively, as is standard practice for the NOAA. Therefore, it was possible to place a lower level discriminator on the rate of precipitation as well, rather than simply relying on a potentially inconsistent, qualitative threshold between what does and does not constitute a significant rain event.

The first major improvement made with this data was the determination of the amount of time the average rain event increases the background count rate signifi-

cantly. This allowed accurate values for values j and k of Eq. 4.1 to be determined in most cases.

Although the behavior of the background count rate during precipitation events had been studied previously, it was not possible to simply extrapolate from this to determine the correct values for those parameters. This was due to the fact that j and k needed to be chosen based upon the length of time within a rain event during which count rate would not only be elevated, but also be greater than the values immediately before and after. This meant that the range not only had to always contain the maximum count rate value for all rain events, but also had to be designed such that extremely large slopes were not encountered just after or before the selected range. Most importantly, the range had to tolerate the delay between the start of precipitation and the actual change in background count rate, meaning that it had to yield the proper result even if transposed by several minutes. Note that while j and k are simply indices, each index has a corresponding time associated with it, and the time elapsed between consecutive indices is a constant.

After a significant amount of trial and error, a search range of 6 minutes prior to the time step and 40 minutes after was chosen. This produced excellent accuracy on a random sample of several 24 hour periods, each of which included at least one rain event. These parameters were chosen by observation out of necessity, in order to permit the setting of the other parameters by mathematical optimization.

The next parameter to be analyzed was the lower-level discriminator (LLD) value. This was determined by running the algorithm against four 24 hour data samples chosen due to the presence of precipitation on those days. This was necessary due to the fact that, were a sample with no precipitation chosen, the ideal LLD value would be infinite and thus would not be conducive to the investigation.

An LLD value of 1.025 was chosen, which resulted in all rain events being correctly detected to within 2 standard deviations with a success rate of 85.6%. False positives occurred only 0.28% of the time at this level, clearly demonstrating the strong correlation between precipitation and increased background count rate. The minimum intensity for a rain event to be considered significant in this analysis was 0.2032 centimeters per hour (0.08 inches per hour); events less intense than this did not create any significant increase in background count rate. The effects of these LLD values can be seen in Fig. 10. Note that the precipitation logic flag is at 10 when the weather station reports precipitation above the previously established value of 0.2032 centimeters per hour, and at -10 when there is no precipitation. Note that the value of -10 is off the scale of this plot, and thus such data points will not be visible. Also, the algorithm success flag is at 25 when there is no actual precipitation and none detected by the algorithm, 35 when there is a properly detected precipitation event and at 15 when there is an error of any sort, whether there was an event detected when none occurred or no event detected when one did occur.

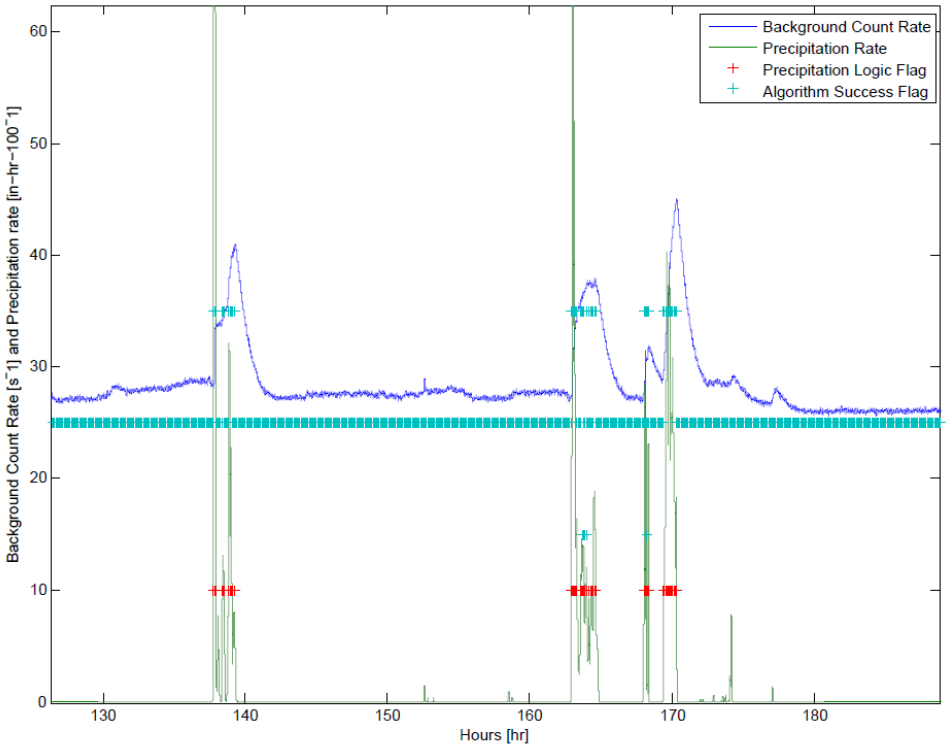

Fig. 10. Effects of LLD values on inverse model.

Once these values were established, the algorithm was run against all available data, covering the period from April 23, 2009 to July 9, 2009. These results can be seen in Table III. The first two columns represent the start and end dates of the period in question. The third column represents the ratio between detected precipitation timesteps and total precipitation timesteps. The fourth column represents the ratio between false positives and timesteps with no precipitation. The fifth column represents the ratio between detected precipitation events and false positives, and the last column represents the average gap between false positives in days, for periods during which this figure was finite. Some periods were intentionally omitted, due to the fact that they had no precipitation events and therefore no usable data. It is worth noting that the inclusion of the omitted periods would have improved the

results considerably. However, this would have also driven some of the values in Table III to infinity, thus rendering the results meaningless. This is also true of the omitted entry in the average gap between false positives column for the period between May 10, 2009 and May 19, 2009.

Table III. Metrics for performance of inverse model algorithm.

Start Date	End Date	Positives Per Event	False Positives per Non-Event	True Positives per False Positive	Average Gap Between False Positives [d]
5/1/2009	5/9/2009	0.888	6.57E-03	8.371	0.531
5/10/2009	5/19/2009	0.721	2.14E-04	80.899	N/A
5/20/2009	5/29/2009	0.812	2.79E-03	3.251	0.942
6/20/2009	6/29/2009	0.908	1.26E-03	4.899	1.409
7/1/2009	7/9/2009	0.967	3.48E-03	4.064	0.239
Overall Average		0.856	2.77E-03	20.883	0.634

While these results might seem unimpressive or even dismal if the false positives were uniformly distributed, that was not the case. The false positives generally occurred in clusters around a spurious rise in background count rate, as seen in Fig. 11. Discounting false positives that occurred within 5 minutes of another false positive, each cluster of false positives was separated by an average of 0.63 days from the next one. This indicated that increases in background count rate from other sources were a rare occurrence relative to those due to precipitation.

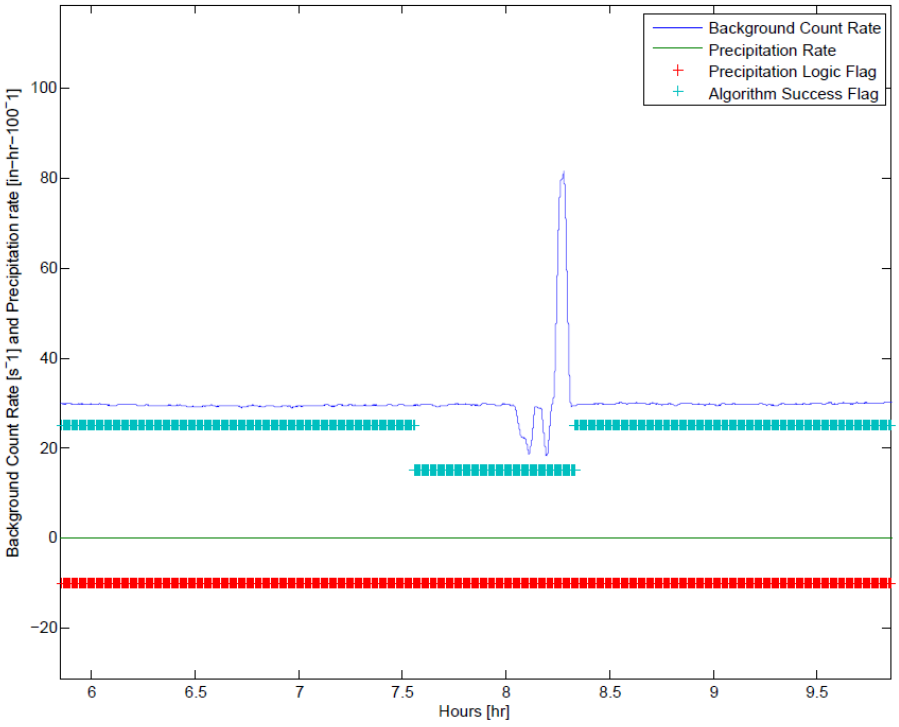

Fig. 11. Clustering of false positives around spurious changes in background count rate.

The above testing was only made possible after extensive reformatting of the data via PERL scripts. Utilization of the data in its existing form was precluded by the fact that the names of the weather data files were in a format that was not machine sortable.

Additional PERL scripts were then created to convert the output from the RPM and weather station to a comma-separated values format that was compatible with MATLAB. These scripts served to strip the tokens from the existing data, and to combine all of the radiation or weather data files from the period of interest into a single, continuous file. These scripts can be seen in Appendix D and Appendix E.

Overall, the improved algorithm demonstrated impressive robustness against the data gathered at ORNL, especially considering the unforgiving laboratory environment the portal was operated in. While "laboratory conditions" are seen as ideal for most experiments, a DOE laboratory is probably one of the most difficult places to operate a RPM due to the relatively frequent transportation of radioactive materials throughout the site. Due to this fact, it can be said with confidence that equal or better results should be expected at any typical border crossing.

C. Forward Model

Based on the data gathered thus far, it was clear that it would be significantly advantageous to suppress the gamma background created by precipitation at several different portal monitor sites. After the initial observations were completed, it was abundantly clear that the algorithm would be dramatically affected by the complex vagaries of meteorology. This fact was also attested to by much of the literature reviewed in previous chapters, some of which contained equations spanning several pages and containing 12 or more variables whose purpose was to account for all the sources and sinks of the various radon daughters in the atmosphere [9].

Broadly speaking, there were two clear approaches that could be taken to resolve this issue. The algorithm would need to either account for all pertinent meteorological factors precisely enough to mitigate their effects, or it would need to be made so robust that most of these effects could be ignored without excessive degradation in performance. Due to the impractical variety and precision of data needed for the former approach, the latter was chosen, although this choice would clearly come at the cost of some accuracy.

1. Portal Monitor Based

The first and most obvious option explored was the modification of the forward model algorithm to automatically suppress the background in real time. This method would be hugely advantageous in that it would require no additional hardware to implement, making its deployment nearly costless. However, it was clear almost immediately that this would not be possible. This is due to the fact that the inverse model algorithm can only detect a rain event after the gamma background levels have dropped back down to normal afterwards, a process which takes roughly 45 minutes. By this time, whatever vehicles bearing radiation sources that could have passed through the portal monitor during that period would already be long gone.

2. Weather Station Based

The next method explored was the use of a weather station to predict the increases in background radiation due to precipitation. This method would clearly have a much better chance of functioning properly in real time, as the advent of precipitation, theoretically, precedes the resulting increase in gamma background radiation.

The results from the ORNL portal monitor immediately confirmed that this was the case, indicating that this approach was theoretically viable. However, in order to implement it, an algorithm correlating a given length or quantity of precipitation to a given increase in background count rate needed to be developed. While algorithms for this purpose had been developed, the vast majority of them were designed solely for pure science purposes, and required an impractically wide range of detailed weather and atmospheric data [9], most of which was far beyond the capabilities of any commercially available weather station to provide.

3. Response Function

In order to create any sort of algorithm designed to predict the portal monitor's response to the radon daughters in precipitation, it was necessary to first determine the portal monitor's response to a given quantity of said radon daughters.

The first step in this process was determining which radon daughters contributed sufficiently to the gamma background to warrant modeling, and what the distribution of said isotopes was. To accomplish this, data gathered by researchers at the Universitat Politècnica de Catalunya with an experimental apparatus designed specifically for this task was utilized [18]. This data demonstrated that ^{214}Bi and ^{214}Pb were the only isotopes of any consequence in terms of gamma background. Furthermore, the ratio between ^{214}Bi and ^{214}Pb was reasonably constant for all events between 0 and 450 minutes in duration, with a value of 3.742 and a standard deviation of 0.689. This correlation can be seen in Fig. 12. Based on this, the ratio between the two isotopes was assumed to be constant for the purpose of simulating the portal monitor's response.

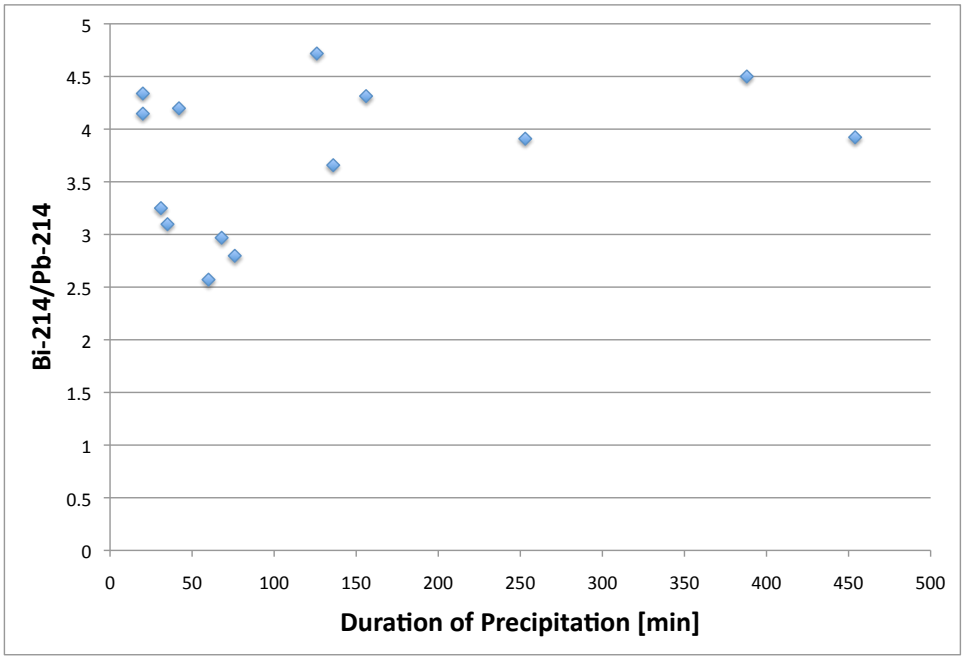

Fig. 12. Ratio of ^{214}Bi to ^{214}Pb for various durations of precipitation [18].

To determine the change in activity over time of these species, the ORIGEN-ARP software was used to simulate the decay of a mixture of ^{214}Bi and ^{214}Pb in the aforementioned ratio. The use of this software was advantageous in that it was able to not only quickly calculate the quantity and activity of each isotope at each time step, but also track the quantity and activity of the daughter isotopes resulting from the decay of the isotopes initially present.

This data was then used to generate MCNP source cards which would be used to simulate the actual behavior of the radiation portal monitor in response to the various resulting concentrations of ^{214}Bi, ^{214}Pb and daughter isotopes. The background radiation emanating from the precipitation was assumed to be an infinite disk source on the ground. To achieve greater computational efficiency, the MCNP deck was designed with the radon daughters represented as a finite disk source with a radius

of 20 meters. Modeling it as such resulted in a negligible 0.2% error, as seen in the following equation [19]:

$$\begin{aligned} \mu &= \frac{\mu}{\rho}\rho \\ \theta &= \text{ArcTan}(R/H) \\ \Phi_f &= \frac{S}{2}E_1(\mu H) - E_1(\mu H \text{Sec}(\theta) - 1) \\ \Phi_i &= \frac{S}{2}E_1(\mu H) \\ \delta &= \text{abs}(\frac{\Phi_f - \Phi_i}{\Phi_i}) * 100 \end{aligned} \tag{4.2}$$

where

$\frac{\mu}{\rho}$ is the mass attenuation coefficient of air in cm^2g^{-1}.

μ is the attenuation coefficient of air in cm^{-1}.

ρ is the density of air in g cm^{-3}.

R is the radius of the finite disk in cm, which is the independent variable in this case.

H is the height of the top of the highest detector on the radiation portal monitor in cm.

S is the source's activity per unit area in cm^{-2}.

Φ_f is the fluence at height H due to a finite disk source or radius R of activity S in $\text{cm}^{-3}\text{s}^{-1}$.

Φ_i is the fluence at height H due to infinite disk source of activity S in $\text{cm}^{-3}\text{s}^{-1}$.

δ is the the percent error due to approximating a given infinite disk source as a finite disk source of radius R.

The above result was calculated with a mass attenuation coefficient of of 0.1356 cm^2g^{-1}, an air density of 0.00122521 g cm^{-3}, a radius of 2000 cm (20 m) and a portal

monitor detector height of 273.5 cm [20]. The top of the highest detector was chosen as the height H in order to achieve the most conservative estimate.

An MCNP deck was then created by modifying an existing deck designed to calculate the effects of background radiation emanating from the concrete beneath the radiation portal monitor [21], as seen in Fig. 13, Fig. 14, Fig. 15, Fig. 16 and Fig. 17. In each of the cross-sectional images in this document, red represents concrete, yellow represents air, pink represents lead, green represents PVT, orange represents lucite, light blue represents SS304 stainless steel, dark blue represents aluminum and peach represents A336 Steel as shown in Table IV. This color scheme does not hold true for any three-dimensional images, or if otherwise noted. Furthermore, each cross-sectional image has a set of reference coordinates included. These coordinates are in centimeters and represent the position of the small black cross in the image. Thus, they may not correspond to the apparent center of the image itself. Also, Please note that these images may be slightly distorted, and should not be used as a reference for the proportions or dimensions of this model. An example of the source code, including the proper dimensions for the model in centimeters, is available in Appendix N.

Table IV. Key for colors and materials in MCNP cross-sectional images for this document.

Color	Material
Red	Concrete
Yellow	Air
Pink	Lead (Pb)
Green	PVT
Orange	Lucite
Light Blue	SS304 Stainless Steel
Dark Blue	Aluminum (Al)
Peach	A336 Steel

A noteworthy design feature of this MCNP deck was the use of cookie cutter cells to exclude the radiation source from the area immediately beneath the radiation portal monitor, as permitting a source in this location would be highly unrealistic and strongly bias the model. The effect of the cookie cutter cells on the source distribution can be seen in Fig. 18, where red represents the presence of a radiation source, and white represents its absence. Please note that in Fig. 13 the cookie cutter cells are visible as red and white dashed lines that normally represent geometry errors. This is simply how the cookie cutter cells are rendered by the MCNP visual editor, and do not reflect the presence of an actual error in this case. In the remainder of the figures, the cookie cutter cells have been removed from the image for better clarity.

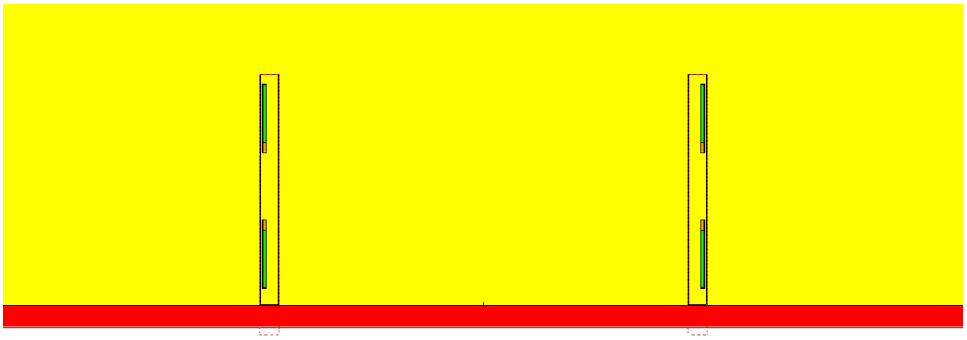

Fig. 13. X-Z cross section of MCNP model of radiation portal monitor centered at (0,-15,0).

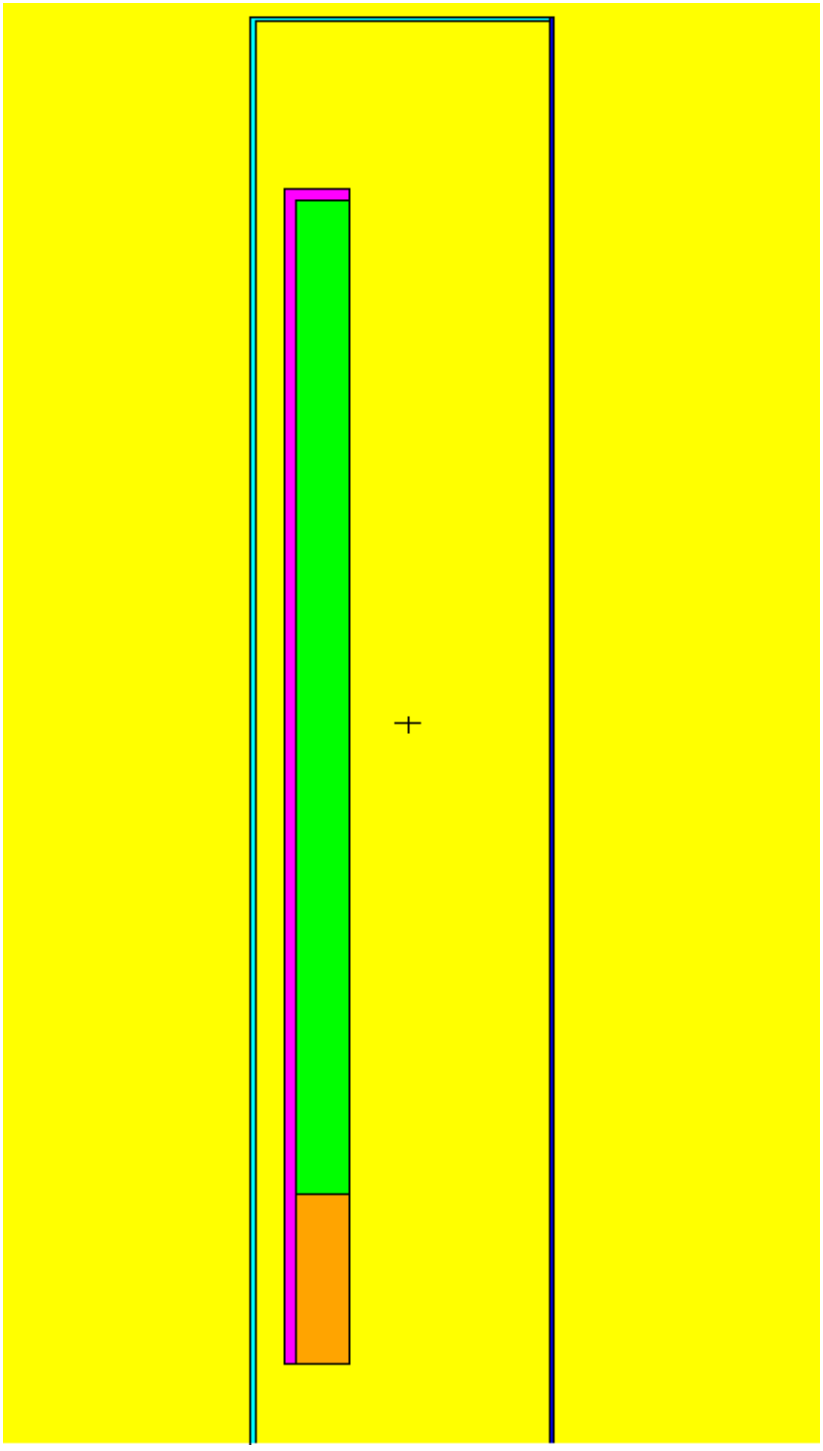

Fig. 14. X-Z cross section of upper left detector of the radiation portal monitor centered at (-265,-15,250).

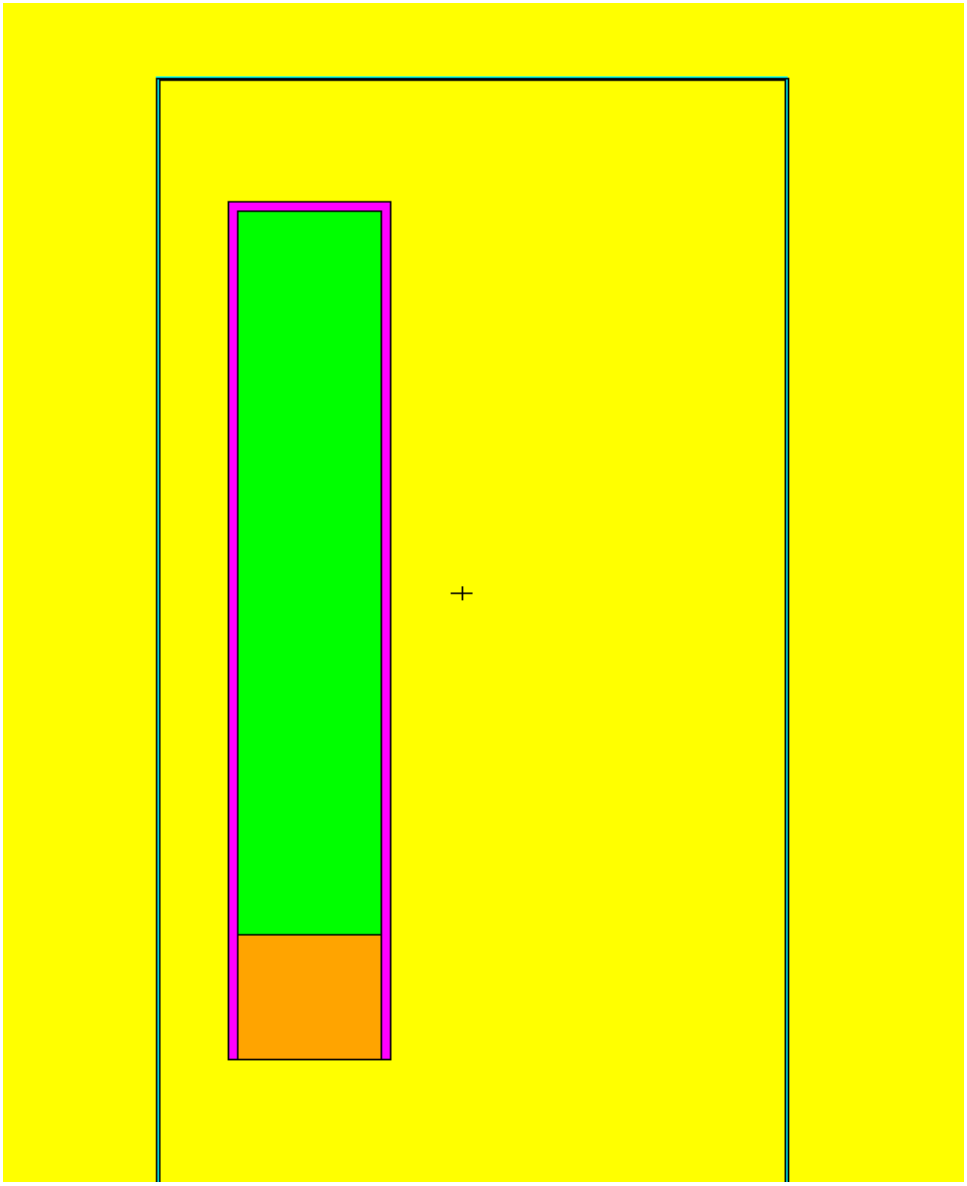

Fig. 15. Y-Z cross section of upper left detector of the radiation portal monitor centered at (-270,0,250).

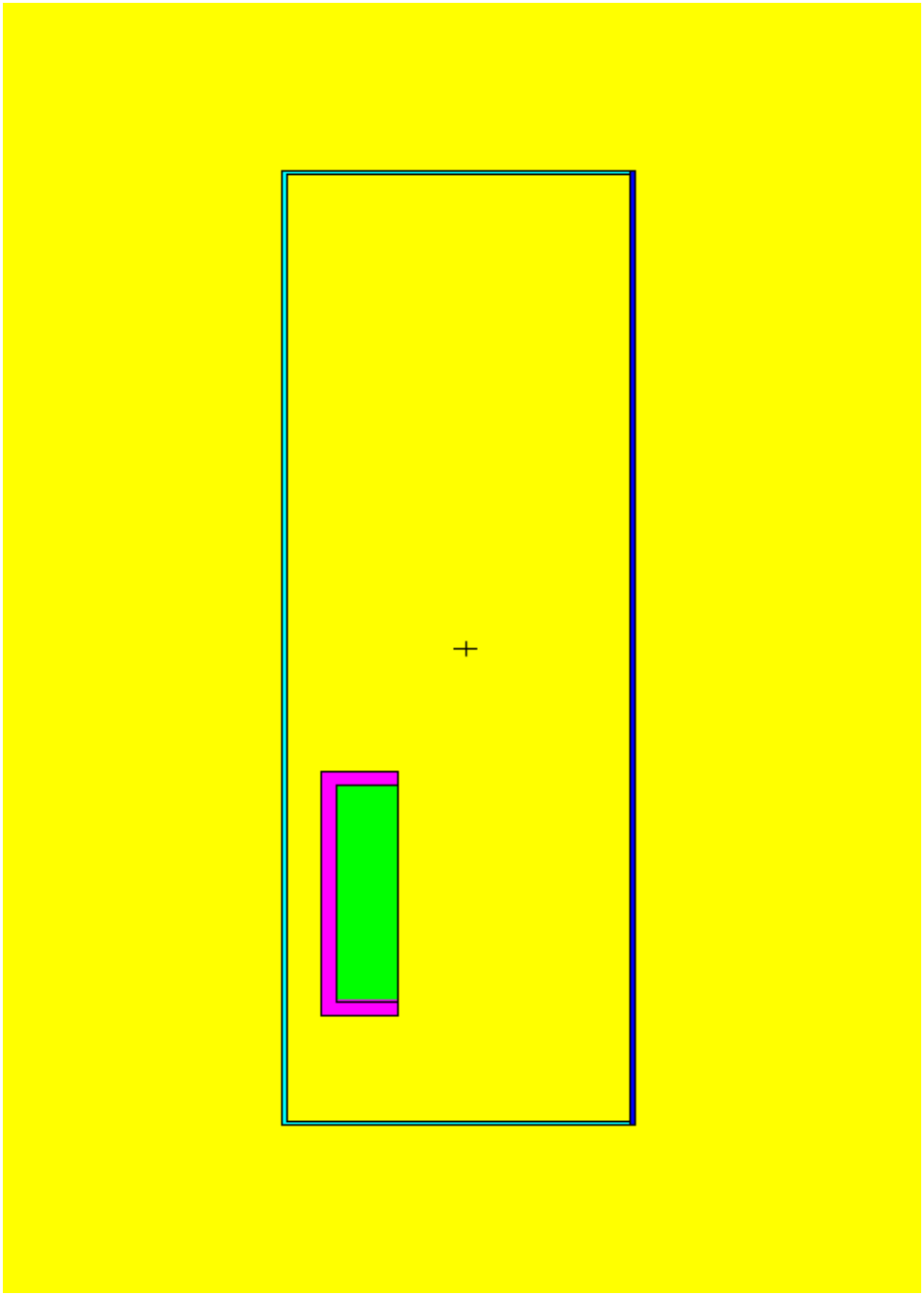

Fig. 16. X-Y cross section of upper left detector of the radiation portal monitor centered at (-265,0,250).

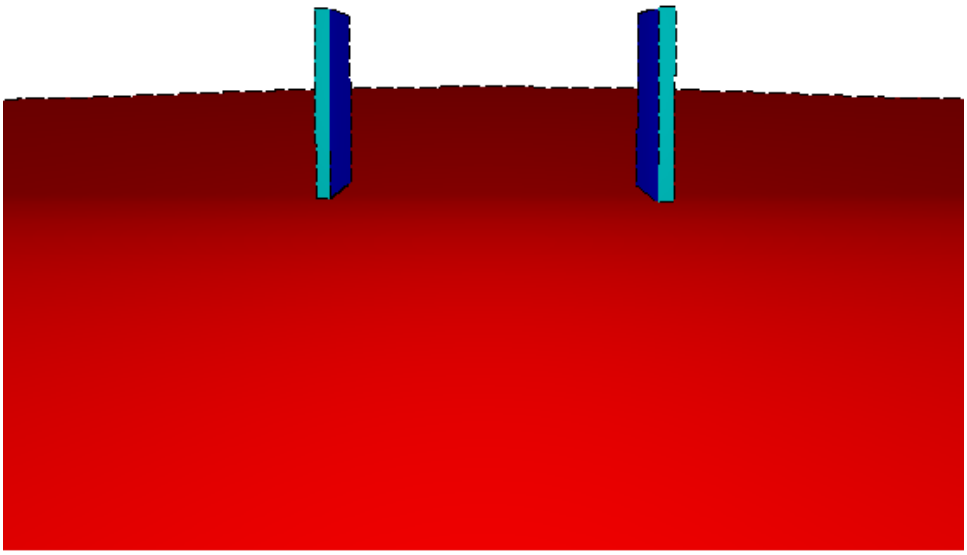

Fig. 17. Three-dimensional rendering of MCNP model of RPM.

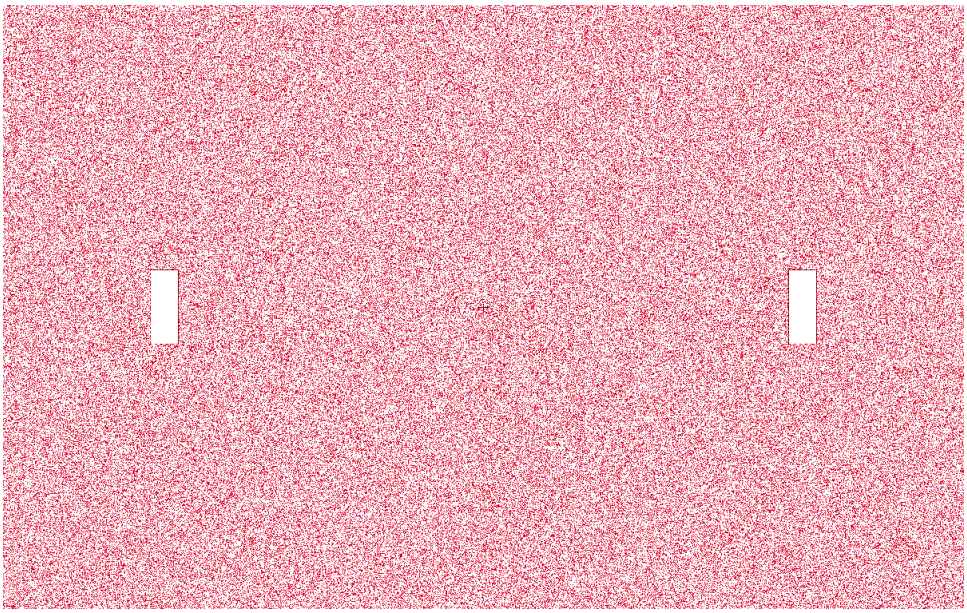

Fig. 18. Effect of cookie cutter cells used to exclude source from footprint of RPM. X-Y cross section centered at (0,0,0) with plot of source distribution within 100 cm of plot plane.

To verify the accuracy of this model, a quality control simulation was performed. First, a ^{152}Eu source of known activity was placed at various distances from the ORNL portal monitor and counted. Once this was completed, MCNP simulations of an identical source in the same positions were run, and the results of each were compared. The results of this simulation can be seen in Fig. 19.

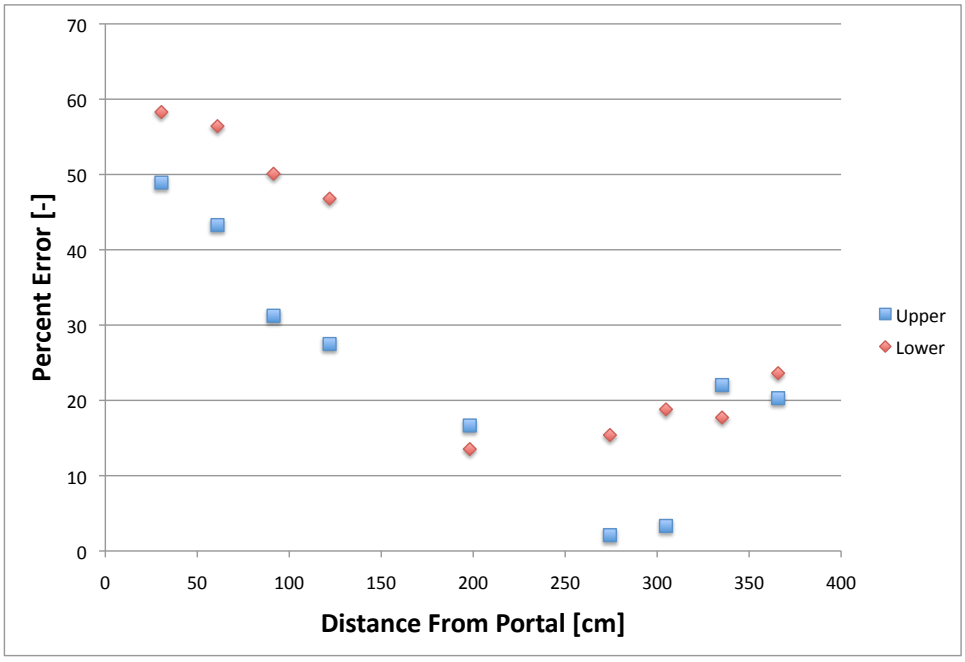

Fig. 19. Percent error of MCNP simulation relative to quality control experiment.

Due to the inherent uncertainties in counting statistics described by Eq. 2.1, the results of MCNP simulation were guaranteed to deviate somewhat from the experimental results, regardless of the accuracy of the simulation itself. This was taken into account by first calculating the percent error of the simulation versus the experiment, then subtracting the uncertainty in the percent error itself, as shown in Eq. 4.3. If this result was a negative number, it could be assumed that said error could be attributed to statistical variance as opposed to a shortcoming in the simulation.

$$\begin{aligned} \varepsilon &= \varepsilon_s + \varepsilon_r \\ \varepsilon_r &= \sigma_\varepsilon \\ \varepsilon_s &= \varepsilon - \sigma_\varepsilon \end{aligned} \tag{4.3}$$

where

ε is the error calculated assuming that the experimental results are the established value and the MCNP results are the estimated value.

ε_s is the systemic error in the MCNP simulation.

ε_r is the random error induced by the statistical uncertainty in the results of the MCNP simulation and the experiment.

σ_ε is the uncertainty in the value of ε.

The results of applying Eq. 4.3 can be seen in Fig. 20. As expected, the results were considerably better. Although a high systemic error for very short distances remained, this was unlikely to cause excessive error in the simulation, due to the fact that the source of the background was located on the ground around the RPM. This meant that the entire source would be located a minimum of 23 cm and 214 cm from the lower and upper detectors respectively. It also guaranteed that any radiation emitted in extremely close proximity to the detectors would need to penetrate a relatively large thickness of steel or aluminum and must pass through a relatively small solid angle due to the orientation of the RPM's housing and the detectors within.

Therefore, the QC results were deemed adequate, and the calculation of the response function proceeded.

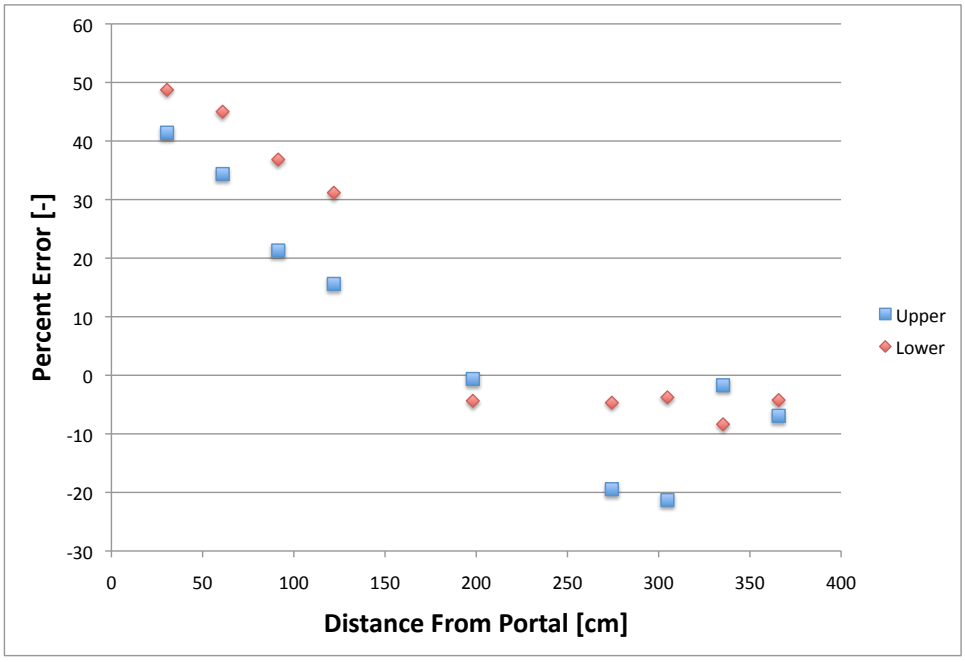

Fig. 20. Percent systemic error of MCNP simulation relative to quality control experiment.

Based on the results of the MCNP simulations, a response function was calculated. This was accomplished by simulating the response of the RPM to the radiation source generated by Origen-ARP then averaging the response of the four detectors at each time step. The values were then normalized and fitted to an exponential function, as seen in Fig. 21. The chosen exponential fit is described by Eq. 4.4 had an R^2 value of 0.9993.

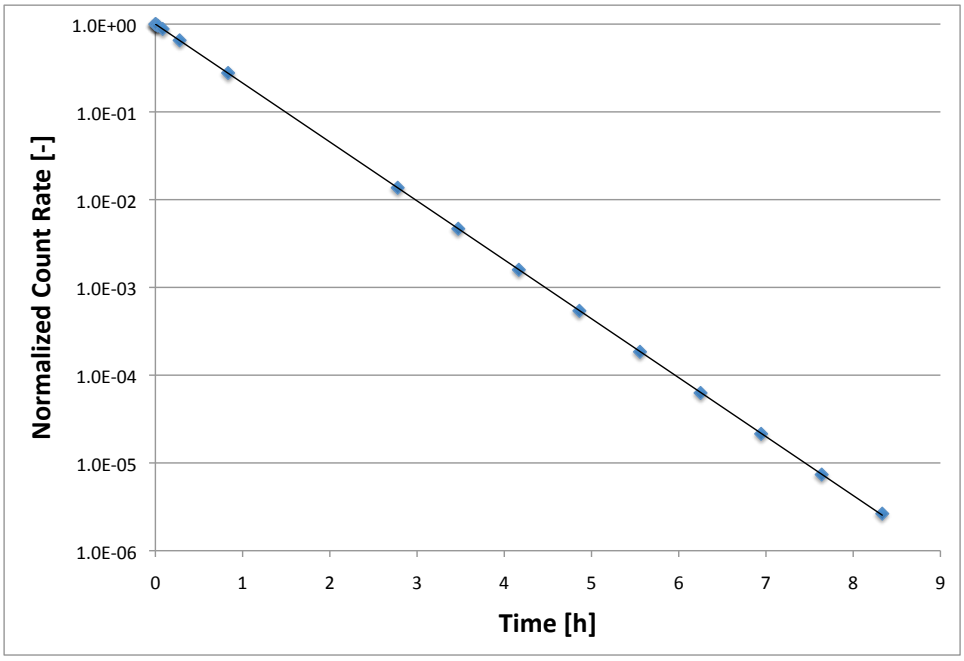

Fig. 21. RPM response function for normalized initial count rate.

The equation resulting from this fit is as follows:

$$C(t) = C_0\, 1.0002269368\, e^{-1.5460100942\, t} \tag{4.4}$$

where

$C(t)$ is the count rate with respect to time due to a precipitation event,

C_0 is the count rate at the end of the precipitation event,

t is the time elapsed after the end of the precipitation event in hours.

4. Algorithm Development

With a response function calculated, it was only necessary to determine some means of predicting the increase in count rate at the end of a given precipitation event in order to calculate its probable effects on the background count rate over time. A

variety of methods for accomplishing this goal have been proposed, but most of them require unfeasibly precise meteorological data, such as the exact path a raincloud took from its formation to when precipitation began [9].

However, one algorithm, developed by K. Fujitaka et. al. at the National Institute of Radiological Sciences in Japan appeared to be well suited to this application. This algorithm was based on an empirical correlation and relied only on the duration of the rainfall to calculate a figure for the percent increase in background count rate [22]. Their algorithm is as follows:

$$\ln y_{max} = logA(1 - e^{-2.21logt}), 1.5 \leq t \leq 24 \tag{4.5}$$

where

y_{max} is the percent increase in background count rate from the baseline.
A is the maximum increase in background count rate from the baseline.
t is the duration of the precipitation in hours.

Although certainly advantageous due to its sheer simplicity, this algorithm's performance was questionable. When compared to its developers' own data, the variance between the trendline and the plotted data was extreme, as seen in Fig. 22. Note that the data is plotted on a log-log scale in this figure, and the variance is thus worse than it might initially appear. Worse still, this trend was not even discernible in the data gathered from the ORNL portal monitor as seen in Fig. 23. This algorithm had an R^2 value of 0.0236 when plotted against the data from the ORNL portal monitor with the value of A set at 28.5, as in the original publication.

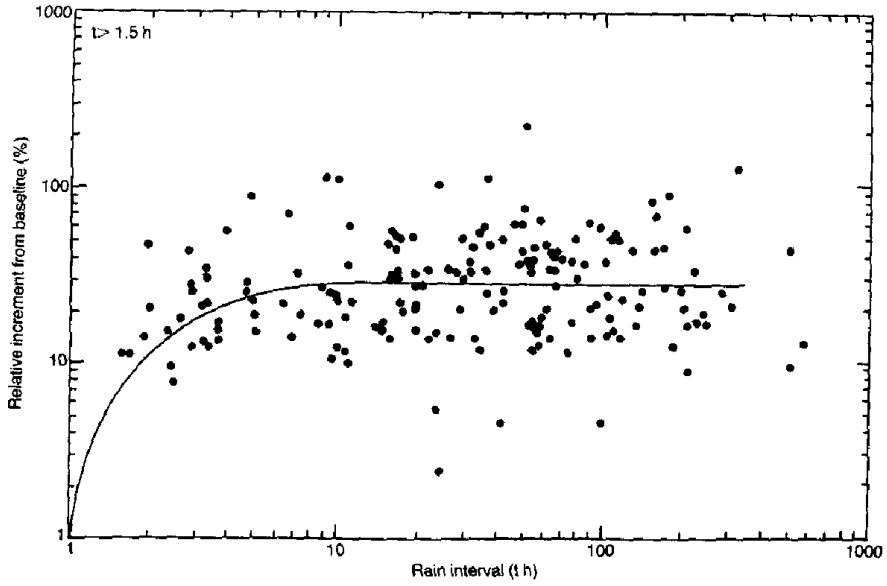

Fig. 22. Dependence of relative increment of external radiation level on rain interval [22].

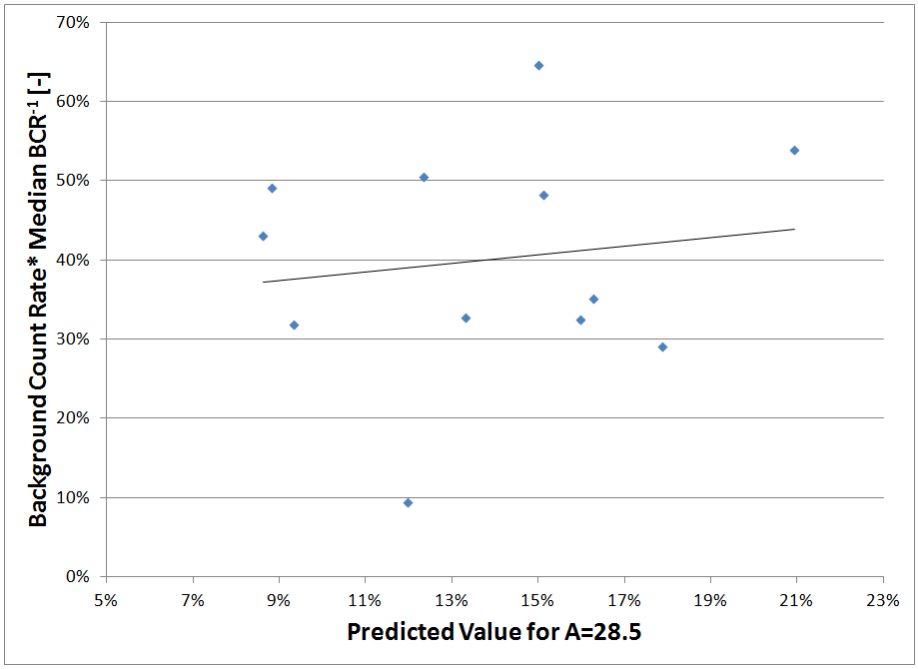

Fig. 23. Eq. 4.5 and linear fit thereof vs. increment of background count rate over median.

However, it should be noted that the value of A in Eq. 4.5 represents the maximum possible value the algorithm is designed to represent, and thus should be set to the maximum value encountered in the data. To determine if this was the cause of the inaccuracy, the algorithm's results were plotted again with A set equal to 45. Nevertheless, this yielded nearly the same result, and an R^2 value of 0.0214.

Although the trend whose existence they postulated was plausible and vaguely visible in their own data, it was clear that this algorithm's performance was weak. Thus, a new, more accurate algorithm needed to be developed.

To improve the performance of the algorithm, it was clear that additional variables would need to be utilized, as relying solely on the duration of the precipitation could produce only a minimal improvement. The behavior of several other variables was investigated, and it was found that the maximum rate of precipitation had a reasonably good correlation with the intensity. However, it too was not sufficiently well correlated in and of itself, and had an R^2 value of only 0.3941, as seen in Fig. 24.

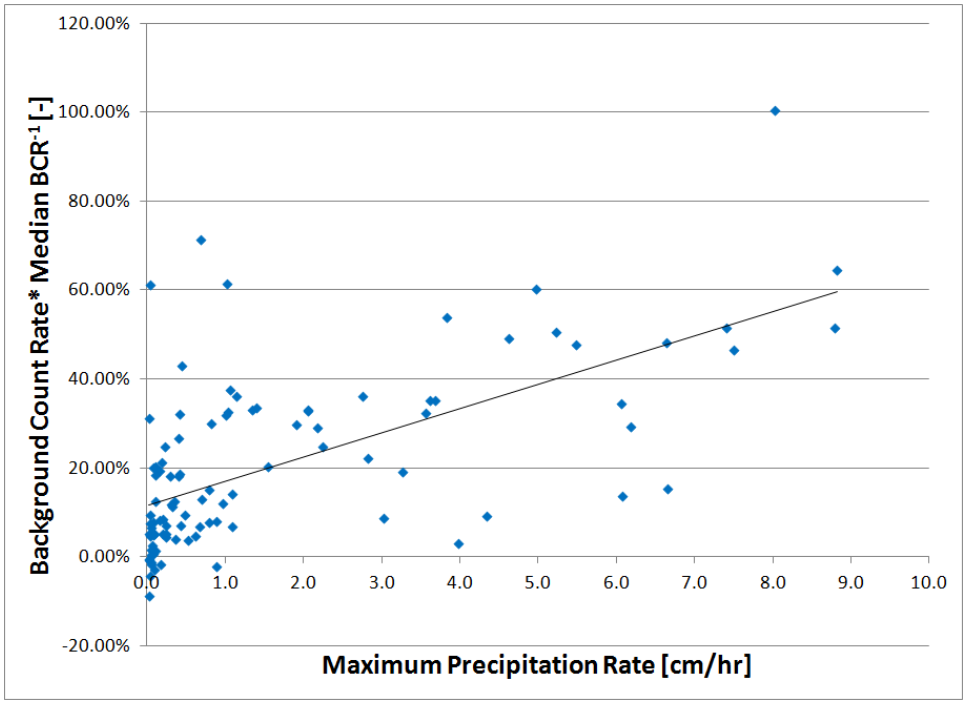

Fig. 24. Maximum rate of precipitation vs. increase in background count rate.

However, combining the two did result in a reasonably accurate algorithm. Optimizing the coefficients governing each set of data resulted in the following equation:

$$C_1 R_{max}^{A} * (1 - e^{-tB-\delta}) + C_2 \tag{4.6}$$

where

C_1 and C_2 are constants. For short precipitation events, C_2 represents the minimum possible increment in background count rate due to a precipitation event of greater intensity than the lower level discriminator.

R_{max} is the maximum precipitation rate during the precipitation event in inch hour^{-1},

A is the constant representing the correlation between the maximum rate of precipitation and the increase in background count rate.

B is the constant representing the correlation between the total duration of precipitation and the resulting increase in background count rate.
t is the duration of the precipitation event in hours.
δ is $\lim_{x\to\ 0} f(x) = x$ This is simply designed to avoid taking the log of zero or a negative number, and is included to increase the computational efficiency of the equation by avoiding more complex means of excluding times of zero from computation.

To improve the algorithm's accuracy, different values of A, B, C_1 and C_2 were calculated for events lasting less than one hour and events lasting more than one hour. In all cases, D should be set to the smallest value permitted by the hardware and/or software that the algorithm is run on. For events less than 1 hour in duration, A equals 0.5, B equals 4.5, C_1 equals 0.24117 and C_2 equals 0.05268. For events of more than one hour in duration, A equals 0.5, B equals 1.5, C_1 equals 0.26196 and C_2 equals 0.1366376.

The resulting correlations for events lasting less than one hour and events lasting more than one hour had R^2 values of 0.524 and 0.616 respectively, as seen in Fig. 25 and Fig. 26. Although these correlations still were imperfect, they were a significant improvement.

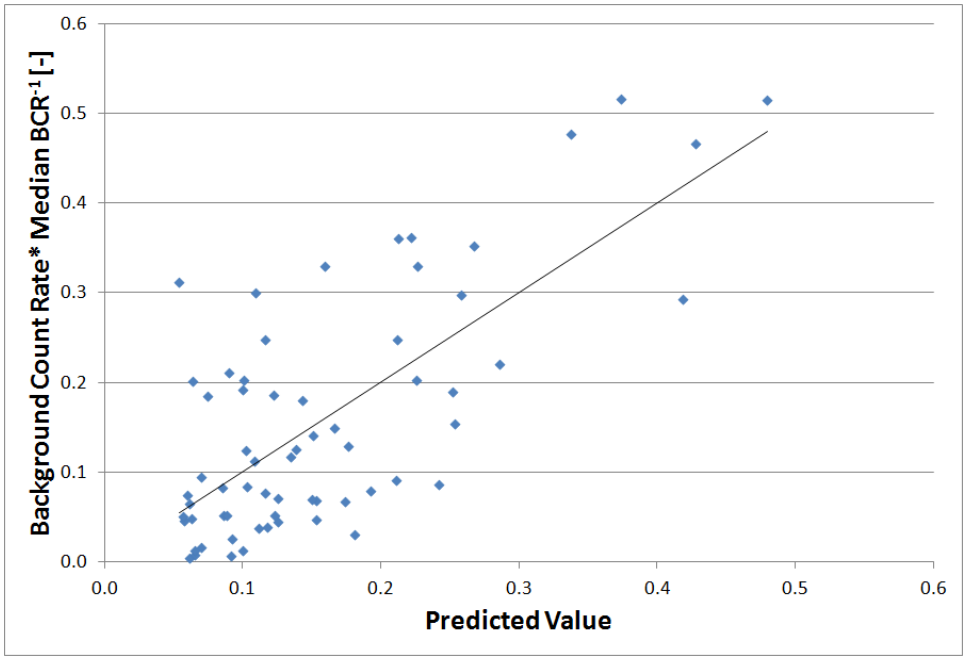

Fig. 25. Eq. 4.6 and linear fit thereof vs. increment of background count rate over median for events of less than 1 hour in duration.

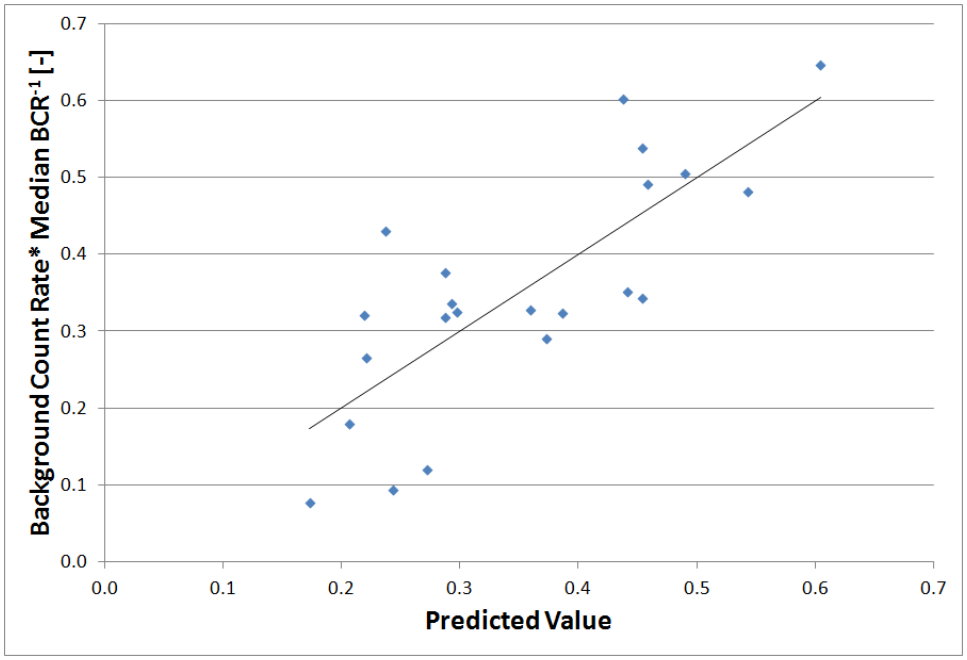

Fig. 26. Eq. 4.6 and linear fit thereof vs. increment of background count rate over median for events of more than 1 hour in duration.

Due to the algorithm's design and the variance in the data, it was necessary to reduce the values of C_1 and C_2 in practice to avoid over-correcting for the precipitation excessively. To accomplish this, C_1 was reduced to 0.15 for events of less than one hour and 0.20 for events over one hour. C_2 was reduced to 0.05 for events of less than one hour and 0.015 for events over one hour. This reduced over-correction to an acceptable margin.

5. Algorithm Performance

After this final change, the algorithm was tested. The results can be seen in Table V. In this table, the first two columns represent the start and end dates of the period in question. The third column represents the average percent attenuation of the increase in background count rate due to precipitation. The increase in background

count rate due to precipitation was calculated as the count rate subtracted from the mean count rate over the entire period. The fourth column represents the percentage of the steps in which the correction algorithm produced a value below the mean value of the background count rate over the entire period. This was expected to occur during normal operation due to the fact that the true baseline count rate fluctuates about this value considerably. The fifth column represents the average percentage below the mean value that the steps from column four possessed. The last column represents the frequency of steps whose values were more than 10% below the baseline or mean value. Any such steps could be considered to be genuine errors as opposed to a result of the rapid fluctuation of the true baseline value. Although the algorithm only attenuated around 50% of the increases, this was a necessary trade-off to avoid excessive over-correction which would inevitably result in a vast quantity of false alarms. An example of the algorithm's behavior can be seen in Fig. 27.

Table V. Performance of forward model.

Start Date	End Date	Average Attenuation	Attenuation Steps Under Baseline	Average Percentage Below Baseline	Steps Exceeding 10% Below Baseline
5/1/2009	5/9/2009	44.310%	29.297%	2.527%	0.000%
5/10/2009	5/19/2009	48.537%	16.076%	1.466%	0.000%
5/20/2009	5/29/2009	47.921%	23.327%	2.085%	0.000%
6/20/2009	6/29/2009	45.672%	31.624%	4.198%	4.290%
7/1/2009	7/9/2009	47.672%	1.566%	0.855%	0.000%
Overall Average		46.857%	20.584%	2.248%	0.894%

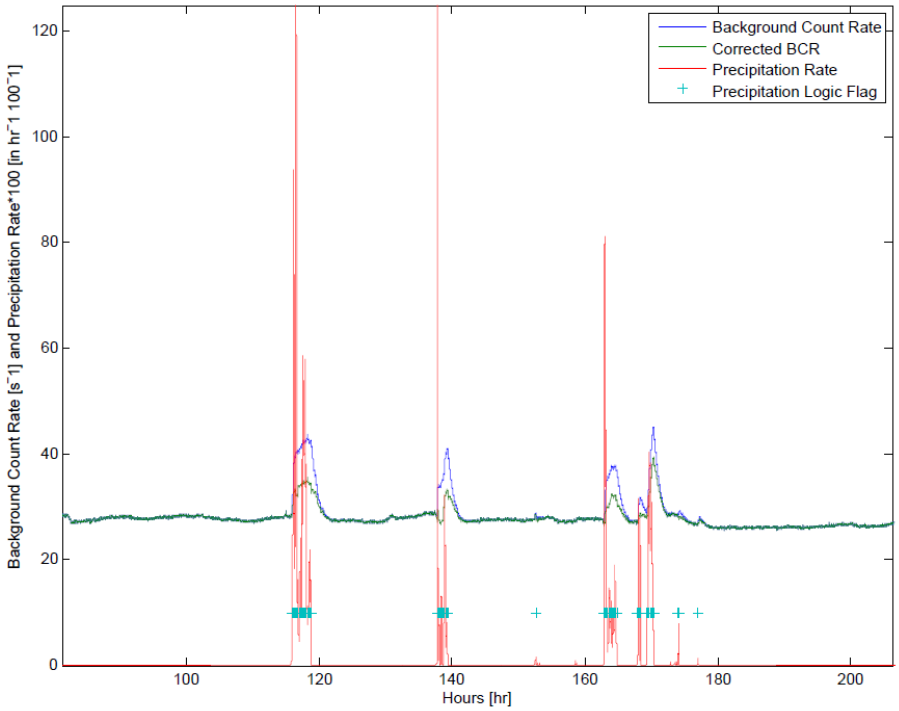

Fig. 27. Behavior of algorithm defined by Eq. 4.6, precipitation rate and background count rate from 5/10/2009 to 5/19/2009.

Based on this algorithm, it should be possible to increase or decrease the alarm threshold based on the predictable behavior of the background count rate during or after precipitation. When precipitation occurs, it is known that the background count rate will rise, along with by how much it will do so. In this case, increasing the value for the alarm level would be advisable. Conversely, it is known that the background count rate will continuously decrease once the rain ends, and the alarm level could be decreased in anticipation of this occurring. As previously discussed, the alarm level itself is not a fixed value, but a multiple of the standard deviation of the background count rate. It is the coefficient that the standard deviation is multiplied by that would thus be increased or decreased.

Unfortunately, it was not possible to perform any actual experiments involving the adjustment of the alarm level. However, adding this capability to an existing SLD site would be very inexpensive, with a weather station costing approximately $3,500 [23].

CHAPTER V

SHIELDING RESULTS

A. Introduction

The final method explored was the use of shielding to reduce the effect of the precipitation on the RPM's background count rate. Unlike most conventional radiation shielding, this approach could be effective not only by preventing unwanted gamma rays from impinging on the detectors, but also by preventing the water containing the radon daughters from coming into close proximity to the detectors. This approach seemed particularly promising as the detectors are already heavily shielded on their outer faces, having a lead shield immediately around the detector and a steel case around the outer faces of the portal monitor. Conversely, the inner faces were made of aluminum and designed to allow gamma radiation in. This directional shielding can be clearly seen in Fig. 16.

Based on the above, it was postulated that most of the background counts were due to radiation sources located in between the RPM's two columns of detectors. This was due to the fact that any source that existed in this area would impinge on the detectors essentially unattenuated, whereas sources from any other direction would need to penetrate a significant amount of shielding.

B. Initial Analysis

To test this theory, two MCNP simulations were created. One simulated a source contained within the area between the detectors, encompassing a radius from 0 m to 2.79 m, which represents a circle whose perimeter encompasses the outer edge of the base of each of the detector units, as seen in Fig. 28. The other simulation covered

the remainder of the source from 2.79 m to 20 m. The source code for each of these simulations is located in Appendices O and P respectively. A source with a radius of 20 m was a sufficient approximation of an infinite disk source as detailed in Eq. 4.2. The inner area was 24.45 m^2, while the outer area was 1232.18 m^2. To obtain the ratio between the fraction of the background count rate emanating from each region, the output of this simulation was manipulated as follows:

$$\frac{C_{in}}{C_{out}} = \frac{A_{in}}{A_{out}} \frac{P_{in}}{P_{out}} \tag{5.1}$$

where

C_{in} is the count rate due to activity within the inner area

C_{out} is the count rate due to activity outside the inner area

A_{in} is the surface area of the inner area

A_{out} is the surface area of the outer area

P_{in} is the number of counts per particle started in the inner area

P_{out} is the number of counts per particle started in the outer area

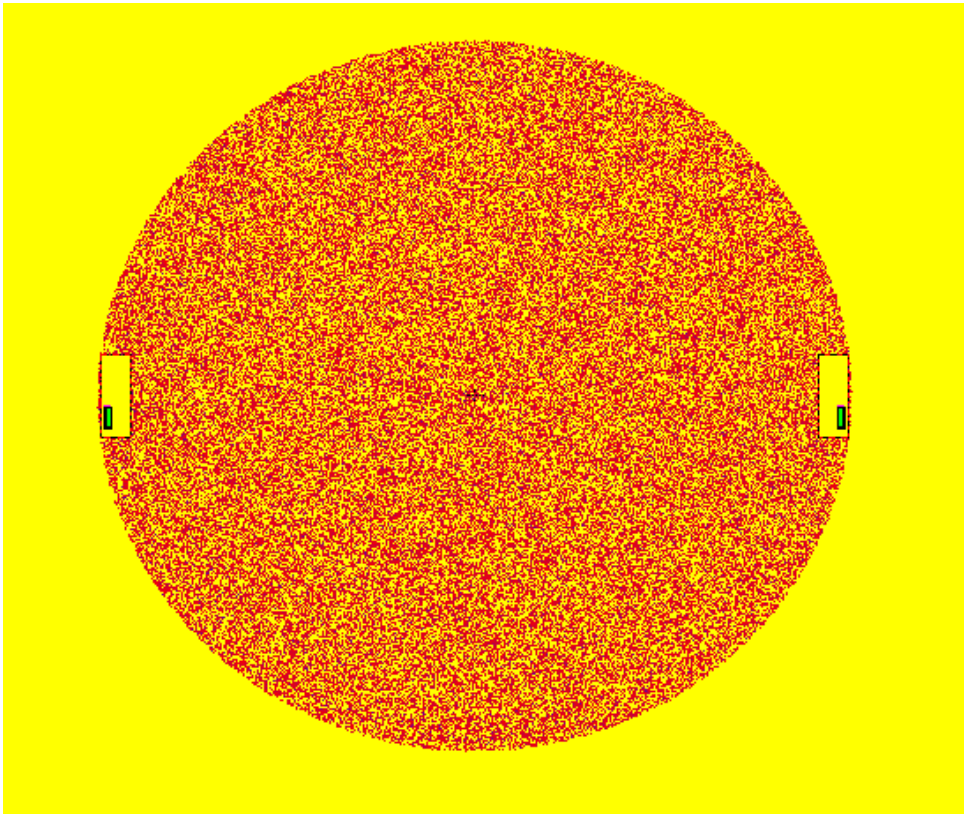

Fig. 28. Image of the source distribution for the MCNP simulation of the inner 2.79 m portion of the radiation source.

As seen in Table VI, the contribution of the inner portion of the source contained within the 2.79 m radius was disproportionate. This table uses the notation found in Eq. 5.1. Please note that in the first column, L stands for left, R stands for right, U stands for upper and L stands for lower. In the second column, the area ratio (AR) is the value of the A_{in}/A_{out} term from Eq. 5.1. The fifth column gives the uncertainty for the values of the fourth column. Given a uniform amount of activity per unit area in both regions, the area inside the 2.79 m radius was responsible for slightly over 37% of the total count rate. This demonstrated that simply keeping all precipitation, and thus the source of background radiation, out of this inner area could dramatically

reduce the effects of the precipitation.

Table VI. Contribution of inner 2.74 m radius vs. remainder of source in counts per particle started.

Detector	P_{in}	P_{in}* AR	P_{out}	P_{in}*AR* P_{out}^{-1}	Uncertainty	% Due to Inner
LU	5.304E-05	1.053E-06	3.140E-06	0.34	0.01	25.106%
LL	1.397E-04	2.772E-06	3.412E-06	0.81	0.02	44.824%
RU	5.327E-05	1.057E-06	3.268E-06	0.32	0.01	24.444%
RL	1.411E-04	2.800E-06	3.142E-06	0.89	0.02	47.125%
U Avg	5.315E-05	1.055E-06	3.204E-06	0.33	0.01	24.770%
L Avg	1.404E-04	2.786E-06	3.277E-06	0.85	0.02	45.951%
Avg	9.676E-05	1.920E-06	3.240E-06	0.59	0.01	37.212%
Uncert.	$<$0.7%	$<$2.3%	$<$2.3%			

C. Shielding Designs

Based on the results of this simulation, several designs for shielding were generated and simulated. The designs simulated were a steel dome enclosing the entire RPM, a concrete building enclosing the RPM and steel panels which would serve to further collimate the RPM. Each of the buildings represents a lower bound for the design's effectiveness. This is due to the fact that in reality, a single large building would be constructed to house all the RPMs at a given location in order to achieve cost savings. A single, large building would have superior shielding properties because it would exclude precipitation from an even larger area than the smaller building sim-

ulated would. Furthermore, such a building would almost certainly cost less per RPM housed due to the fact that the materials and labor used to construct it could be purchased and hired more efficiently in quantity. The steel dome and concrete building designs included a 4 m wide and 4.5 m tall penetration to permit vehicle access to the RPM, a size which is sufficient for any standard commercial vehicle in the United States [24].

The steel dome and concrete building designs were intended to attenuate the background radiation by both serving as shielding and by preventing precipitation from entering the aforementioned area. Conversely, the steel panels simply function as shielding.

1. Steel Panels

The steel panels consisted of a series of u-shaped steel panels designed to shield the sides and rear of the RPM without obstructing the inner face, as seen in Fig. 29. These were designed to maximize cost effectiveness, with a materials cost of only $700 to $1000 per set of panels, depending on how many were used. It was thought that these would have some effect, as a significant amount of background comes from the area outside the inner 2.74m. However, they were a complete failure, attenuating only 2% of the background if a set of three panels per detector unit was used. Although they were roughly as cost-effective as the steel dome, they were of no practical value.

Fig. 29. X-Y cross section of MCNP simulation of steel panel shields centered at (0,0,15).

2. Steel Dome

The steel dome shield consisted of a half-sphere of .3175 cm (.125 in., 11 ga.) thick steel surrounding the RPM and adjacent area, as seen in Fig. 30 and Fig. 31. It was modeled so that the radiation source due to the precipitation that would ordinarily fall on the building was distributed with a standard radial power law distribution on the surface of the building itself. To put it simply, the source was distributed as if a planar circle had been projected onto the surface of the spherical building. This likely served to underestimate the design's actual performance, as water would obviously tend not to collect on the building itself due to its shape. To simplify the modeling of the source distribution, two models were made for each case, one for the source on the shield and another for the remainder of the source, as seen in Fig. 32 and Fig. 33. Please note that the colors in the graphics correspond to the materials listed in

Table IV. An example of the source code for the 20 m diameter case can be found in Appendix Q and Appendix R.

The results were then were combined and scaled with Eq. 5.1. In reality, it would also be advisable to add additional shielding around the lower rim of the building, as this is where a large amount of water is likely to collect during precipitation. Additionally, the floor of the building should be designed so that rainwater tends to drain away from the RPM and out of the building.

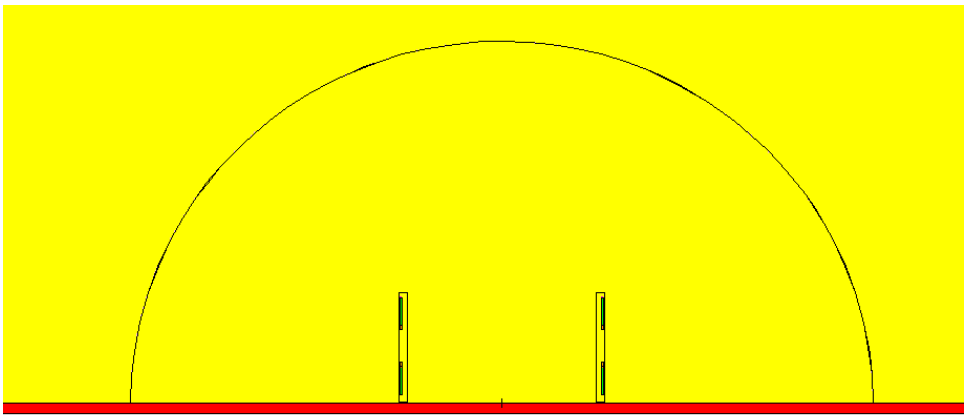

Fig. 30. X-Z cross section of 20 m diameter steel dome shield centered at (0,-15,0).

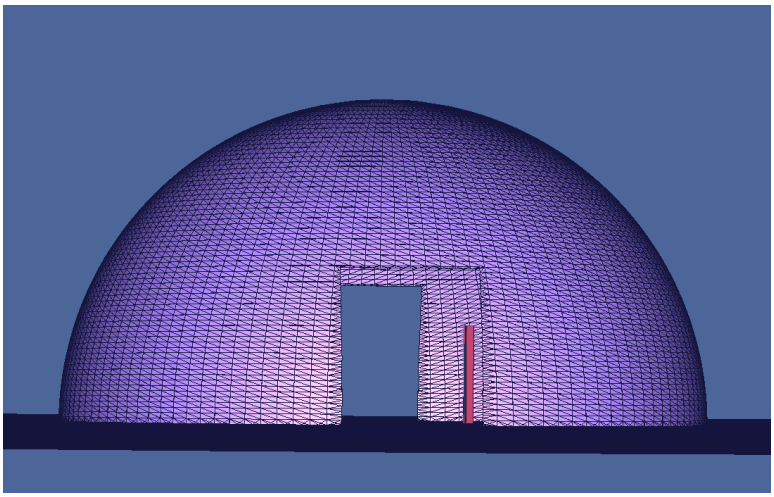

Fig. 31. Three-dimensional image of 20 m diameter steel dome shield with one side of the RPM visible inside.

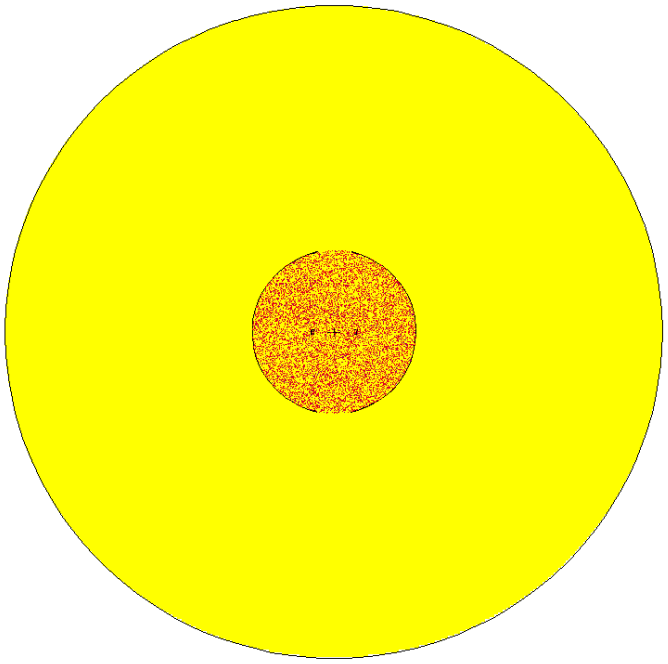

Fig. 32. X-Y cross section of simulation of inner radiation source distribution for 20m diameter steel dome shield centered at (0,0,2).

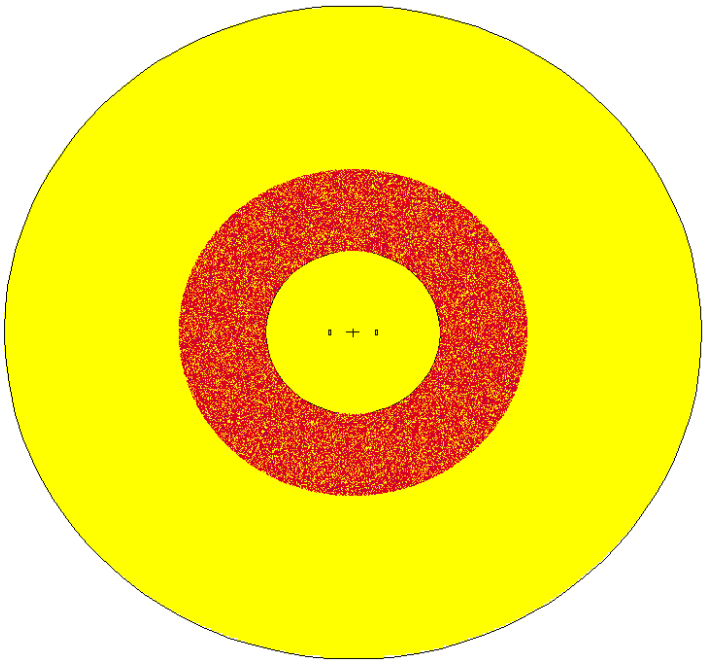

Fig. 33. X-Y cross section of simulation of outer radiation source distribution for 20m diameter steel dome shield centered at (0,0,2).

The steel dome design was able to reduce the background count rate due to precipitation up to 51% if made with a 20 m diameter. Unfortunately, this performance comes at a significant cost, as the sheet metal to construct this shield would have a materials cost of around $41,700 [25, 26], or only slightly less than the portal monitor itself [17]. The smaller domes were far more cost-effective, with a 14 m diameter dome producing just under 40% attenuation at a materials cost of only $20,000. As steel buildings are generally prefabricated, the cost of labor would be negligible. It is worth noting that the majority of this reduction came from the two lower detectors, particularly for the smaller diameter buildings.

The steel dome's prefabricated design makes it far easier to set up in parts of the world that lack skilled labor and infrastructure; the steel panels are physically small

enough that they could be prefabricated then shipped to any site in the world from a single manufacturer. This would assure uniform quality and uniform attenuation.

Table VII. Performance of spherical shields of various diameters at a materials cost of $66.52 per square meter of steel.

Shield Diameter [m]	Percent Attenuation	Uncertainty	Estimated Materials Cost	Dollars Per % Attenuation
20	50.7%	0.57%	$ 41,796	$ 825.20
18	47.6%	0.61%	$ 33,855	$ 711.73
16	43.3%	0.65%	$ 26,749	$ 618.24
14	39.8%	0.69%	$ 20,480	$ 514.66
12	34.5%	0.75%	$ 15,046	$ 435.64
10	28.3%	0.82%	$ 10,449	$ 368.85

Although certainly effective, the steel dome design was somewhat costly, and could be unsuitable for regions with strict building codes or extreme weather conditions. However, a concrete building can easily be designed to accommodate any inclement conditions that might be encountered.

3. Concrete Building

Three different designs for a square concrete building were simulated, one with walls 20 cm thick, one with walls 25 cm thick and one with walls 30 cm thick. All three were designed with an inner length and width of 10m, an inner height of 5m and a 10 cm thick roof, as seen in Fig. 34 and Fig. 35. The minimum wall thickness of 20 cm was chosen to correspond with the minimum thickness recommended in the Reinforced Concrete Designer's Handbook [27]. As with the steel dome, two models were made for each case, one for the source on the shield and another for the remain-

der of the source, as seen in Fig. 36 and Fig. 37. The results were then were scaled with Eq. 5.1. Please note that the colors in the graphics correspond to the materials listed in Table IV. An example of the source code for the 30 cm wall thickness case can be found in Appendix S and Appendix T.

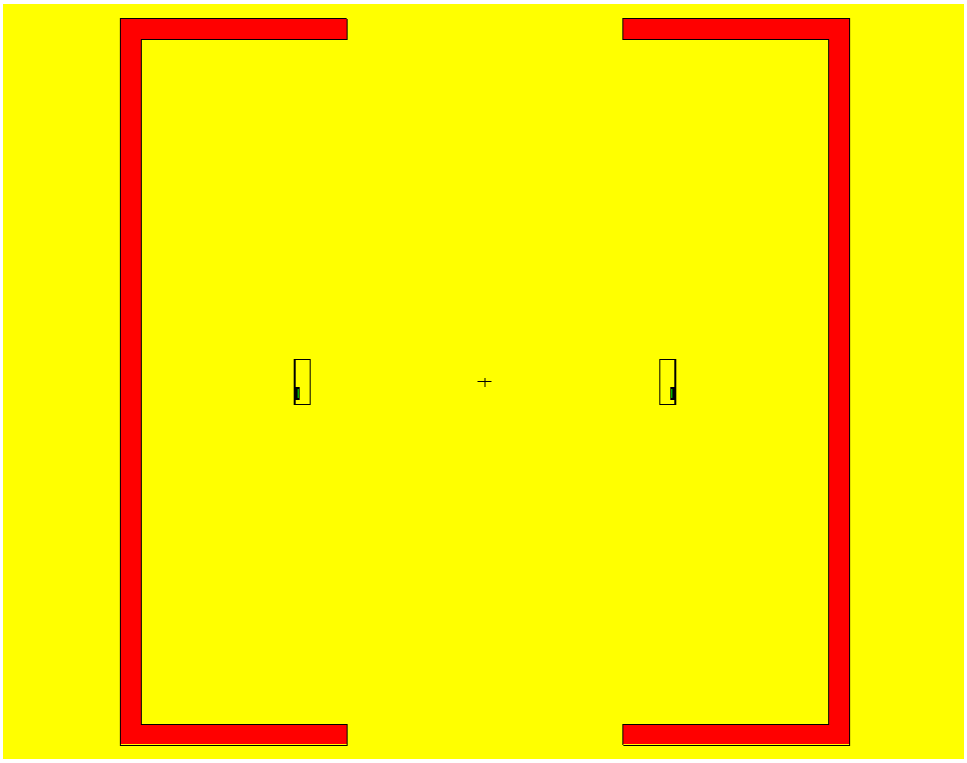

Fig. 34. X-Y cross section of concrete shield MCNP model with 30 cm thick walls, centered at (0,0,250)

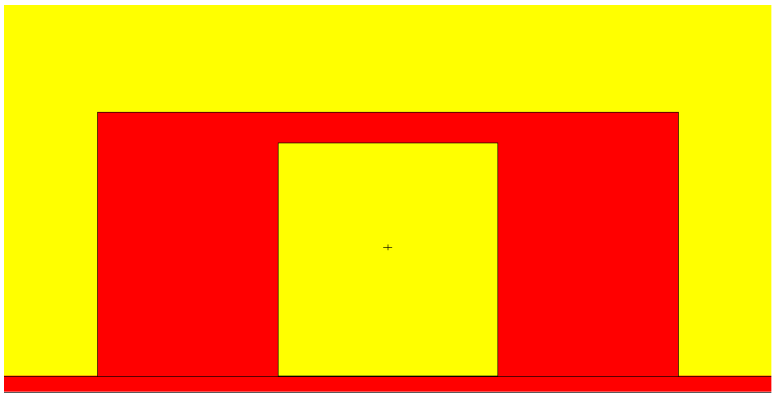

Fig. 35. X-Z cross section of concrete shield MCNP model with 30 cm thick walls, centered at (0,-515,250).

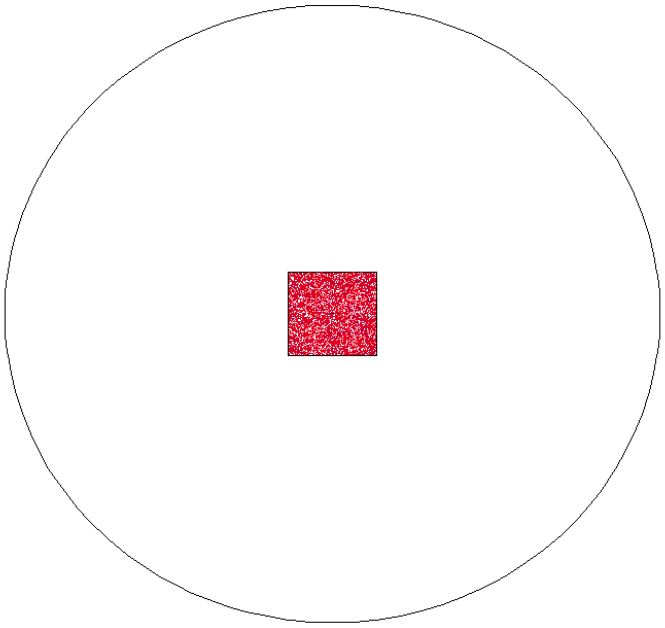

Fig. 36. X-Y cross section of simulation of inner radiation source distribution for the 30 cm wall thickness concrete shield centered at (0,0,505).

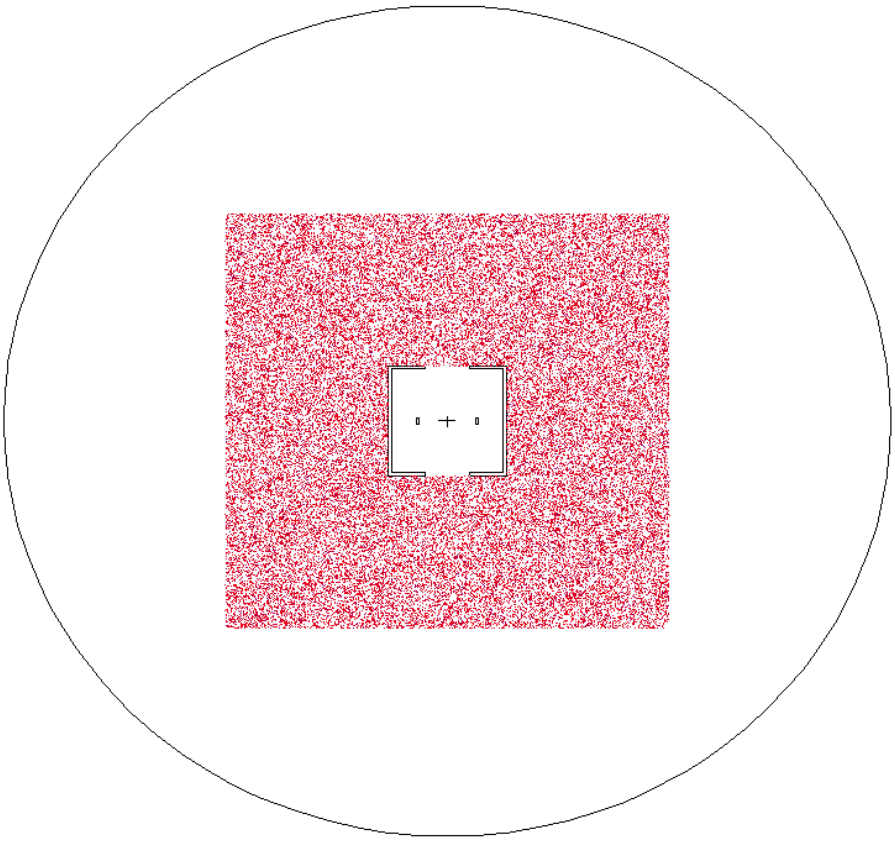

Fig. 37. X-Y cross section of simulation of outer radiation source distribution for the 30 cm wall thickness concrete shield centered at (0,0,2).

Again, it would also be advisable to add additional shielding around the lower rim of the building, as this is where a large amount of water is likely to collect during precipitation. Additionally, the floor of the building should be designed such that rainwater tends to drain away from the RPM and out of the building.

The concrete shields proved to be the most effective design from both a pure attenuation and cost effectiveness perspective. The 30 cm wall thickness model was able to attenuate 71.2% of the incoming background radiation, at an estimated materials cost of only $6,045. However, it must be noted that this is an unfair comparison

to the steel structures, as the majority of the cost of concrete construction is that of labor. The effectiveness of the 20 and 25 cm wall thickness designs can be seen in Table VIII.

The cost estimate for concrete was far more complex than that of steel, as concrete requires reinforcement, usually in the form of metal bars, forms to be poured into, and other components that increase its cost beyond the materials cost of the concrete itself. The formula used to estimate the price of the concrete is as follows:

$$P = V * (C + R) + 5A * F\, 1.0002269368\, e^{-1.5460100942\, t} \tag{5.2}$$

where

P is the total cost of the of the concrete and associated materials

V is the Volume of the concrete in cubic meters

C is the price of the concrete per cubic meter

R is the price of reinforcement per cubic meter

A is the surface are of one side of the building

F is the cost of the concrete forms per square meter

Table VIII. Performance of concrete shields of various wall thicknesses at a materials cost of $98.10 per cubic yard of concrete.

Wall Thickness [cm]	Percent Attenuation	Uncertainty	Estimated Materials Cost	Dollars Per % Attenuation
20	66.59%	0.85%	$ 4,747	$ 71.29
25	69.49%	0.89%	$ 5,390	$ 77.57
30	71.17%	0.92%	$ 6,045	$ 84.94

For this project, C was \$98.10 m^{-3}, R was \$10.00 m^{-3} and F was \$16.15 m^{-2} [28]. At \$98.10 per cubic meter, concrete is far less expensive than steel per unit volume or unit mass, the latter of which correlates directly with gamma ray attenuation. However, it does have some significant drawbacks as well. First and foremost, the cost of labor for construction with concrete is far greater, and the logistical issues are more severe. This is particularly true for small-scale construction, thus steel structures could be a better choice if shielding is only needed for one or two portal monitors. Additionally, construction is more time consuming, which can be a severe issue at a busy port. Also, the above cost assumes that a nearby supplier is available; if that is untrue, the concrete could end up being significantly more expensive. While it is unlikely that concrete would be difficult to obtain near any major port in the developed world, such a difficulty could potentially arise in some cases.

Secondly, the concrete can itself contribute significant amounts of background radiation, depending on what sort of rocks and aggregate were used to form it [29]. If the concrete available in the region is of a type that contains large amounts of radioactive materials, such a structure could actually increase the overall background count rate rather than attenuating it, or produce so little net attenuation that it is no longer cost effective. For this reason, the source of concrete must be analyzed prior to any construction for this purpose. Furthermore, the quality and density of concrete varies from region to region, meaning that a uniform amount of attenuation cannot be guaranteed for a structure of a given wall thickness.

Lastly, concrete is less dense than steel, and thus requires a greater thickness to achieve equal attenuation of gamma ray radiation. This can be a severe drawback where space is a serious concern.

CHAPTER VI

CONCLUSION

A. Inverse Model Capabilities

The inverse model algorithm was able to correctly identify 85.6% of the precipitation events recorded by the portal monitor testbed at Oak Ridge National Laboratory solely based on the behavior of the background count rate. Furthermore, actual precipitation events were detected over 20 times as often as false positives occurred, and false positives occurred once every 0.63 days on average. This proved that precipitation was correlated with almost all rapid background count rate increases. It also demonstrated that these increases are likely a serious issue both in terms of potential false alarms and loss of sensitivity due to increased alarm levels.

Additionally, the results from the inverse model demonstrated a clear statistical correlation between precipitation and increased background count rate at portal monitors worldwide, although the magnitude of this correlation was rather poorly characterized due to the quality of the data available.

B. Inverse Model Limitations

The inverse model algorithm was not capable of functioning as a means of mitigating the effects of precipitation on the radiation portal monitor. This is due to the fact that in order to detect the occurrence of a rain event, the algorithm must be fed background count rate data from the end of the event to at least 40 minutes after the event. By this time, whatever vehicles were passing through the portal monitor when the rain occurred would be long gone. Therefore, this algorithm was mainly used for understanding precipitation mitigation, but a dynamic algorithm would be needed if

one was actually to be used in practice.

The algorithm was designed specifically for precipitation events no longer than several hours in duration. This algorithm would therefore be inappropriate for use in extreme weather conditions such as monsoon rains, hurricanes, typhoons and the like. However, this decision was appropriate, as short rain events cause the greatest change in background count rate in the least amount of time and therefore are the most disruptive to a portal monitor's operation.

C. Forward Model Capabilities

The forward model was able to predict the increase in background count rate due to precipitation. It was able to attenuate the background count rate due to precipitation by an average of 45.9%, and attenuated the background count rate more than 10% below the median value only 0.9% of the time. When the algorithm did decrease the count rate below the median, it did so by an average of only 2.25%, an amount less than the average fluctuation of the baseline background count rate over the 9 or 10 day periods that the data was analyzed over. Furthermore, the forward model was never observed to generate a false positive. That is to say that no case where a significant amount of precipitation occurred but a background count rate increase did not occur was ever observed. The purchase of of a weather station to support this algorithm would cost approximately $3,500 per SLD site.

The forward model's prediction capabilities could be utilized to adjust the alarm level more intelligently. Raising the alarm level during precipitation and lowering it after the precipitation ends could prevent false alarms and false negatives respectively.

D. Forward Model Limitations

As expected, the behavior of very short rain events was extremely difficult to predict. This is due to the fact that the quantity of radionuclides deposited by a shorter event is almost totally depended on the initial concentration of radionuclides in the cloud, a figure that no commercially available meteorology apparatus is capable of measuring.

E. Shielding Designs

37.2% of the background count rate increase was found to be caused by the radon daughters deposited in a circle with a radius of 2.79 m encompassing the outer edges of the two RPM detector units. Preventing precipitation from entering the area between the two detector units of the radiation portal monitor proved to be a very effective method of reducing the resulting background count rate.

1. Steel Dome

The steel dome shield design was able to reduce the background count rate due to precipitation by up to 50.7%, at a materials cost of approximately $41,797 per RPM. Its design could easily be scaled from 10 to 20m in diameter to attenuate from 28.3% to 50.7% of the background count rate, with the cost effectiveness decreasing dramatically as the dome's size increased. Materials costs ranged from $368.85 to $825.20 per percent attenuation.

2. Concrete Building

The concrete building design was able to reduce the background count rate by up to 71.3% at a materials cost of $6,045 per RPM. Its wall thickness was scaled from

20 to 30 cm, resulting in the attenuation of 66.6% to 71.3% of the background count rate, with the cost effectiveness decreasing marginally as the wall thickness increased. Materials costs ranged from $71.29 to $84.94 per percent attenuation.

F. Recommendations

The construction of a concrete building is likely the most effective method of mitigating the effects of background count rate due to precipitation. Although the total cost of the concrete structure is likely at least double the actual materials cost, it is still far less expensive than the steel shield.

However, the use of concrete can have severe drawbacks. The most serious of these is the tendency of the concrete to contain large concentrations of radionuclides which can themselves cause the background count rate to increase. Also the density of concrete can vary between different batches and manufacturers, resulting in nonuniform gamma ray attenuation for a given thickness. As such, the quality and activity of the concrete must be carefully monitored before such construction is undertaken.

Overall, the construction of a concrete building is the best option for mitigation of these effects, with the steel dome as a standby option should concrete of adequate density or low enough activity be unavailable. The forward model, although useful as a predictive tool and inexpensive to implement, can only do so much to improve the performance of a device that does not discriminate based on energy and has essentially no energy resolution. Nothing except for shielding can reduce the inherent increase in uncertainty caused by an increased background count rate. However, such an algorithm could prove very useful for improving the performance of a spectroscopic portal monitor. This is due to the fact that it can easily be modified to estimate the type and quantity of radionuclides transported to the surface during precipitation, and

thus the exact spectrum of the resulting background activity. This could dramatically improve the performance of such a device.

G. Future Work

In the future, the inverse model should be tested against higher quality data from other SLD sites to determine whether its applicability is universal, or if changes in its coefficients must be made at each site.

The forward model could be improved by the gathering of additional data, less than three months of information is too little to generate a strong correlation for a phenomenon controlled by as many variables as the absorption of radon daughters by atmospheric moisture is. Additionally, the exact amount by which the RPM's sensitivity can be raised or lowered in response to precipitation should be calculated. This figure obviously will necessitate a tradeoff between sensitivity and false alarms and will likely depend on local conditions.

Lastly, the shielding structures proposed should be constructed and tested to determine their effectiveness at mitigating the background count rate increases due to precipitation.

REFERENCES

[1] T. J. Colin, Nuclear proliferation and terrorism, CQ Researcher 14 (12) (2004) 297–320.

[2] IAEA, IAEA illicit tracking database (ITDB), Available From <http://www.iaea.org/NewsCenter/Features/RadSources/PDF/itdb_31122004.pdf> (November 2010).

[3] International Atomic Energy Agency, IAEA Safeguards Glossary, International Atomic Energy Agency, 2002, Available From <http://www-pub.iaea.org/books/IAEABooks/6570/IAEA-Safeguards-Glossary-2001-Edition>.

[4] Graeme Hosken, Attack at Pelindaba Nuclear Facility, Pretoria News, Pretoria, Gauteng, South Africa, November 9, 2007, Available From http://www.iol.co.za/news/south-africa/attack-at-pelindaba-nuclear-facility-1.378127.

[5] Micah Zenko, A Nuclear Site Is Breached, Washington Post, Washington, DC, December 20, 2007, Available From http://www.washingtonpost.com/wp-dyn/content/article/2007/12/19/AR2007121901857.html.

[6] Testimony on "NNSA's megaports initiative and its role in the secure freight initiative (SFI)" before the senate commerce, science, and transportation subcommittee, Available From <http://nnsa.energy.gov/mediaroom/congressionaltestimony/06.12.08> (June 2008).

[7] M. Takeyasu, T. Iida, T. Tsujimoto, K. Yamasaki, Y. Ogawa, Concentrations and their ratio of ^{222}Rn decay products in rainwater measured by gamma-ray spectrometry using a low background Ge detector, Journal of Environmental Radioactivity 88 (2006) 74–89.

[8] Cothern, Smith, Environmental Radon, Plenum Press, New York, New York, 1987.

[9] J. Mercier, B. Tracy, R. d'Amours, F. Changon, I. Hoffman, E. Korpach, S. Johnson, R. Ungar, Inceased environmental gamma-ray dose rate during precipitation: a strong correlation with contributing air mass, Journal of Environmental Radioactivity 100 (2009) 527–533.

[10] R. M. Keyser, T. R. Twomey, False positive probability as a function of background for short data collection times in a germanium detector portal monitor, in: INMM 50th Annual Meeting, Institute of Nuclear Materials Managment, Tuscon, Arizona, 2009.

[11] D. Stromswold, E. Siciliano, J. Schweppe, J. Ely, B. Milbrath, R. Kouzes, B. Geelhood, Nuclear Instruments and Methods in Physics Research Section A: Accelerators, Spectrometers Detector and Associated Equipment 550 (3) (2005) 647–674.

[12] J. Ely, R. Kouzes, B. D. Geelhood, J. Schweppe, R. Warner, Discrimination of naturally occurring radioactive material in plastic scintillator material, IEEE Transactions on Nuclear Science 54 (4) (2004) 1672–1676.

[13] NOAA, NNDC climate data online, Available From <http://cdo.ncdc.noaa.gov/cdo/3505doc.txt> (November 2010).

[14] Portal Monitor Fundamentals, Oak Ridge National Laboratory, Oak Ridge, Tennessee, 2010.

[15] G. F. Knoll, Radiation Detection and Measurement, Third Edition, John Wiley and Sons, Inc., New York, New York, 2000.

[16] Nucsafe, Selecting gamma detector, Available From <http://www.nucsafe.com/cms/Selecting+Gamma+Detector/43.html> (January 2011).

[17] T. Cochran, R. C. Byrd, J. Lewis, D. R. Obey, Combating nuclear smuggling: DHS's cost-benefit analysis to support the purchase of new radiation detection portal monitors was not based on available performance data and did not fully evaluate all the monitors' costs and benefits, Tech. rep., Available From <www.gao.gov/new.items/d07133r.pdf> (2006).

[18] G. Cortès, J. Sempau, X. Ortega, Automated measurement of radon daughters Bi-214 and Pb-214, Nukleonika 46 (4) (2001) 161–164.

[19] Shultis, Faw, Radiation Shielding, American Nuclear Society, La Grange Park, Illinois, 2000.

[20] National Institute of Standards and Technology, Air, dry (near sea level), Available From <http://physics.nist.gov/PhysRefData/XrayMassCoef/ComTab/air.html> (May 2011).

[21] A. A. Solodov, C. M. Ryan, MCNP deck, Texas A&M University, College Station, Texas.

[22] K. Fujitaka, M. Matsumoto, K. Kaiho, S. Abe, Effect of rain interval on wet deposition of radon daughters, Radiation Protection Dosimetry 45 (1) (1992) 333–336.

[23] Ambient Weather, Columbia weather systems 9510-B-1 / 9511B1 orion weather station with WeatherMaster software, Available From <http://www.ambientweather.com/coco9510b1.html> (2011).

[24] U.S. Department of Transportation, Commercial vehicle size and weight program, Available From <ops.whwa.dot.gov/freight/sw/overview/index.htm> (2011).

[25] Metals depot, Available From <www.metalsdepot.com/products/hrsteel2.phtml?page=sheet\&LimAcc=\protect\T1\textdollarLimAcc> (2011).

[26] Discount Steel Buildings, Steel building specials, Available From <www.discountsteelbuildings.com/building_specials.htm> (2011).

[27] C. E. Reynolds, J. C. Stedman, Reinforced Concrete Designer's Handbook, Taylor and Francis, Abingdon, Oxfordshire, UK, 1988.

[28] Concrete Network, Concrete price considerations-cost of concrete, Available From <http://www.concretenetwork.com/concrete-prices.html> (2008).

[29] C. M. Ryan, Determining the impact of concrete roadways on gamma ray background readings for radiation portal monitor systems, Master's thesis, Texas A&M University, College Station, Texas (2011).

APPENDIX A

SLD PORTAL MONITOR SITES AND SITE IDS

countryName	countryId	siteName	siteId	CountOflaneNumber
Azerbaijan	250	Shirvanovka	38	4
Azerbaijan	250	Samur	40	2
Azerbaijan	250	Balakan	42	2
Azerbaijan	250	Sadikhli	43	4
Azerbaijan	250	Baku Seaport	56	2
Azerbaijan	250	Turkan Trainin	57	2
Azerbaijan	250	Xanoba	58	3
Azerbaijan	250	Julfa	69	6
Bahamas	19	Freeport	2	9
Belgium	24	Bear	15	26
Belgium	24	Beal	28	14
Belgium	24	Zeebrugge	60	10
Colombia	255	Port of Cartage	55	6
Dominican Rep	251	Caucedo	44	5
Estonia	253	Koidula	48	1
Estonia	253	Narva	49	1
Georgia	82	Batumi Sea Po	20	6
Georgia	82	Lilo Training C	21	2
Georgia	82	Poti Sea Port	22	11
Georgia	82	Red Bridge	23	5
Georgia	82	Sadakhlo	30	6
Georgia	82	Vakhtangisi	41	4
Georgia	82	Gardabani	46	4
Georgia	82	Tbilisi Airport	66	27
Greece	86	Evzoni VC-Site	4	12
Greece	86	Kakavia	5	9
Greece	86	Athens AP	6	7
Greece	86	Piraeus Cargo	7	5
Greece	86	Piraeus Passe	8	6
Greece	86	Promahonas	9	11
Honduras	99	Cortez	16	3
Israel	109	Haifa	31	1
Jamaica	258	PortOfKingston	63	2
Kyrgyzstan	121	Ak-Tilek	24	3
Mexico	257	PortOfVeracruz	62	4
Mongolia	260	Zamiin Uud VC	67	9
Mongolia	260	Chinggis Khaa	68	13
Netherlands	157	Rotterdam	10	5
Oman	248	Salalah	37	1
ORNL	259	ORNL	65	1
Panama	256	Balboa	59	3
Panama	256	Manzanillo	61	1
Philippines	176	MICT	17	10
Philippines	176	South Harbor	19	9
Portugal	261	PortOfLisbon	70	7
Singapore	199	Singapore	11	2

countryName	countryId	siteName	siteId	CountOflaneNumber
Slovakia	254	Cierna Nad Tis	50	2
Slovakia	254	Matovce	51	1
Slovakia	254	Ubla	52	3
Slovakia	254	Velke Slemenc	53	1
Slovakia	254	Vysne-Nemeck	54	6
Slovakia	254	MDS	64	4
Slovenia	201	PortofKoper	25	7
Slovenia	201	Obrezje VC	26	14
South Korea	252	Busan Gamma	47	4
Spain	206	Algeciras	12	9
Sri Lanka	1	Colombo	1	18
Thailand	218	Laem Chabang	13	20
United Kingdo	232	Southampton	29	3

APPENDIX B

NOAA SURFACE HOURLY DATA ABBREVIATED FORMAT

04/11/2005

SURFACE HOURLY ABBREVIATED FORMAT

ONE HEADER RECORD FOLLOWED BY DATA RECORDS:

COLUMN	DATA DESCRIPTION
01-06	USAF = AIR FORCE CATALOG STATION NUMBER\\
08-12	WBAN = NCDC WBAN NUMBER\\
14-25	YR--MODAHRMN = YEAR-MONTH-DAY-HOUR-MINUTE IN GREENWICH MEAN TIME (GMT)\\
27-29	DIR = WIND DIRECTION IN COMPASS DEGREES, 990 = VARIABLE, REPORTED AS\\ '***' WHEN AIR IS CALM (SPD WILL THEN BE 000)\\
31-37	SPD \& GUS = WIND SPEED \& GUST IN MILES PER HOUR \\
39-41	CLG = CLOUD CEILING--LOWEST OPAQUE LAYER\\ WITH 5/8 OR GREATER COVERAGE, IN HUNDREDS OF FEET,\\ 722 = UNLIMITED \\
43-45	SKC = SKY COVER -- CLR-CLEAR, SCT-SCATTERED-1/8 TO 4/8,\\ BKN-BROKEN-5/8 TO 7/8, OVC-OVERCAST, \\ OBS-OBSCURED, POB-PARTIAL OBSCURATION \\
47-47	L = LOW CLOUD TYPE, SEE BELOW\\
49-49	M = MIDDLE CLOUD TYPE, SEE BELOW\\
51-51	H = HIGH CLOUD TYPE, SEE BELOW \\
53-56	VSB = VISIBILITY IN STATUTE MILES TO NEAREST TENTH \\ NOTE: FOR SOME STATIONS, VISIBILITY IS REPORTED ONLY UP TO A\\ MAXIMUM OF 7 OR 10 MILES IN METAR OBSERVATIONS, BUT TO HIGHER\\ VALUES IN SYNOPTIC OBSERVATIONS, WHICH CAUSES THE VALUES TO \\ FLUCTUATE FROM ONE DATA RECORD TO THE NEXT. ALSO, VALUES\\ ORIGINALLY REPORTED AS '10' MAY APPEAR AS '10.1' DUE TO DATA\\ BEING ARCHIVED IN METRIC UNITS AND CONVERTED BACK TO ENGLISH.\\
58-65	WW WW WW = PRESENT WEATHER--LISTED BELOW\\
67-67	W = PAST WEATHER INDICATOR, SEE BELOW\\
69-77	TEMP \& DEWP = TEMPERATURE \& DEW POINT IN FAHRENHEIT \\
79-84	SLP = SEA LEVEL PRESSURE IN MILLIBARS TO NEAREST TENTH \\
86-90	ALT = ALTIMETER SETTING IN INCHES TO NEAREST HUNDREDTH \\
92-97	STP = STATION PRESSURE IN MILLIBARS TO NEAREST TENTH\\
99-101	MAX = MAXIMUM TEMPERATURE IN FAHRENHEIT (TIME PERIOD VARIES)\\
103-105	MIN = MINIMUM TEMPERATURE IN FAHRENHEIT (TIME PERIOD VARIES)\\
107-111	PCP01 = 1-HOUR LIQUID PRECIP REPORT IN INCHES AND HUNDREDTHS --\\ THAT IS, THE PRECIP FOR THE PRECEDING 1 HOUR PERIOD\\
113-117	PCP06 = 6-HOUR LIQUID PRECIP REPORT IN INCHES AND HUNDREDTHS --\\ THAT IS, THE PRECIP FOR THE PRECEDING 6 HOUR PERIOD\\
119-123	PCP24 = 24-HOUR LIQUID PRECIP REPORT IN INCHES AND HUNDREDTHS\\ THAT IS, THE PRECIP FOR THE PRECEDING 24 HOUR PERIOD\\
125-129	PCPXX = LIQUID PRECIP REPORT IN INCHES AND HUNDREDTHS, FOR \\ A PERIOD OTHER THAN 1, 6, OR 24 HOURS (USUALLY FOR 12 HOUR PERIOD\\ FOR STATIONS OUTSIDE THE U.S., AND FOR 3 HOUR PERIOD FOR THE U.S.)\\ T = TRACE FOR ANY PRECIP FIELD\\
131-132	SD = SNOW DEPTH IN INCHES \\

NOTES: \\

- *'s IN FIELD INDICATES ELEMENT NOT REPORTED.\\

- SOME VALUES WERE CONVERTED FROM METRIC TO ENGLISH UNITS. THIS WILL\\
OCCASIONALLY RESULT IN MINOR DIFFERENCES VS ORIGINAL DATA DUE TO ROUNDING.\\

- COLUMN POSITION REFERS TO ASCII TEXT DATA. \\

- THIS FORMAT CAN BE EASILY IMPORTED INTO A SPREADSHEET OR A DATABASE\\
MANAGEMENT SYSTEM SINCE FIELDS ARE SPACE-DELIMITED.\\

- THIS FORMAT DOES NOT INCLUDE QUALITY CONTROL FLAGS, WHICH ARE AVAILABLE\\
IN THE ADVANCED FORMAT THROUGH THE CLIMATE DATA ONLINE SYSTEM.\\

PRESENT WEATHER CODE TABLE

The code that denotes a specific type of weather observed.\\
----------\\
00-49 No precipitation at the station at the time of observation\\
----------\\
00-19 No precipitation, fog, ice fog (except for 11 and 12),\\
duststorm, sandstorm, drifting or blowing snow at the station at the\\
time of observation or, except for 09 and 17, during the preceding\\
hour\\
----------\\
00: Cloud development not observed or not observable\\
01: Clouds generally dissolving or becoming less developed\\
02: State of sky on the whole unchanged\\
03: Clouds generally forming or developing\\
04: Visibility reduced by smoke, e.g. veldt or forest fires,\\
industrial smoke or volcanic ashes\\
05: Haze\\
06: Widespread dust in suspension in the air, not raised by wind at\\
or near the station at the time of observation\\
07: Dust or sand raised by wind at or near the station at the time of\\
observation, but no well-developed dust whirl(s) or sand whirl(s),\\
and no duststorm or sandstorm seen or, in the case \\
of ships, blowing spray at the station\\
08: Well developed dust whirl(s) or sand whirl(s) seen at or near the\\
station during the preceding hour or at the time of observation, but\\
no duststorm or sandstorm\\
09: Duststorm or sandstorm within sight at the time of observation,\\
or at the station during the preceding hour\\
10: Mist\\
11: Patches of shallow fog or ice fog at the station, whether on land\\
or sea, not deeper than about 2 meters on land or 10 meters at sea\\
12: More or less continuous shallow fog or ice fog at the station,\\
whether on land or sea, not deeper than about 2 meters on land or 10\\
meters at sea \\
13: Lightning visible, no thunder heard\\
14: Precipitation within sight, not reaching the ground or the\\
surface of the sea\\
15: Precipitation within sight, reaching the ground or the surface of\\
the sea, but distant, i.e., estimated to be more than 5 km from the\\
station\\
16: Precipitation within sight, reaching the ground or the surface of\\
the sea, near to, but not at the station\\
17: Thunderstorm, but no precipitation at the time of observation\\
18: Squalls at or within sight of the station during the preceding\\
hour or at the time of observation\\
19: Funnel cloud(s) (Tornado cloud or waterspout) at or within sight\\
of the station during the preceding hour or at the time of\\
observation

```
20-29  Precipitation, fog, ice fog or thunderstorm at the station
during the preceding hour, but not at the time of observation
---------------------------------------------------------------
20: Drizzle (not freezing) or snow grains not falling as shower(s)
21: Rain (not freezing) not falling as shower(s)
22: Snow not falling as shower(s)
23: Rain and snow or ice pellets not falling as shower(s)
24: Freezing drizzle or freezing rain not falling as shower(s)
25: Shower(s) of rain
26: Shower(s) of snow or of rain and snow
27: Shower(s) of hail (Hail, small hail, snow pellets), or rain and
hail
28: Fog or ice fog
29: Thunderstorm (with or without precipitation)
---------------------------------------------------------------
30-39  Duststorm, sandstorm, or blowing snow
---------------------------------------------------------------
30: Slight or moderate duststorm or sandstorm has decreased during
the preceding hour
31: Slight or moderate duststorm or sandstorm no appreciable change
during the preceding hour
32: Slight or moderate duststorm or sandstorm has begun or has
increased during the preceding hour
33: Severe duststorm or sandstorm has decreased during the preceding
hour
34: Severe duststorm or sandstorm no appreciable change during the
preceding hour
35: Severe duststorm or sandstorm has begun or has increased during
the preceding hour
36: Slight or moderate drifting snow generally low (below eye level)
37: Heavy drifting snow generally low (below eye level)
38: Slight or moderate blowing snow generally high (above eye level)
39: Heavy blowing snow generally high (above eye level)
---------------------------------------------------------------
40-49  Fog or ice fog at the time of observation
---------------------------------------------------------------
40: Fog or ice fog at a distance at the time of observation, but not
at the station during the preceding hour, the fog or ice fog
extending to a level above that of the observer
41: Fog or ice fog in patches
42: Fog or ice fog, sky visible, has become thinner during the
preceding hour
43: Fog or ice fog, sky invisible, has become thinner during the
preceding hour
44: Fog or ice fog, sky visible, no appreciable change during the
preceding hour
45: Fog or ice fog, sky invisible, no appreciable change during the
preceding hour
46: Fog or ice fog, sky invisible, has begun or has become thicker
during the preceding hour
47: Fog or ice fog, sky invisible, has begun or has become thicker
during the preceding hour
48: Fog, depositing rime, sky visible
49: Fog, depositing rime, sky invisible
---------------------------------------------------------------
50-99  Precipitation at the station at the time of observation
---------------------------------------------------------------
50-59  Drizzle
---------------------------------------------------------------
50: Drizzle, not freezing, intermittent, slight at time of
observation
51: Drizzle, not freezing, continuous, slight at time of observation
52: Drizzle, not freezing, intermittent, moderate at time of
observation
```

```
53: Drizzle, not freezing, continuous, moderate at time of
observation
54: Drizzle, not freezing, intermittent, heavy (dense) at time of
observation
55: Drizzle, not freezing, continuous, heavy (dense) at time of
observation
56: Drizzle, freezing, slight
57: Drizzle, freezing, moderate or heavy (dense)
58: Drizzle and rain, slight
59: Drizzle and rain, moderate or heavy
---------------------------------------------------------------
60-69  Rain
---------------------------------------------------------------
60: Rain, not freezing, intermittent, slight at time of observation
61: Rain, not freezing, continuous, slight at time of observation
62: Rain, not freezing, intermittent, moderate at time of observation
63: Rain, not freezing, continuous, moderate at time of observation
64: Rain, not freezing, intermittent, heavy at time of observation
65: Rain, not freezing, continuous, heavy at time of observation
66: Rain, freezing, slight
67: Rain, freezing, moderate or heavy
68: Rain or drizzle and snow, slight
69: Rain or drizzle and snow, moderate or heavy
---------------------------------------------------------------
70-79  Solid precipitation not in showers
---------------------------------------------------------------
70: Intermittent fall of snowflakes, slight at time of observation
71: Continuous fall of snowflakes, slight at time of observation
72: Intermittent fall of snowflakes, moderate at time of observation
73: Continuous fall of snowflakes, moderate at time of observation
74: Intermittent fall of snowflakes, heavy at time of observation
75: Continuous fall of snowflakes, heavy at time of observation
76: Diamond dust (with or without fog)
77: Snow grains (with or without fog)
78: Isolated star-like snow crystals (with or without fog)
79: Ice pellets
---------------------------------------------------------------
80-99  Showery precipitation, or precipitation with current or recent
thunderstorm
---------------------------------------------------------------
80: Rain shower(s), slight
81: Rain shower(s), moderate or heavy
82: Rain shower(s), violent
83: Shower(s) of rain and snow mixed, slight
84: Shower(s) of rain and snow mixed, moderate or heavy
85: Show shower(s), slight
86: Snow shower(s), moderate or heavy
87: Shower(s) of snow pellets or small hail, with or without rain or
rain and snow mixed, slight
88: Shower(s) of snow pellets or small hail, with or without rain or
rain and snow mixed, moderate or heavy
89: Shower(s) of hail (hail, small hail, snow pellets) , with or
without rain or rain and snow mixed, not associated with thunder,
slight
90: Shower(s) of hail (hail, small hail, snow pellets), with or
without rain or rain and snow mixed, not associated with thunder,
moderate or heavy
91: Slight rain at time of observation, thunderstorm during the
preceding hour but not at time of observation
92: Moderate or heavy rain at time of observation, thunderstorm
during the preceding hour but not at time of observation
93: Slight snow, or rain and snow mixed or hail (Hail, small hail,
snow pellets), at time of observation, thunderstorm during the
preceding hour but not at time of observation
```

94: Moderate or heavy snow, or rain and snow mixed or hail(Hail, small hail, snow pellets) at time of observation, thunderstorm during the preceding hour but not at time of observation
95: Thunderstorm, slight or moderate, without hail (Hail, small hail, snow pellets), but with rain and/or snow at time of observation, thunderstorm at time of observation
96: Thunderstorm, slight or moderate, with hail (hail, small hail, snow pellets) at time of observation, thunderstorm at time of observation
97: Thunderstorm, heavy, without hail (Hail, small hail, snow pellets), but with rain and/or snow at time of observation, thunderstorm at time of observation
98: Thunderstorm combined with duststorm or sandstorm at time of observation, thunderstorm at time of observation
99: Thunderstorm, heavy, with hail (Hail, small hail, snow pellets) at time of observation, thunderstorm at time of observation

PAST WEATHER CODE TABLE

The code that denotes a specific type of past weather observed.
0: Cloud covering 1/2 or less of the sky throughout the appropriate period
1: Cloud covering more than 1/2 of the sky during part of the appropriate period and covering 1/2 or less during part of the period
2: Cloud covering more than 1/2 of the sky throughout the appropriate period
3: Sandstorm, duststorm or blowing snow
4: Fog or ice fog or thick haze
5: Drizzle
6: Rain
7: Snow, or rain and snow mixed
8: Shower(s)
9: Thunderstorm(s) with or without precipitation

LOW CLOUD TYPE

0: No low clouds
1: Cumulus humulis or Cumulus fractus other than of bad weather or both
2: Cumulus mediocris or congestus, with or without Cumulus of species fractus or humulis or Stratocumulus all having bases at the same level
3: Cumulonimbus calvus, with or without Cumulus, Stratocumulus or Stratus
4: Stratocumulus cumulogenitus
5: Stratocumulus other than Stratocumulus cumulogenitus
6: Stratus nebulosus or Stratus fractus other than of bad weather, or both
7: Stratus fractus or Cumulus fractus of bad weather, or both (pannus) usually below Altostratus or Nimbostratus
8: Cumulus and Stratocumulus other than Stratocumulus cumulogenitus, with bases at different levels
9: Cumulonimbus capillatus (often with an anvil), with or without Cumulonimbus calvus, Cumulus, Stratocumulus, Stratus or pannus

MIDDLE CLOUD TYPE

0: No middle clouds
1: Altostratus translucidus
2: Altostratus opacus or Nimbostratus
3: Altocumulus translucidus at a single level

4: Patches (often lenticular) of Altocumulus translucidus,
continually changing and occurring at one or more levels
5: Altocumulus translucidus in bands, or one or more layers of
Altocumulus translucidus or opacus, progressively invading the sky;
these Altocumulus clouds generally thicken as a whole
6: Altocumulus cumulogentis (or cumulonimbogentus)
7: Altocumulus translucidus or opacus in two or more layers, or
Altocumulus opacus in a single layer, not progressively invading the
sky, or Altocumulus with Altostratus or Nimbostratus
8: Altocumulus castellanus or floccus
9: Altocumulus of a chaotic sky; generally at several levels

HIGH CLOUD TYPE

0: No High Clouds
1: Cirrus fibratus, sometimes uncinus, not progressively invading
the sky
2: Cirrus spissatus, in patches or entangled sheaves, which usually
do not increase and sometimes seem to be the remains of the upper
part of a Cumulonimbus; or Cirrus castellanus or floccus
3: Cirrus spissatus cumulonimbogenitus
4: Cirrus unicinus or fibratus, or both, progressively invading the
sky; they generally thicken as a whole
5: Cirrus (often in bands) and Cirrostratus, or Cirrostratus alone,
progressively invading the sky; they generally thicken as a whole,
but the continuous veil does not reach 45 degrees above the horizon
6: Cirrus (often in bands) and Cirrostratus, or Cirrostratus alone,
progressively invading the sky; they generally thicken as a whole;
the continuous veil extends more than 45 degrees above the horizon,
without the sky being totally covered
7: Cirrostratus covering the whole sky
8: Cirrostratus not progressively invading the sky and not entirely
covering it
9: Cirrocumulus alone, or Cirrocumulus predominant among the High
clouds

APPENDIX C

PERL SCRIPT DESIGNED TO RENAME WEATHER DATA FILES IN A MACHINE-SORTABLE FORMAT

```
# this script reads weather data files and creates copies with a machine-sortable file name in
# the specified destination folder. It accounts for all of the whimsical, inconsistent formats
# used to specify the date and time by the apparently computer-illiterate creator of this data



use File::Copy;

# This script can be easily modified to run from the command line.
# I leave that as an exercise to the end user.

#Input and output directories
$input_dir="/Users/Steve/Documents/ORNL Stuff/Steves Stuff/Archive_Weather";
$search_wildcard="^._";
$output_dir="/Users/Steve/Documents/workspace/Final Draft/Fixed_Weather";

#Log file name
$log_file ="copylog.txt";

@all_files = directory_search($input_dir,$search_wildcard);
$output_directory = $output_dir;
$log_output_path = ">".$output_directory."\/".$log_file;

printf "Outputing Log File to: \n";
printf "\n%s\n%s\n\n",$log_output_path;

#Create Logfile
open(COPYLOG,$log_output_path) or die "can't open output file: $!";


# open each daily file_____________________________________________________________
print "Processing Data Files...\n\n";
foreach $input_file (@all_files)
{

  @input_file_name_parts = $input_file;
  # open the file
  $input_path = "<".$input_dir."\/".$input_file;
  printf "$input_path\n";

  #convert space to underscore if necessary
  $original_input_file=$input_file;
  $input_file=~s/ /_/g;

  # Break filename up into array
  @inarr=split(/_/,$input_file);
  $inmonth=@inarr[0];
  $inday=@inarr[1];
  $inyear=@inarr[2];
  $inhour=@inarr[3];
  $inminute=@inarr[4];
```

```
  $inampm=@inarr[5];

  #Year and minutes need no adjustment
  $outyear=$inyear;
  $outminute=$inminute;

  #Convert to 24 hour time, Add 12 hours if time is PM
  if (($inampm=~/AM/) && ($inhour==12)){
   $twentyfour=0;
  }elsif (($inampm=~/PM/) && ($inhour<12)) {
   $twentyfour=$inhour+12;
  }else{
   $twentyfour=$inhour;
  }

  #Add leading zeros for numbers less than 10
  if ($inmonth < 10) {
   $outmonth="0".$inmonth;
  }else{
   $outmonth=$inmonth;
  }

  if ($inday < 10) {
   $outday="0".$inday;
  }else{
   $outday=$inday;
  }

  if ($twentyfour < 10) {
   $outhour="0".$twentyfour;
  } else {
   $outhour=$twentyfour;
  }

  #Create machine sortable output from components
$output_file = $outyear."_".$outmonth."_".$outday."_".$outhour."_".$outminute;
$output_path = "<".$output_dir."\/".$output_file;

#Actually copy the original file to a file with the desired, machine-sortable name
$source_filename=$input_dir."\/".$original_input_file;
$destination_filename=$output_dir."\/".$output_file;

#output input and output filenames to log file
print COPYLOG $source_filename."\n";
print COPYLOG $destination_filename."\n";

copy($source_filename,$destination_filename) or die "Copy failed: $!";


printf "saved as\n";
printf "$output_path\n\n";




} # END <<<< foreach $input_file (@all_files) >>>>

close(OUTPUT);


#------------------------------------------------------------------------

sub directory_search()
{
```

```
  #function arguments
  my($directory_name)=@_[0];
  my($wild_card)=@_[1];

  my($i);
  my($x_file);
  my(@all_files);
  my(@selected_files);

  opendir(THISDIR,$directory_name) or die "directory not found";
  @all_files = readdir THISDIR;
  closedir THISDIR;

  $i = 0;
  foreach $x_file (@all_files)
  {

    if ($x_file =~ $wild_card)
    {
      $selected_files[$i] = $x_file;
      $i+=1;
    }
  }

  if ($i==0)
  {
    printf "(directory search) ...no file meets the search criteria\n"
  }

  return @selected_files;
}

sub clean_queue()
{
  # this is a hack, but it works ....
  my(@queue) = @_;

  @queue=0;shift(@queue);

  return @queue;
}
```

APPENDIX D

PERL SCRIPT DESIGNED TO CONVERT RPM OUTPUT INTO COMMA-SEPARATED VALUES FORMAT

```
# Radiation Portal Monitor Token Remover by Stephen M. Revis, Texas A&M University


# This script reads Radiation Portal Monito (RPM) data files and outputs the data
# as comma separated values in each line as follows:

# Upper-Left Detector Count Rate [1/s], Lower-Left Detector Count Rate [1/s],
# Upper-Right Detector  Count Rate [1/s], Upper-left detector Count Rate [1/s],
# Date [yyyymmdd], Time[hhmmss]

# It combines all files meeting the search criteria into one single file formatted
# as shown above.  Please name your input files in a machine-sortable manner

# This script can be easily modified to run from the command line.
# I leave that as an exercise to the end user.

# INPUT_____________________________________________________
# Arguments are space delimited and sequential on the command line following
# the script name; arguments can not be omitted!:

# ARGV[0] is the target directory
# ARGV[1] is the input wildcard
#
$input_dir="/Users/Steve/Documents/ORNL Stuff/Steves Stuff/Archive_RPM";
$search_wildcard="^Weather_2009-05-0";
$output_dir="/Users/Steve/Documents/workspace/Final Draft/Output_R";
$output_file ="report.txt";
$do_five_point_sum = 0;



# INPUT_____________________________________________________
# Arguments are space delimited and sequential on the command line following
# the script name; arguments can not be omitted!:

# ARGV[0] is the search wildcard
#
#@all_files = directory_search($ARGV[0],$ARGV[1]);
@all_files = directory_search($input_dir,$search_wildcard);
#print @all_files;


# ARGV[2] is the output directory
#$output_directory = $ARGV[2];
$output_directory = $output_dir;

# ARGV[3] is the output file name prefix
#$output_file = $ARGV[3];


$G_output_path = ">".$output_directory."\/G_".$output_file;
```

```
$N_output_path = ">".$output_directory."\/N_".$output_file;
printf "Outputting to\:\n";
printf "\n%s\n%s\n\n",$G_output_path,$N_output_path;
open(G_OUTPUT,$G_output_path) or die "can't open output file: $!";
open(N_OUTPUT,$N_output_path) or die "can't open output file: $!";


# Options_____________________________________________
# if true, do a five point sum on the gamma data
#$do_five_point_sum = $ARGV[4];

print "Processing Files...\n";

# open each daily file_____________________________________________________________
foreach $input_file (@all_files)
{
  @input_file_name_parts = split /\./ ,$input_file;

  # open the file
  $input_path = "<".$input_dir."\/".$input_file;  printf "$input_path\n";
  open(INPUT,$input_path);
  $Day_count++;

  # go thru the file line by line
  while($line = <INPUT>)
  {
    chomp($line);
    $line=~tr/\://d;
    $line=~tr/-//d;
    @words = split /,/ ,$line;

    # determine new occupancy state_____________________________________________

    # build profile
    if (($words[0] eq "GS") || ($words[0] eq "GA") || ($words[0] eq "GB"))
    {
       push @G1,$words[1];
       push @G2,$words[2];
       push @G3,$words[3];
       push @G4,$words[4];
       push @G5,$words[5];
       push @G6,$words[6];
    }

    if (($words[0] eq "NS") || ($words[0] eq "NA") || ($words[0] eq "NB"))
    {
       push @N1,$words[1];
       push @N2,$words[2];
       push @N3,$words[3];
       push @N4,$words[4];
       push @N5,$words[5];
       push @N6,$words[6];
    }
  }

  #Do the five second gamma sum if requested
  if ($do_five_point_sum)
  {
    @G1 = five_point_running_sum(@G1);
    @G2 = five_point_running_sum(@G2);
    @G3 = five_point_running_sum(@G3);
    @G4 = five_point_running_sum(@G4);
  }
  if ($do_five_point_sum)
```

```
  {
    @N1 = five_point_running_sum(@N1);
    @N2 = five_point_running_sum(@N2);
    @N3 = five_point_running_sum(@N3);
    @N4 = five_point_running_sum(@N4);
  }


for ($i=0;$i<scalar(@G1);$i++)
    {
  printf G_OUTPUT "%s,%s,%s,%s,%s,%s\n",$G1[$i],$G2[$i],$G3[$i],$G4[$i],$G5[$i],$G6[$i];
    }
    for ($i=0;$i<scalar(@N1);$i++)
    {
  printf N_OUTPUT "%s,%s,%s,%s,%s,%s\n",$N1[$i],$N2[$i],$N3[$i],$N4[$i],$N5[$i],$N6[$i];
    }

      @G1 = clean_queue(@G1);
      @G2 = clean_queue(@G2);
      @G3 = clean_queue(@G3);
      @G4 = clean_queue(@G4);
      @G5 = clean_queue(@G5);
      @G6 = clean_queue(@G6);



      @N1 = clean_queue(@N1);
      @N2 = clean_queue(@N2);
      @N3 = clean_queue(@N3);
      @N4 = clean_queue(@N4);
      @N5 = clean_queue(@N5);
      @N6 = clean_queue(@N6);


  close(INPUT);

} # END <<<< foreach $input_file (@all_files) >>>>

close(OUTPUT);




#-------------------------------------------------------------------------

sub directory_search()
{
  #function arguments
  my($directory_name)=@_[0];
  my($wild_card)=@_[1];

  my($i);
  my($x_file);
  my(@all_files);
  my(@selected_files);

  opendir(THISDIR,$directory_name) or die "serious dainbramage: $!";
  @all_files = readdir THISDIR;
  closedir THISDIR;

  $i = 0;
  foreach $x_file (@all_files)
  {
```

```
    if ($x_file =~ $wild_card)
    {
      $selected_files[$i] = $x_file;
      $i+=1;
    }
  }

  if ($i==0)
  {
    printf "(directory search) ...no file meets the search criteria\n"
  }

  return @selected_files;
}

sub clean_queue()
{
  # this is a hack, but it works ....
  my(@queue) = @_;

  @queue=0;shift(@queue);

  return @queue;
}


# This subroutine takes an array and returns the 5-point running sum
#     of the array
sub five_point_running_sum()
{
  my(@Originals)=@_;
  my(@OneSecondSums);
  my($i);

  for($i=0;$i<scalar(@Originals)-4;$i++)
  {
   $OneSecondSums[$i] = $Originals[$i]
                       +$Originals[$i+1]
                       +$Originals[$i+2]
                       +$Originals[$i+3]
                       +$Originals[$i+4];
  }

  return @OneSecondSums;
}

# This subrouting returns the peak value of an array
sub peak_value()
{
  my(@queue) = @_;
  my($peak);
  my($i);

  $peak = 0;
  for ($i=0;$i<scalar(@queue);$i++)
  {
   if ($peak < $queue[$i])
   {
     $peak = $queue[$i];
   }
  }
  return $peak;
}
```

APPENDIX E

PERL SCRIPT DESIGNED TO CONVERT WEATHER STATION OUTPUT INTO COMMA-SEPARATED VALUES FORMAT

```
# Weather Station Token Remover by Stephen M. Revis, Texas A&M University

# This script reads weather data files and outputs the data as comma
# separated values in each line as follows:

# Elappesed time [s] (relative to initial time),
# Wind direction minimum [degrees], Wind direction Avg [degrees]
# Wind direction Max [degrees], Wind speed min [mph], Wind speed avg [mph],
# Wind speed max [mph], Air Temp [degree F], Sensor Temp [degree F], RH [%],
# Barometer [Pa], Rain Accumulation [Inches], Rain Duration [s],
# Rain Intensity [Inch/hour], Supply Voltage [V],Initial Date[yyyymmdd],
# Initial Time [hhmmss]

# It combines all files meeting the search criteria into one single file formatted
# as shown above.  Please name your input files in a machine-sortable manner

# This script can be easily modified to run from the command line.
# I leave that as an exercise to the end user.

$input_dir="/Users/Steve/Documents/workspace/Final Draft/Fixed_Weather";
$search_wildcard="^2009_05_0";
$output_dir="/Users/Steve/Documents/workspace/Final Draft/Output_W";
$output_file ="report.txt";


# INPUT_____________________________________________________
# Arguments are space delimited and sequential on the command line following
# the script name; arguments can not be omitted!:

# ARGV[0] is the search wildcard
#
#@all_files = directory_search($ARGV[0],$ARGV[1]);
@all_files = directory_search($input_dir,$search_wildcard);
#print @all_files;


# ARGV[2] is the output directory
#$output_directory = $ARGV[2];
$output_directory = $output_dir;

# ARGV[3] is the output file name prefix
#$output_file = $ARGV[3];


$G_output_path = ">".$output_directory."\/".$output_file;
print "Outputing to: \n";
printf "\n%s\n%s\n\n",$G_output_path;
open(G_OUTPUT,$G_output_path) or die "can't open output file: $!";

# Options_____________________________________________
# if true, do a five point sum on the gamma data
```

```
#$do_five_point_sum = $ARGV[4];
$do_five_point_sum = 0;



# open each daily file_____________________________________________________________
print "Processing Data Files...\n\n";
foreach $input_file (@all_files)
{

  @input_file_name_parts = $input_file;

  # open the file
  $input_path = "<".$input_dir."\/".$input_file;
  printf "$input_path\n";
  # SAVE STRINGS OF INTEREST
  my $string = "";
  my $counter = 0;
  my $maxcount = 0;
  my $start = 0;
  my $date = "";
  my $time = "";
  open (TMP, "$input_path") || die("Error Reading File: $input_path $!");
     while($string = <TMP>)
     {
      $counter++;
     }
  close(TMP);
  $maxcount = $counter;
  printf "$maxcount"." lines\n";
  $counter = 0;

  open(INPUT,$input_path);
  #$Day_count++;

  # go thru the file line by line
  while($string = <INPUT>)
  {
    # Get Date and Time from Header
      if ($counter == 0)
     {
            @arr = split(/ /,$string);
            $mydate = @arr[0];
            $mytime = @arr[1];
            print "Data start time is\: "."$mydate"."$mytime";

      }
      if ($counter > 3 and $counter < $maxcount-1){
            $string=~s/ //g;
            $string=~s/=//g;
            $string=~s/Vr.*$//g;
            $string=$string.$mydate.$mytime;
            $string=~s/\n//g;
            $string=~s/^p$//g;
            $string=~s/0r0\,//g;
            $string=~tr/a-z//d;
            $string=~tr/A-Z//d;
            $string=~tr/\://d;
            $string=~tr/-//d;
            print G_OUTPUT $string."\n";
      }
      $counter++;
  }
```

```
  close(INPUT);

} # END <<<< foreach $input_file (@all_files) >>>>

close(OUTPUT);



#-------------------------------------------------------------------------

sub directory_search()
{
  #function arguments
  my($directory_name)=@_[0];
  my($wild_card)=@_[1];

  my($i);
  my($x_file);
  my(@all_files);
  my(@selected_files);

  opendir(THISDIR,$directory_name) or die "serious dainbramage: $!";
  @all_files = readdir THISDIR;
  closedir THISDIR;

  $i = 0;
  foreach $x_file (@all_files)
  {

    if ($x_file =~ $wild_card)
    {
      $selected_files[$i] = $x_file;
      $i+=1;
    }
  }

  if ($i==0)
  {
    printf "(directory search) ...no file meets the search criteria\n"
  }

  return @selected_files;
}

sub clean_queue()
{
  # this is a hack, but it works ....
  my(@queue) = @_;

  @queue=0;shift(@queue);

  return @queue;
}


# This subroutine takes an array and returns the 5-point running sum
#     of the array
sub five_point_running_sum()
{
  my(@Originals)=@_;
  my(@OneSecondSums);
  my($i);
```

```
  for($i=0;$i<scalar(@Originals)-4;$i++)
  {
   $OneSecondSums[$i] = $Originals[$i]
                       +$Originals[$i+1]
                       +$Originals[$i+2]
                       +$Originals[$i+3]
                       +$Originals[$i+4];
  }

  return @OneSecondSums;
}

# This subrouting returns the peak value of an array
sub peak_value()
{
  my(@queue) = @_;
  my($peak);
  my($i);

  $peak = 0;
  for ($i=0;$i<scalar(@queue);$i++)
  {
   if ($peak < $queue[$i])
   {
     $peak = $queue[$i];
   }
  }
  return $peak;
}
```

APPENDIX F

MATLAB FUNCTION DESIGNED TO LOAD RPM AND WEATHER STATION DATA PROCESSED INTO CSV BY PERL SCRIPTS FROM PREVIOUS APPENDICES

```
function [wdate,wrain,gammaSerialDate,gammaavg]=loadportal(wfile,gfile)

%Radiation Portal Monitor and Weather Data Loading Fuction
%Stephen M. Revis, Texas A&M University

%This function is designed to load RPM and weather station data in CSV
%format and re-format said data into MATLAB vectors in census date format


%All inputs are strings and must be in quotes!

clc
disp('Loading Weather and Radiation Data from Local Source')
%fig=1;
    weather=load(wfile);
    gamma=load(gfile);
    wdvec=zeros(max(length(weather)),6);
    wdvec(:,1)=floor(weather(:,16)./1e4);
    wdvec(:,2)=floor(weather(:,16)./1e2-wdvec(:,1).*1e2);
    wdvec(:,3)=floor(weather(:,16)-wdvec(:,1).*1e4-wdvec(:,2)*1e2);
    %    wadd=weather(:,17)+weather(:,1);
    wdvec(:,4)=floor(weather(:,17)./1e4)+floor(weather(:,1)./3600);
    wdvec(:,5)=floor(weather(:,17)./1e2)-floor(weather(:,17)./1e4)*...
        1e2+floor(weather(:,1)./60)-floor(weather(:,1)./3600)*60;
    wdvec(:,6)=weather(:,17)-floor(weather(:,17)./1e2)*1e2+weather(:,1)...
        -floor(weather(:,1)./60)*60;
    wdate2=datenum(wdvec); %use datestr(date) to convert SLD
    %(MATLAB) type dates into human readable

    gdvec=zeros(max(length(gamma)),6);
    gdvec(:,1)=floor(gamma(:,5)./1e4);
    gdvec(:,2)=floor(gamma(:,5)./1e2-gdvec(:,1).*1e2);
    gdvec(:,3)=floor(gamma(:,5)-gdvec(:,1).*1e4-gdvec(:,2).*1e2);
    gdvec(:,4)=floor(gamma(:,6)./1e4);
    gdvec(:,5)=floor(gamma(:,6)./1e2)-gdvec(:,4).*1e2;
    gdvec(:,6)=gamma(:,6)-gdvec(:,5).*1e2-gdvec(:,4).*1e4;
    gdate=datenum(gdvec);




    gammaSerialDate2=gdate;
    gammaavg2=mean([gamma(:,1),gamma(:,2),gamma(:,3),gamma(:,4)],2);
    bigmean=mean(gammaavg2);
    bigstd=std(gammaavg2);

    ll=1;
    mm=1;
    datehold=gammaSerialDate2(1);
```

```
    for ii=1:length(gammaSerialDate2)
        if gammaSerialDate2(ii) ~= datehold
            kk=ii-1;
            gammaavg3(mm)=mean(gammaavg2(ll:kk));
            gammaSerialDate3(mm)=gammaSerialDate2(ll);
            mm=mm+1;
            ll=ii;
            datehold=gammaSerialDate2(ii);
        end
    end

    jj=1;
    kk=1;

    gammaavg=zeros(length(gammaavg3)-200,1);
    gammaSerialDate=zeros(length(gammaavg3)-200,1);
    for ii=101:length(gammaavg3)-100
        gammaavg(jj)=mean(gammaavg3(ii-50:ii+50));
        gammaSerialDate(jj)=gammaSerialDate3(ii);
        jj=jj+1;
    end

    jj=1;

    wrain=zeros(length(weather)-200,1);
    wdate=zeros(length(weather)-200,1);
    for ii=101:length(weather)-100
        wrain(jj)=mean(weather((ii-100:ii+100),14));
        wdate(jj)=wdate2(ii);
        jj=jj+1;
    end
    beep


disp('Load Complete')
```

APPENDIX G

MATLAB FUNCTION DESIGNED TO ACCEPT USER INPUT AND CREATE PLOTS AND ARRAY OUTPUT FOR BACKGROUND SUPRESSION ALGORITHM

```
function [meangamma,corrgamma,attenout]=rainfunction(weatherfile,gammafile)
tic
%Portal Monitor Background Supression Function
%Stephen M. Revis, Texas A&M University
%This function is designed to analyze RPM and weather station data that
%has been converted by the PERL scripts included in previous appendices

%The inputs are the location of the text files containing the
%aforementioned weather station output and RPM output enclosed in single
%quotes.

%The outputs are:

%meangamma, an array with the following columns:
%mean count rate during period,
%precipitation intensity (zero means no precip.),
%MATLAB census format date,
%Event type flag (1= precipitation beginning, 0=precipitation continuing
%-1=no precipitation),
%Logic Flag (1= event correctly identified, 0=no event (due to continuing
%precipitation, -1= event incorrectly identified
%Pulse height logic flag (1=pulse correctly identified, 0= no pulse (due to
%continuing precipitation, -1=pulse incorrectly identified (false negative
%or false positive)
%Algorithm rain detection flag (1=rain, 0=no rain) independent of weather
%data, solely based on gamma CR
%range start if rain detected by algorithm
%range end if rain detected by algorithm

%corrgamma, an array with the following columns:
%corrected count rate [1/s], date, a rain logic flag (1=rain, 0=no rain,
%rain intensity [in/hr], index, radfactor value [-]

%attenout, an array with the following columns:
%Output structure is as follows:
%Average percent attenuation,
%Percentage of steps in which attenuation exceeded baseline
%Percentage of steps in which attenuation exceeded baseline by > 10 percent
%Average amount by which attenuation exceeded baseline

%All averages are taken over steps in which the condition is met, i.e.
%attenuation is averaged over only steps with attenuation, the amount by
%which the baseline is exceeded is only averaged over steps where the
%baseline was exceeded, etc.

%Baseline is the median value of the background count rate over the period
%being analyzed.
```

```
close all hidden
%clear all
clc
%fig=0;
%disp('enter 1 to load new data, 0 to use existing data')
%loadflag=input('');
%if loadflag==1
%Load data from local files
[wdate,wrain,gammaSerialDate,gammaavg]=loadportal(weatherfile,gammafile);
%end
fig=0;
%Analyze data
tshift=0;
rlld=0.01;
lld=1.025;
[meangamma,true,truepos,false,falsepos,rainavg,norainavg,gapmean]=...
autoportal_correct(wdate,wrain,gammaSerialDate,gammaavg,tshift,lld,rlld);

%correction script, knocks down excess CR from rain
corrgamma=revis(gammaSerialDate,gammaavg,meangamma);



% Create Plots
fig=fig+1;
figure(fig)
plot(gammaSerialDate,gammaavg,meangamma(:,3),corrgamma(:,1),wdate,wrain*100)
hold on
xlabel('Census Date')
ylabel('Background Count Rate [s^-1] and Precipitation Rate*100 [in hr^-1 100^-1]')
legend('Background Count Rate','Corrected BCR', 'Precipitation Rate',...
'Precipitation Logic Flag', 'Algorithm Success Flag')
hold off

fig=fig+1;
figure(fig)
plot((gammaSerialDate-min(wdate)).*24,gammaavg,(meangamma(:,3)-min(wdate)).*24,corrgamma(:,1),...
(wdate-min(wdate)).*24,wrain*100,(meangamma(:,3)-min(wdate)).*24,meangamma(:,4).*10,'+')
xlabel('Hours [hr]')
hold on
ylabel('Background Count Rate [s^-1] and Precipitation Rate*100 [in hr^-1 100^-1]')
legend('Background Count Rate','Corrected BCR', 'Precipitation Rate', 'Precipitation Logic Flag')
hold off
%axis([0 300 0 100])

% fig=fig+1;
% figure(fig)
% [AX,H1,H2] = plotyy(gammaSerialDate,gammaavg,wdate,wrain,'plot');
% %legend('Background Count Rate', 'Precipitation Rate')
% xlabel('Time')
% set(get(AX(1),'Ylabel'),'String','Background Count Rate [s^-1]')
% set(get(AX(2),'Ylabel'),'String','Precipitation Rate [in hr^-1]')
% datetick(AX(1),'x',15)
% datetick(AX(2),'x',15)


disp('positives per event')
disp(truepos/true)
disp('false positives per non-event')
disp(falsepos/false)
disp(' ')
disp('total events')
disp(true)
```

```
disp(' ')
disp('total non-events')
disp(false)
disp(' ')
disp('true positives per false positive')
disp(truepos/falsepos)
attenout=attenuation(meangamma,corrgamma);
disp('Postprocessing Complete')
toc
```

APPENDIX H

MATLAB FUNCTION DESIGNED TO SYNCHRONIZE TIMESTEPS FROM ASYNCHRONOUS WEATHER AND RADIATION DATA SOURCES

```
function[meangamma,true,truepos,false,falsepos,rainavg,norainavg,gapmean]=...
...autoportal_correct(wdate,wrain,gammaSerialDate,gammaavg,tshift,lld,rlld)

%Stephen Revis, Texas A&M University

%wdate is a census date vector corresponding to weather
%weather is a vector of qualitative weather values
%gammaSerialDate is a census date vector corresponding to gammaavg
%gammaavg is a vector of gamma count rates
%tshift is a time shift between the portal monitor and the weather station.
%sign convention is such that a positive value indicates that the portal
%monitor experiences a weather event before the weather station
%lld is a lower level discriminator defined by a multiple of the average
%value.  This value must be greater than unity to produce meaningful
%results.

% disp(' ')
% disp('Postprocessing: Calculating Values and Generating Plots')
% disp(' ')
%tshift=input('Enter time shift between weather station and portal monitor in hours \n');
%tshift=tshift/24;
%tshift=input('Enter time shift between weather station and portal monitor in minutes \n');
%lld=input('Enter Lower Level Discriminator Value in Terms of Average Count Rate \n');
tshift=tshift/(24*60);
%tshift=0;
wdate=wdate-tshift;


%summation of average gamma counts within +/- trange hour of each weather
%observation
jjo=1; %Start index for search for 1/2 hour before and end 2 hours after (like a shift register)
%jj=1;
kk=1;
ll=1;
%qq=1;
%rr=1;
% true=0; %percipitation events
% false=0;%no percipitation recorded
% truepos=0; %event recorded, peak detected (good)
% trueneg=0; %event recorded, peak not detected (bad)
% falsepos=0; %no event, peak erroneously detected (bad)
% falseneg=0; % no event, no peak (good)
%     highweather=zeros(size(weather));
%     lowweather=zeros(size(weather));
vecsize=length(wrain);
% highweather=zeros(1,vecsize);
% lowweather=zeros(1,vecsize);
spot=0;
tback=(1/(24*3600))*0.5; %start of range associated with weather data point, value in seconds
tforward=(1/(24*3600))*0.5; %end of range associated with weather data point, value in minutes
%if (min(wdate)-5*((1/24)/60))<min(gammaSerialDate)  %Find first weather point with corresponding
```

```
%radiation data, 5 minute buffer to prevent array overruns
while wdate(ll)<(min(gammaSerialDate)+5*((1/24)/60)+tback)
    ll=ll+1;
end
%end
%if max(gammaSerialDate)<(max(wdate)+5*((1/24)/60))  %Find last weather point with corresponding
%radiation data, 5 minute buffer to prevent array overruns
while kk<length(wdate) && wdate(kk)<(max(gammaSerialDate)-5*((1/24)/60)-tforward)
    kk=kk+1;
end
%else
%    kk=length(wdate);
%end
kk=kk-1;
glength=kk-ll;
cumgamma=zeros(glength,1);
truthvec=zeros(glength,1);
meangamma=zeros(glength,9);


%meangamma data structure is as follows:
% NINE (9) columns
%[mean count rate during period,
%precipitation intensity (zero means no precip.),
%MATLAB census format date,
%Event type flag (1= precipitation beginning, 0=precipitation continuing
%-1=no precipitation),
%Logic Flag (1= event correctly identified, 0=no event (due to continuing
%precipitation, -1= event incorrectly identified
%Pulse height logic flag (1=pulse correctly identified, 0= no pulse (due to
%continuing precipitation, -1=pulse incorrectly identified (false negative
%or false positive)
%Algorithm rain detection flag (1=rain, 0=no rain) independent of weather
%data, solely based on gamma CR
%range start if rain detected by algorithm
%range end if rain detected by algorithm

%rlld=0.00; % historical data is qualitative, anything above zero really is rain


for ii=ll+1:kk %analyze weather-radiation correlation over previously determined range of
%weather data
    spot=spot+1; %position in correlation matrix
    meangamma(spot,3)=wdate(ii);
    meangamma(spot,2)=wrain(ii);
    if wrain(ii)<=rlld
        meangamma(spot,4)=-1;
        %         wdateii=wdate(ii);
        jj=jjo;
        while gammaSerialDate(jj)<wdate(ii)-(tback)
            jj=jj+1;
        end
        jjstart=jj;
        jjo=jj;
        while gammaSerialDate(jj)<wdate(ii)+(tforward)
            jj=jj+1;
        end
        jjend=jj-1;
        if jjend>=jjstart   %Avoid NaNs
            meangamma(spot,1)=mean(gammaavg(jjstart:jjend));
        else
            meangamma(spot,1)=gammaavg(jjstart);
        end
        if meangamma(spot,1)>=lld*mean(gammaavg(jjstart-10:jjstart)) && meangamma(spot,1)>=lld*...
```

```
        mean(gammaavg(jjend:jjend+10));
            meangamma(spot,6)=-1; %algorithm success flag (fail)
            meangamma(spot,7)=1;  %algorithm rain detection flag (yes)
            meangamma(spot,8)=jjstart;
            meangamma(spot,9)=jjend;
        end
    else
        meangamma(spot,4)=1;
        jj=jjo; %start search for next start point at last start point for efficiency
        while gammaSerialDate(jj)<wdate(ii)-(tback) %search for end of period
            jj=jj+1;
        end
        jjstart=jj;
        jjo=jj;
        while gammaSerialDate(jj)<wdate(ii)+(tforward)
            jj=jj+1;
        end
        jjend=jj-1;
        if jjend>=jjstart   %Avoid NaNs
            meangamma(spot,1)=mean(gammaavg(jjstart:jjend));
        else
            meangamma(spot,1)=gammaavg(jjstart);
        end
        if meangamma(spot,1)<lld*mean(gammaavg(jjstart-10:jjstart)) && meangamma(spot,1)<lld*...
        mean(gammaavg(jjend:jjend+10));
            meangamma(spot,6)=-1; %lower level discriminator: does peak area have higher CR than
            %before and after?, algorithm successs flag (fail)
        else
            meangamma(spot,6)=1; %algorithm success flag (success)
            meangamma(spot,7)=1; %algorithm rain detection flag (yes)
            meangamma(spot,8)=jjstart;
            meangamma(spot,9)=jjend;
        end
    end
end

%logic to determine algorithm's success
scratchsum=meangamma(:,4)==1;
true=sum(scratchsum);
scratchsum=meangamma(:,6)==1 & meangamma(:,4)==1;
truepos=sum(scratchsum);
% scratchsum=meangamma(:,6)==-1 & meangamma(:,4)==1;
% trueneg=sum(scratchsum);
scratchsum=meangamma(:,4)==-1;
false=sum(scratchsum);
% scratchsum=meangamma(:,6)==1 & meangamma(:,4)==-1;
% falseneg=sum(scratchsum);
scratchsum=meangamma(:,6)==-1 & meangamma(:,4)==-1;
falsepos=sum(scratchsum);

%Determine average counts with and without rain
rain=0;
norain=0;
aa=1;
bb=1;
for ii=ll:kk
    if wrain(ii)>rlld
        rain(aa)=meangamma(ii-ll+1);
        aa=aa+1;
    else
        norain(bb)=meangamma(ii-ll+1);
        bb=bb+1;
    end
end
```

```
rainavg=mean(rain);
norainavg=mean(norain);

%Determine average gap between false positives
aa=1;
for ii=1:length(meangamma)
    if meangamma(ii,6)==-1 && meangamma(ii,7)==1
        fvec(aa)=meangamma(ii,3);
        aa=aa+1;
    end
end
if aa >= 2
    fvec=fvec';
    bb=1;
    %gapvec=zeros(length(fvec)-1,1);
    for ii=2:length(fvec)
        scratch=fvec(ii)-fvec(ii-1);
        if scratch>5*((1/24)/60)
            gapvec(bb)=scratch;
            bb=bb+1;
        end
    end

else
    gapvec=0;
    %disp('no false positives')
end
if bb==1;
    gapvec=0;
end
gapmean=mean(gapvec);
gapmedian=median(gapvec);

%disp(gapmean)
%disp(gapmedian)


% avgvec=[rainavg,norainavg];
% fprintf('When raining, the average background count rate is %6.2f \n',rainavg)
% fprintf('When not raining, the average background count rate is %6.2f \n',norainavg)
end
```

APPENDIX I

MATLAB FUNCTION DESIGNED TO SUPPRESS BACKGROUND COUNT RATE DUE TO PRECIPITATION

```
function [correct]=revis(gammaavg,meangamma)


%Correction Function, knocks down excess CR from rain
%Stephen Revis, Texas A&M University

%Initial Calculations
A=0.5;     % originally 0.5
B=1.5;     % originally 1.5
C=0.05;   % originally 0.1366
D=0.15;   % originally 0.262

A2=0.5;    % originally 0.5
B2=4.5;    % originally 4.5
C2=0.015;   % originally 0.0454
D2=0.2;    %originally 0.2412

tstep=(1/3600)/24; %Data time step length in days
%Find Baseline Countrate
wrain=gammaavg;
wrain=sort(wrain);
wlow=ceil((1-0.9545)./2.*length(wrain)); %lowest CR in day to 2 standard deviations
%(actual lowest value may be spurious)
whigh=ceil((1-((1-0.9545)./2)).*length(wrain)); %lowest CR in day to 2 standard deviations
%(actual lowest value may be spurious)
noraincr=wrain(wlow);
wmean=mean(wrain);
wstd=std(wrain);
if noraincr < wmean-3*wstd
    disp('Warning, Low CR value is more than three standard deviations below average CR')
end

%ratio=1-(wrain(wlow)./wrain(whigh)); %maximum decrease amount)

%Initialize Corrgamma
corrgamma=zeros(length(meangamma),8);
corrgamma(:,1)=meangamma(:,1); %corrected count rate
corrgamma(:,2)=meangamma(:,3);% date
%column 3 is a rain logic flag
corrgamma(:,4)=meangamma(:,2); % rain intensity
corrgamma(:,5)=1:length(corrgamma); %index
% colum 6 is to check the radfactor value
kkstart=0;
kkend=0;
datelength=length(corrgamma);
datemax=corrgamma(datelength,2);


ii=datelength;
while datemax-corrgamma(ii,2)<(5/60)/24
    ii=ii-1;
```

```
end
datelength=ii;
datemax=corrgamma(datelength,2);

%Initialize counters and flags
ii=2;
gap=0;
gflag=0;
jjstart=1;

%Determine periods of rain
while ii<length(meangamma)
    if meangamma(ii,2)>0.01 && meangamma (ii-1,2) < 0.01 && gflag == 0 %see if there's new rain
        jjstart=(ii);
    elseif meangamma(ii,2)<0.01 && meangamma (ii-1,2)>0.01 %activate gflag and record
    %position if rain stopped
        gflag=1;
        jjend=ii;
    end

    if gflag==1
        gap=meangamma(ii,3)-meangamma(jjstart,3); % see how long rain stopped for
        if gap > (1/24)*(60/60) %If it was more than 1 hour, the rain really did stop
            gflag=0; %deactivate gflag
            corrgamma(jjstart:jjend,3)=1; %Record duration of rain
        end
    end
    ii=ii+1;
end



%Apply Japanese Correction Factor
rainflag=0;
radfactor=C2;
for ii=2:datelength
    if corrgamma(ii-1,3)==0 && corrgamma(ii,3)==1 % log start of event
        rainflag=1;
        kkstart=ii;
    elseif  corrgamma(ii-1,3)==1 && corrgamma(ii,3)==0%log end of event
        rainflag=0;
        kkend=ii;
        spikestart=corrgamma(ii,2);
        if corrgamma(kkend,2)+(5/24)<datemax
            qq=kkend;
            datefind=corrgamma(qq,2);
            while datefind<corrgamma(kkend,2)+(5/24);
                datefind=corrgamma(qq,2);
                qq=qq+1;
            end
            spikeend=qq;
        else
            spikeend=datelength;
        end
        ll=kkend;
        while ll<spikeend
            corrgamma(ll,1)=-(corrgamma(ll,1)*radfactor)*1.0002269268*exp(-3.7104242261e1*...
            (corrgamma(ll,2)-spikestart))+corrgamma(ll,1);
            ll=ll+1;
        end
    end
```

```
    if rainflag==1
        rainlength=corrgamma(ii,2)-corrgamma(kkstart,2);
        rainhour=rainlength*24;
        rainmax=max(corrgamma(kkstart:ii,4));
        if rainhour > 1.0
            radfactor=D*rainmax^A*(1-exp(-rainhour*B))+C;
        else
            if ii>kkstart
                intavg=sum(corrgamma(kkstart:ii,4))./(ii-kkstart);
            else
                intavg=corrgamma(ii,4);
            end
            radfactor=D2*rainmax^A2*(1-exp(-rainhour*B2-0.00001))+C2;
        end
        corrgamma(ii,6)=radfactor; %check on this, see where it's too high!!!
        corrgamma(ii,7)=rainlength;
        corrgamma(ii,1)=corrgamma(ii,1)./(1+radfactor); %Adjust
    end


end

correct=corrgamma;

end
```

APPENDIX J

MATLAB SCRIPT DESIGNED TO EVALUATE EFFECTIVENESS OF BACKGROUND SUPRESSION ALGORITHM

```
function output=attenuation(meangamma,corrgamma)

%Stephen Revis, Texas A&M University

%This script determines the average level of attenuation that the
%background suppression algorithm achieves relative to the median value of
%background count rate, and how often it over-corrects (decrease the
%BCR value below the median)

%Output structure is as follows:
%Average percent attenuation,
%Percentage of steps in which attenuation exceeded baseline
%Percentage of steps in which attenuation exceeded baseline by > 10 percent
%Average amount by which attenuation exceeded baseline

%All averages are taken over steps in which the condition is met, i.e.
%attenuation is averaged over only steps with attenuation, the amount by
%which the baseline is exceeded is only averaged over steps where the
%baseline was exceeded, etc.

%Baseline is the median value of the background count rate over the period
%being analyzed.

corrlength=length(corrgamma);
meanlength=length(meangamma);
baseline=median(meangamma(:,1));
tenbaseline=baseline*-0.1;

stepcount=0;
subbasecount=0;
attenuation=0;
baserate=0;
subbaserate=0;
attentotal=0;
subbasetotal=0;
tentotal=0;

if corrlength ~= meanlength
    disp('uh oh')
end

for ii=1:corrlength
    if corrgamma(ii,3)==1
        meanbase=meangamma(ii,1)-baseline;
        corrbase=corrgamma(ii,1)-baseline;
        if meanbase > 0 && corrbase < 0
            stepcount=stepcount+1;
            subbasecount=subbasecount+1;
            subbasetotal=subbasetotal+corrbase;
            if corrbase < tenbaseline
                tentotal=tentotal+1;
```

```
            end
        elseif meanbase > 0 && corrbase > 0
            attenuation=1-(corrbase./meanbase);
            stepcount=stepcount+1;
            attentotal=attenuation+attentotal;
        end
    end
end

attenavg=attentotal./stepcount;
subbaserate=subbasecount./stepcount;
subbaseavg=subbasetotal./subbasecount./baseline;
subtenrate=tentotal./stepcount;

disp('average attenuation is')
disp('')
disp(attenavg*100)
disp('')
disp('attenuation exceeded baseline')
disp('')
disp(subbaserate*100)
disp('percent of the time')
disp('')
disp('attenuation exceeded baseline by 10% or more')
disp(subtenrate*100)
disp('percent of the time')
disp('')
disp('attenuation exceeded baseline by an average of')
disp(subbaseavg*100)
disp(' percent')

output=[attenavg,subbaserate,subbaseavg,subtenrate];
```

APPENDIX K

MATLAB FUNCTION DESIGNED TO ACCEPT USER INPUT AND CREATE PLOTS AND ARRAY OUTPUT FOR PRECIPITATION DETECTION ALGORITHM

```
function [statout,meangamma]=inversemod(weatherfile,gammafile)

%Stephen Revis, Texas A&M University


%Portal Monitor lld sensitivity analysis
close all hidden
%clear all
clc
fig=0;
%Load data from local files
[wdate,wrain,gammaSerialDate,gammaavg]=loadportal(weatherfile,gammafile);

%Analyze data
tshift=0;
rlld=0.08;
lld=1.025;
[meangamma,true,truepos,false,falsepos,rainavg,norainavg,gapmean]=...
autoportal(wdate,wrain,gammaSerialDate,gammaavg,tshift,lld,rlld);

%Create Plots
fig=fig+1;
figure(fig)
plot(gammaSerialDate,gammaavg,wdate,wrain*100,meangamma(:,3),meangamma(:,4).*10,'+',...
meangamma(:,3),meangamma(:,6).*10+25,'+')
hold on
xlabel('Census Date')
ylabel('Background Count Rate [s^-1] and Precipitation Rate*100 [in hr^-1 100^-1]')
legend('Background Count Rate', 'Precipitation Rate', 'Precipitation Logic Flag',...
'Algorithm Success Flag')

fig=fig+1;
figure(fig)
plot((gammaSerialDate-min(wdate)).*24,gammaavg,(wdate-min(wdate)).*24,wrain*100,...
(meangamma(:,3)-min(wdate)).*24,meangamma(:,4).*10,'+',(meangamma(:,3)-min(wdate)).*24,...
meangamma(:,6).*10+25,'+')
xlabel('Hours [hr]')
ylabel('Background Count Rate [s^-1] and Precipitation rate [in-hr-100^-1]')
legend('Background Count Rate', 'Precipitation Rate', 'Precipitation Logic Flag',...
'Algorithm Success Flag')

%The function that generates this plot is buggy, zooming in will result in
%the scale reading incorrectly.
fig=fig+1;
figure(fig)
[AX,H1,H2] = plotyy((gammaSerialDate-min(wdate)).*24,gammaavg,(wdate-min(wdate)).*24,wrain,'plot');
%legend('Background Count Rate', 'Precipitation Rate')
xlabel('Time')
set(get(AX(1),'Ylabel'),'String','Background Count Rate [s^-1]')
```

```
set(get(AX(2),'Ylabel'),'String','Precipitation Rate [in hr^-1]')
%datetick(AX(1),'x',15)
%datetick(AX(2),'x',15)


disp('positives per event')
disp(truepos/true)
disp('false positives per non-event')
disp(falsepos/false)
disp(' ')
disp('total events')
disp(true)
disp(' ')
disp('total non-events')
disp(false)
disp(' ')
disp('true positives per false positive')
disp(truepos/falsepos)
statout=[truepos/true,falsepos/false,truepos/falsepos,gapmean];
disp('Postprocessing Complete')
```

APPENDIX L

MATLAB FUNCTION DESIGNED TO SYNCHRONIZE TIMESTEPS FROM ASYNCHRONOUS WEATHER AND RADIATION DATA SOURCES

```
function[meangamma,true,truepos,false,falsepos,rainavg,norainavg,gapmean]=...
...autoportal(wdate,wrain,gammaSerialDate,gammaavg,tshift,lld,rlld)

%Stephen Revis, Texas A&M University

%wdate is a census date vector corresponding to weather
%weather is a vector of qualitative weather values
%gammaSerialDate is a census date vector corresponding to gammaavg
%gammaavg is a vector of gamma count rates
%tshift is a time shift between the portal monitor and the weather station.
%sign convention is such that a positive value indicates that the portal
%monitor experiences a weather event before the weather station
%lld is a lower level discriminator defined by a multiple of the average
%value.  This value must be greater than unity to produce meaningful
%results.

% disp(' ')
% disp('Postprocessing: Calculating Values and Generating Plots')
% disp(' ')
%tshift=input('Enter time shift between weather station and portal monitor in hours \n');
%tshift=tshift/24;
%tshift=input('Enter time shift between weather station and portal monitor in minutes \n');
%lld=input('Enter Lower Level Discriminator Value in Terms of Average Count Rate \n');
tshift=tshift/(24*60);
%tshift=0;
wdate=wdate-tshift;


%summation of average gamma counts within +/- trange hour of each weather
%observation
jjo=1; %Start index for search for 1/2 hour before and end 2 hours after (like a shift register)
%jj=1;
kk=1;
ll=1;
%qq=1;
%rr=1;
% true=0; %percipitation events
% false=0;%no percipitation recorded
% truepos=0; %event recorded, peak detected (good)
% trueneg=0; %event recorded, peak not detected (bad)
% falsepos=0; %no event, peak erroneously detected (bad)
% falseneg=0; % no event, no peak (good)
%     highweather=zeros(size(weather));
%     lowweather=zeros(size(weather));
vecsize=length(wrain);
% highweather=zeros(1,vecsize);
% lowweather=zeros(1,vecsize);
spot=0;
tback=(1/(24*60))*6; %start of range associated with weather data point, value in minutes
tforward=(1/(24*60))*45; %end of range associated with weather data point, value in minutes
%if (min(wdate)-5*((1/24)/60))<min(gammaSerialDate)  %Find first weather point with corresponding
```

```
%radiation data, 5 minute buffer to prevent array overruns
while wdate(ll)<(min(gammaSerialDate)+5*((1/24)/60)+tback)
    ll=ll+1;
end
%end
%if max(gammaSerialDate)<(max(wdate)+5*((1/24)/60))  %Find last weather point with corresponding
%radiation data, 5 minute buffer to prevent array overruns
while kk<length(wdate) && wdate(kk)<(max(gammaSerialDate)-5*((1/24)/60)-tforward)
    kk=kk+1;
end
%else
%    kk=length(wdate);
%end
kk=kk-1;
glength=kk-ll;
cumgamma=zeros(glength,1);
truthvec=zeros(glength,1);
meangamma=zeros(glength,9);


%meangamma data structure is as follows:
% NINE (9) columns
%[mean count rate during period,
%precipitation intensity (zero means no precip.),
%MATLAB census format date,
%Event type flag (1= precipitation beginning, 0=precipitation continuing
%-1=no precipitation),
%Logic Flag (1= event correctly identified, 0=no event (due to continuing
%precipitation, -1= event incorrectly identified
%Pulse height logic flag (1=pulse correctly identified, 0= no pulse (due to
%continuing precipitation, -1=pulse incorrectly identified (false negative
%or false positive)
%Algorithm rain detection flag (1=rain, 0=no rain) independent of weather
%data, solely based on gamma CR
%range start if rain detected by algorithm
%range end if rain detected by algorithm

%rlld=0.00; % historical data is qualitative, anything above zero really is rain


for ii=ll+1:kk %analyze weather-radiation correlation over previously determined range of
%weather data
    spot=spot+1; %position in correlation matrix
    meangamma(spot,3)=wdate(ii);
    meangamma(spot,2)=wrain(ii);
    if wrain(ii)<=rlld
        meangamma(spot,4)=-1;
        %         wdateii=wdate(ii);
        jj=jjo;
        while gammaSerialDate(jj)<wdate(ii)-(tback)
            jj=jj+1;
        end
        jjstart=jj;
        jjo=jj;
        while gammaSerialDate(jj)<wdate(ii)+(tforward)
            jj=jj+1;
        end
        jjend=jj-1;
        if jjend>=jjstart   %Avoid NaNs
            meangamma(spot,1)=mean(gammaavg(jjstart:jjend));
        else
            meangamma(spot,1)=gammaavg(jjstart);
        end
        if meangamma(spot,1)>=lld*mean(gammaavg(jjstart-10:jjstart)) && meangamma(spot,1)>=lld*...
```

```
        mean(gammaavg(jjend:jjend+10));
            meangamma(spot,6)=-1; %algorithm success flag (fail)
            meangamma(spot,7)=1;  %algorithm rain detection flag (yes)
            meangamma(spot,8)=jjstart;
            meangamma(spot,9)=jjend;
        end
    else
        meangamma(spot,4)=1;
        jj=jjo; %start search for next start point at last start point for efficiency
        while gammaSerialDate(jj)<wdate(ii)-(tback) %search for end of period
            jj=jj+1;
        end
        jjstart=jj;
        jjo=jj;
        while gammaSerialDate(jj)<wdate(ii)+(tforward)
            jj=jj+1;
        end
        jjend=jj-1;
        if jjend>=jjstart   %Avoid NaNs
            meangamma(spot,1)=mean(gammaavg(jjstart:jjend));
        else
            meangamma(spot,1)=gammaavg(jjstart);
        end
        if meangamma(spot,1)<lld*mean(gammaavg(jjstart-10:jjstart)) && meangamma(spot,1)<lld*...
        mean(gammaavg(jjend:jjend+10));
            meangamma(spot,6)=-1; %lower level discriminator: does peak area have higher CR than
            %before and after?, algorithm successs flag (fail)
        else
            meangamma(spot,6)=1; %algorithm success flag (success)
            meangamma(spot,7)=1; %algorithm rain detection flag (yes)
            meangamma(spot,8)=jjstart;
            meangamma(spot,9)=jjend;
        end
    end
end

%logic to determine algorithm's success
scratchsum=meangamma(:,4)==1;
true=sum(scratchsum);
scratchsum=meangamma(:,6)==1 & meangamma(:,4)==1;
truepos=sum(scratchsum);
% scratchsum=meangamma(:,6)==-1 & meangamma(:,4)==1;
% trueneg=sum(scratchsum);
scratchsum=meangamma(:,4)==-1;
false=sum(scratchsum);
% scratchsum=meangamma(:,6)==1 & meangamma(:,4)==-1;
% falseneg=sum(scratchsum);
scratchsum=meangamma(:,6)==-1 & meangamma(:,4)==-1;
falsepos=sum(scratchsum);

%Determine average counts with and without rain
rain=0;
norain=0;
aa=1;
bb=1;
for ii=ll:kk
    if wrain(ii)>rlld
        rain(aa)=meangamma(ii-ll+1);
        aa=aa+1;
    else
        norain(bb)=meangamma(ii-ll+1);
        bb=bb+1;
    end
end
```

```
rainavg=mean(rain);
norainavg=mean(norain);

%Determine average gap between false positives
aa=1;
for ii=1:length(meangamma)
    if meangamma(ii,6)==-1 && meangamma(ii,7)==1
        fvec(aa)=meangamma(ii,3);
        aa=aa+1;
    end
end
if aa >= 2
    fvec=fvec';
    bb=1;
    %gapvec=zeros(length(fvec)-1,1);
    for ii=2:length(fvec)
        scratch=fvec(ii)-fvec(ii-1);
        if scratch>5*((1/24)/60)
            gapvec(bb)=scratch;
            bb=bb+1;
        end
    end

else
    gapvec=0;
    %disp('no false positives')
end
if bb==1;
    gapvec=0;
end
gapmean=mean(gapvec);
gapmedian=median(gapvec);

%disp(gapmean)
%disp(gapmedian)


% avgvec=[rainavg,norainavg];
% fprintf('When raining, the average background count rate is %6.2f \n',rainavg)
% fprintf('When not raining, the average background count rate is %6.2f \n',norainavg)
end
```

APPENDIX M

MATLAB FUNCTION DESIGNED TO EVALUATE THE RELATIONSHIP BETWEEN PRECIPITATION-RELATED VARIABLES AND BACKGROUND COUNT RATE INCREASES

```
function outvec=correlator(corrgamma,meangamma,filename)

%Stephen Revis, Texas A&M University

%This script is designed to analyze the relationship between the duration,
%average intensity and maximum intensity of precipitation evnents relative
%to the resulting increase in background activity.  Increase is calculated
%in terms of both gross counts above median and percent increase from
%median.

%inputs are corrgamma, meangamma, 'filename'

corrlength=length(corrgamma);
meanlength=length(meangamma);
baseline=median(meangamma(:,1));
scratchvec=zeros(ceil(corrlength./2+1),5);
%1.)Duration, 2.)Avg. Rate, 3.)Max. Rate, 4.)CR increase over baseline,
% 5.)percent over baseline,

stepcount=0;
flagtrack=0;

if corrlength ~= meanlength
    disp('uh oh')
end

for ii=1:corrlength
    if corrgamma(ii,3) == 1 && flagtrack == 0
        flagtrack=1;
        rstart=corrgamma(ii,2);
        rsindex=ii;
    elseif flagtrack == 1 && corrgamma(ii,3) == 0

        flagtrack=0;

        if rsindex==ii-1
            break
        end

        stepcount=stepcount+1;

        scratchvec(stepcount,1)=corrgamma(ii-1,2)-rstart; %duration
        scratchvec(stepcount,2)=mean(corrgamma(rsindex:ii-1,4)); %avg rate
        scratchvec(stepcount,3)=max(corrgamma(rsindex:ii-1,4)); %max rate
        scratchvec(stepcount,4)=meangamma(ii,1)-baseline; %CR over baeline
        scratchvec(stepcount,5)=scratchvec(stepcount,4)./baseline; %percent over baseline
    end
end
format long
```

```
outvec=scratchvec(1:stepcount,:);
save(filename, 'outvec', '-ascii', '-double')
format short
disp('correlation calculation complete')
```

APPENDIX N

RADIATION PORTAL MONITOR MCNP MODEL

```
c Portal Monitor Environmental Gamma Background Study
c Created by Alexander Solodov, GNSTD, Oak Ridge National Laboratory
c Modified by Christopher Ryan, NSSPI, Texas A&M University
c Further Modified by Stephen Revis, NSSPI, Texas A&M University
c
c * CELL CARDS *
1  1  -2.301    -100 101 -99    imp:p=1 $ Concrete Slab
11 4  -1.032    -112            imp:p=1 $ PVT (Right Lower Detector)
12 4  -1.032    -113            imp:p=1 $ PVT (Right Upper Detector)
14 6  -11.34    -114 112 116    imp:p=1 $ Shielding, Lead (Right Lower Detector)
15 6  -11.34    -115 113 117    imp:p=1 $ Shielding, Lead (Right Upper Detector)
16 7  -1.19     -116            imp:p=1 $ PMMA (Right Lower Detector)
17 7  -1.19     -117            imp:p=1 $ PMMA (Right Upper Detector)
21 4  -1.032    -122            imp:p=1 $ PVT (Left Lower Detector)
22 4  -1.032    -123            imp:p=1 $ PVT (Left Upper Detector)
24 6  -11.34    -124 122 126    imp:p=1 $ Shielding, Lead (Left Lower Detector)
25 6  -11.34    -125 123 127    imp:p=1 $ Shielding, Lead (Left Upper Detector)
26 7  -1.19     -126            imp:p=1 $ PMMA (Left Lower Detector)
27 7  -1.19     -127            imp:p=1 $ PMMA (Left Upper Detector)
c begin new stuff
c right
c 100 1 -2.301  -200 -100 101   imp:p=1 $ concrete under portal (no source here)
110 2 -2.700    -200 100 -210   imp:p=1 $ right portal inner face (Aluminum)
111 5  -7.920  (-220:221:-290:291:211)
               -200 210 100     imp:p=1 $ SS304 (Right Portal, Back & Sides)
112 3 -1.205E-3 210 -211 220 -221
               290 -291 112 113
               114 115          imp:p=1 $ Interior Air (Right Portal Arm)
c left
c 200 1 -2.301   -201 -100 101  imp:p=1 $ concrete under portal (no source here)
210 2 -2.700   -201 100  213    imp:p=1 $ left portal inner face (Aluminum)
211 5  -7.920  (-220:221:-290:291:-212)
               -201 -213 100    imp:p=1 $ SS304 (Left Portal, Back & Sides)
212 3 -1.205E-3 212 -213 220 -221
               290 -291 122 123
               124 125          imp:p=1 $ Interior Air (Left Portal Arm)
c other
998 3 -1.205E-3 100 200 201
                -99             imp:p=1 $ Universe Sphere
999 0           +99:-101        imp:p=0 $ The edge of the universe...
1000 0          903 904         imp:p=1 $ Cookie Cutter Cell
c end new stuff
c * END CELL CARDS *

c * SURFACE CARDS *
100 pz  0      $ top of concrete slab
101 pz  -30.48 $ bottom of concrete slab
112 RPP 269.5 273.5 -24.5 -9.5 23 99 $ right lower detector surf
113 RPP 269.5 273.5 -24.5 -9.5 214 290 $ right upper detertor surf
114 RPP 269.5 274.4525 -25.4525 -8.5475 22.0475 112 $ lead around right lower det surf
115 RPP 269.5 274.4525 -25.4525 -8.5475 201 290.9525 $ lead around right upper det surf
116 RPP 269.5 273.5 -24.5 -9.5 99 112 $ lucite right lower
117 RPP 269.5 273.5 -24.5 -9.5 201 214 $ lucite right upper
122 RPP -273.5 -269.5 -24.5 -9.5 23 99 $ left lower detector surf
```

```
123 RPP -273.5 -269.5 -24.5 -9.5 214 290 $ left upper detector surf
124 RPP -274.4525 -269.5 -25.4525 -8.5475 22.0475 112 $ lead around left lower det surf
125 RPP -274.4525 -269.5 -25.4525 -8.5475 201 290.9525 $ lead around left upper det surf
126 RPP -273.5 -269.5 -24.5 -9.5 99 112 $ lucite left lower
127 RPP -273.5 -269.5 -24.5 -9.5 201 214 $ lucite left upper
c new stuff
200 RPP 254 277 -33 33 -40 304 $ right portal outer
201 RPP -277 -254 -33 33 -40 304 $ left portal outer
210 px 254.3175 $right portal inner face
211 px 276.6825 $right portal outer face
212 px -276.6825 $left portal outer face
213 px -254.3175 $left portal inner face
220 py -32.6825 $ right portal side
221 py  32.6825 $ right portal side
290 pz  0.3175  $ portal bottom
291 pz 303.6825 $ portal top
99 so 4000 $ universe sphere
903 RPP 253.99 277.01 -33.01 33.01 -40.01 304.01 $ right portal ccc
904 RPP -277.01 -253.99 -33.01 33.01 -40.01 304.01 $ left portal ccc
c * END SURFACE CARDS *

c * DATA CARDS *
NPS 1.00E9
c   -- Source Specifications --
c Source
c Located +/- 1mm from surface of concrete (surface 100)
c 3.742:1 initial ratio of Bi-214 to Pb-214
c This source represents the spectrum found 1s after rain ends.
c Source is isotropic
MODE p
SDEF  ERG D2 PAR 2 AXS 0 0 1 VEC 0 0 1 POS 0 0 -0.025 DIR D1 EXT D4 RAD D3
      CCC 1000
si1 -1   0    1 $Isotropic Source
sp1  0   0.5  1
sb1  0   0.1  1
si4  -0.075 0.125 $Pos is not 0 0 0
sp4  0 1          $to avoid placing pos on surface 100
si3  0 2000
sp3  -21 1  $ power law distribution
C      ---------------------------------------------------------------
C      Photon Source Definition - generated from ORIGEN F71 file
C         total strength:  2.2668E11 gammas/second
C         discrete lines:  2.2668E11 gammas/second in 242 lines
C                          100.00% of energy
C         multigroup bins: 0.0000E00 gammas/second in 18 bins
C                          0.00% of energy
C         not counted:     0.0000E00 gammas/second
C      ---------------------------------------------------------------
C
C      discrete lines (in MeV) and their probabilities
si2    l 1.2213E-02 1.2614E-02 1.2614E-02 1.2614E-02 1.3024E-02  $ Bi-210 Tl-206 Po-210 Po-214 Pb-210
         1.3024E-02 1.3446E-02 4.6520E-02 5.3226E-02 7.0832E-02  $ Pb-214 Bi-214 Pb-210 Pb-214 Bi-210
         7.2805E-02 7.2805E-02 7.2805E-02 7.2873E-02 7.4815E-02  $ Tl-206 Po-210 Po-214 Bi-210 Pb-214
         7.4969E-02 7.4969E-02 7.4969E-02 7.6861E-02 7.7107E-02  $ Tl-206 Po-210 Po-214 Bi-214 Pb-214
         7.9291E-02 8.2344E-02 8.4685E-02 8.4694E-02 8.4694E-02  $ Bi-214 Bi-210 Bi-210 Tl-206 Po-210
         8.4694E-02 8.7089E-02 8.7111E-02 8.7111E-02 8.7111E-02  $ Po-214 Pb-214 Tl-206 Po-210 Po-214
         8.9527E-02 8.9588E-02 9.2110E-02 1.3745E-01 1.4130E-01  $ Bi-214 Pb-214 Bi-214 Pb-214 Pb-214
         1.9630E-01 2.4191E-01 2.5879E-01 2.6560E-01 2.7370E-01  $ Pb-214 Pb-214 Pb-214 Bi-210 Bi-214
         2.7453E-01 2.8094E-01 2.8690E-01 2.9517E-01 2.9800E-01  $ Pb-214 Bi-214 Bi-214 Pb-214 Po-214
         3.0443E-01 3.0460E-01 3.0560E-01 3.1420E-01 3.2430E-01  $ Bi-214 Bi-210 Pb-214 Pb-214 Pb-214
         3.3361E-01 3.3490E-01 3.3850E-01 3.4710E-01 3.5190E-01  $ Bi-214 Bi-214 Bi-214 Bi-214 Pb-214
         3.6420E-01 3.7660E-01 3.8700E-01 3.8910E-01 3.9400E-01  $ Bi-214 Bi-214 Bi-214 Bi-214 Bi-214
         3.9601E-01 4.0574E-01 4.2650E-01 4.4040E-01 4.5477E-01  $ Bi-214 Bi-214 Bi-214 Bi-214 Bi-214
         4.6210E-01 4.6969E-01 4.7060E-01 4.7438E-01 4.8042E-01  $ Pb-214 Bi-214 Pb-214 Bi-214 Pb-214
```

```
          4.8708E-01 4.9460E-01 5.0220E-01 5.1100E-01 5.2040E-01  $ Pb-214 Bi-214 Bi-214 Pb-214 Bi-214
          5.2500E-01 5.3369E-01 5.3694E-01 5.3870E-01 5.4340E-01  $ Bi-214 Pb-214 Bi-214 Pb-214 Bi-214
          5.4410E-01 5.4710E-01 5.7283E-01 5.8015E-01 5.9600E-01  $ Pb-214 Bi-214 Bi-214 Pb-214 Bi-214
          6.0932E-01 6.1578E-01 6.1710E-01 6.2640E-01 6.3120E-01  $ Bi-214 Bi-214 Bi-214 Bi-214 Bi-214
          6.3314E-01 6.3937E-01 6.4918E-01 6.6140E-01 6.6545E-01  $ Bi-214 Bi-214 Bi-214 Bi-214 Bi-214
          6.8322E-01 6.8770E-01 6.9330E-01 6.9790E-01 7.0311E-01  $ Bi-214 Bi-214 Bi-214 Bi-214 Bi-214
          7.1080E-01 7.1986E-01 7.2340E-01 7.2780E-01 7.3365E-01  $ Bi-214 Bi-214 Bi-214 Bi-214 Bi-214
          7.4150E-01 7.5284E-01 7.6600E-01 7.6836E-01 7.8591E-01  $ Bi-214 Bi-214 Pb-214 Bi-214 Pb-214
          7.8610E-01 7.9970E-01 7.9976E-01 8.0310E-01 8.0310E-01  $ Bi-214 Po-214 Bi-214 Tl-206 Po-210
          8.0617E-01 8.1508E-01 8.2118E-01 8.2620E-01 8.3235E-01  $ Bi-214 Bi-214 Bi-214 Bi-214 Bi-214
          8.3903E-01 8.4720E-01 9.0425E-01 9.1580E-01 9.3405E-01  $ Pb-214 Bi-214 Bi-214 Bi-214 Bi-214
          9.4330E-01 9.6408E-01 9.7620E-01 9.8920E-01 1.0134E00  $ Bi-214 Bi-214 Bi-214 Bi-214 Bi-214
          1.0205E00 1.0324E00 1.0380E00 1.0454E00 1.0520E00  $ Bi-214 Bi-214 Bi-214 Bi-214 Bi-214
          1.0669E00 1.0700E00 1.1037E00 1.1048E00 1.1203E00  $ Bi-214 Bi-214 Bi-214 Bi-214 Bi-214
          1.1308E00 1.1337E00 1.1552E00 1.1731E00 1.2077E00  $ Bi-214 Bi-214 Bi-214 Bi-214 Bi-214
          1.2268E00 1.2305E00 1.2381E00 1.2810E00 1.3038E00  $ Bi-214 Bi-214 Bi-214 Bi-214 Bi-214
          1.3170E00 1.3300E00 1.3415E00 1.3530E00 1.3777E00  $ Bi-214 Bi-214 Bi-214 Bi-214 Bi-214
          1.3853E00 1.3925E00 1.4015E00 1.4080E00 1.4197E00  $ Bi-214 Bi-214 Bi-214 Bi-214 Bi-214
          1.4711E00 1.4792E00 1.5092E00 1.5385E00 1.5433E00  $ Bi-214 Bi-214 Bi-214 Bi-214 Bi-214
          1.5832E00 1.5947E00 1.5993E00 1.6366E00 1.6574E00  $ Bi-214 Bi-214 Bi-214 Bi-214 Bi-214
          1.6613E00 1.6840E00 1.7296E00 1.7645E00 1.7821E00  $ Bi-214 Bi-214 Bi-214 Bi-214 Bi-214
          1.8137E00 1.8384E00 1.8474E00 1.8732E00 1.8903E00  $ Bi-214 Bi-214 Bi-214 Bi-214 Bi-214
          1.8963E00 1.8987E00 1.9358E00 1.9947E00 2.0045E00  $ Bi-214 Bi-214 Bi-214 Bi-214 Bi-214
          2.0107E00 2.0218E00 2.0529E00 2.0850E00 2.0895E00  $ Bi-214 Bi-214 Bi-214 Bi-214 Bi-214
          2.1099E00 2.1185E00 2.1478E00 2.1768E00 2.1926E00  $ Bi-214 Bi-214 Bi-214 Bi-214 Bi-214
          2.2041E00 2.2512E00 2.2597E00 2.2666E00 2.2700E00  $ Bi-214 Bi-214 Bi-214 Bi-214 Bi-214
          2.2844E00 2.2934E00 2.3122E00 2.3248E00 2.3313E00  $ Bi-214 Bi-214 Bi-214 Bi-214 Bi-214
          2.3609E00 2.3693E00 2.3770E00 2.3909E00 2.4235E00  $ Bi-214 Bi-214 Bi-214 Bi-214 Bi-214
          2.4477E00 2.4828E00 2.5056E00 2.5510E00 2.6045E00  $ Bi-214 Bi-214 Bi-214 Bi-214 Bi-214
          2.6309E00 2.6620E00 2.6948E00 2.6994E00 2.7194E00  $ Bi-214 Bi-214 Bi-214 Bi-214 Bi-214
          2.7700E00 2.7861E00 2.8270E00 2.8609E00 2.8804E00  $ Bi-214 Bi-214 Bi-214 Bi-214 Bi-214
          2.8936E00 2.9221E00 2.9287E00 2.9349E00 2.9400E00  $ Bi-214 Bi-214 Bi-214 Bi-214 Bi-214
          2.9788E00 2.9887E00 3.0000E00 3.0539E00 3.0817E00  $ Bi-214 Bi-214 Bi-214 Bi-214 Bi-214
          3.0939E00 3.1363E00 3.1426E00 3.1605E00 3.1836E00  $ Bi-214 Bi-214 Bi-214 Bi-214 Bi-214
          3.2333E00 3.2697E00                                $ Bi-214 Bi-214
sp2     d 4.4729E-23 3.6645E-28 3.3541E-31 2.3003E-07 1.4604E-10  $ Bi-210 Tl-206 Po-210 Po-214 Pb-210
          2.2506E-02 3.3687E-03 2.4340E-11 1.7956E-03 2.9819E-23  $ Pb-214 Bi-214 Pb-210 Pb-214 Bi-210
          1.2721E-28 2.2392E-31 1.5132E-07 5.0500E-23 1.0454E-02  $ Tl-206 Po-210 Po-214 Bi-210 Pb-214
          2.1254E-28 3.7815E-31 2.5627E-07 2.1421E-03 1.7613E-02  $ Tl-206 Po-210 Po-214 Bi-214 Pb-214
          3.5884E-03 1.7314E-23 4.9538E-24 7.6431E-29 1.3008E-31  $ Bi-214 Bi-210 Bi-210 Tl-206 Po-210
          8.7863E-08 6.0504E-03 1.8322E-29 3.8279E-32 2.5627E-08  $ Po-214 Pb-214 Tl-206 Po-210 Po-214
          1.2389E-03 1.8265E-03 3.8509E-04 9.6187E-05 6.4124E-05  $ Bi-214 Pb-214 Bi-214 Pb-214 Pb-214
          8.0156E-05 1.2168E-02 8.9774E-04 2.1585E-22 1.0796E-03  $ Pb-214 Pb-214 Pb-214 Bi-210 Bi-214
          5.2903E-04 4.9182E-04 1.9793E-04 3.1260E-02 3.0508E-07  $ Pb-214 Bi-214 Bi-214 Pb-214 Po-214
          2.0992E-04 2.7299E-22 3.6872E-05 1.2825E-04 3.2062E-05  $ Bi-214 Bi-210 Pb-214 Pb-214 Pb-214
          5.8179E-04 3.4787E-04 2.3991E-04 3.5987E-04 6.0437E-02  $ Bi-214 Bi-214 Bi-214 Bi-214 Pb-214
          3.8386E-05 2.9989E-05 2.2192E-03 2.5191E-03 5.3980E-05  $ Bi-214 Bi-214 Bi-214 Bi-214 Bi-214
          1.8593E-04 1.0197E-03 6.5977E-04 1.7993E-04 1.9433E-03  $ Bi-214 Bi-214 Bi-214 Bi-214 Bi-214
          2.7253E-04 8.0972E-04 1.6031E-05 7.1976E-04 5.5147E-04  $ Pb-214 Bi-214 Pb-214 Bi-214 Pb-214
          7.1659E-04 5.3980E-05 1.0796E-04 4.8093E-05 3.4787E-05  $ Pb-214 Bi-214 Bi-214 Pb-214 Bi-214
          9.5966E-05 3.0940E-04 4.3185E-04 8.0156E-06 5.1581E-04  $ Bi-214 Pb-214 Bi-214 Pb-214 Bi-214
          3.6872E-05 1.9793E-04 4.9782E-04 5.9315E-04 7.1976E-05  $ Pb-214 Bi-214 Bi-214 Pb-214 Bi-214
          2.8130E-01 4.1985E-04 2.0992E-04 2.9989E-05 1.0197E-04  $ Bi-214 Bi-214 Bi-214 Bi-214 Bi-214
          3.6587E-04 1.9193E-04 3.5987E-04 2.6390E-04 9.5368E-03  $ Bi-214 Bi-214 Bi-214 Bi-214 Bi-214
          4.7983E-04 3.5987E-05 3.5987E-05 2.2791E-04 2.8789E-03  $ Bi-214 Bi-214 Bi-214 Bi-214 Bi-214
          4.5584E-04 2.4591E-03 2.7590E-04 9.5966E-05 2.8789E-04  $ Bi-214 Bi-214 Bi-214 Bi-214 Bi-214
          2.3991E-04 8.0972E-04 1.2825E-04 2.9809E-02 1.7794E-03  $ Bi-214 Bi-214 Pb-214 Bi-214 Pb-214
          1.9193E-03 6.3456E-05 2.5191E-04 3.1992E-29 9.8486E-29  $ Bi-214 Po-214 Bi-214 Tl-206 Po-210
          7.4973E-03 2.4591E-04 9.1768E-04 5.6379E-04 1.3795E-04  $ Bi-214 Bi-214 Bi-214 Bi-214 Bi-214
          9.5706E-04 1.0197E-04 6.4177E-04 1.3795E-04 1.9313E-02  $ Pb-214 Bi-214 Bi-214 Bi-214 Bi-214
          1.0197E-04 2.3391E-03 1.3795E-04 7.1976E-05 5.9978E-05  $ Bi-214 Bi-214 Bi-214 Bi-214 Bi-214
          7.1976E-05 5.8778E-04 1.0197E-04 1.7394E-04 1.9253E-03  $ Bi-214 Bi-214 Bi-214 Bi-214 Bi-214
          1.7394E-04 1.7394E-03 5.9978E-04 4.8582E-04 9.1768E-02  $ Bi-214 Bi-214 Bi-214 Bi-214 Bi-214
          2.7590E-04 1.5535E-03 1.0316E-02 3.5387E-04 2.8070E-03  $ Bi-214 Bi-214 Bi-214 Bi-214 Bi-214
```

```
         1.6194E-04 1.3195E-04 3.6107E-02 8.9967E-03 7.3770E-04  $ Bi-214 Bi-214 Bi-214 Bi-214 Bi-214
         5.2181E-04 6.5977E-05 1.3795E-04 2.7590E-05 2.4531E-02  $ Bi-214 Bi-214 Bi-214 Bi-214 Bi-214
         4.7383E-03 1.1396E-04 8.4566E-03 1.5115E-02 3.1189E-05  $ Bi-214 Bi-214 Bi-214 Bi-214 Bi-214
         7.1976E-05 4.1985E-04 1.3375E-02 2.5191E-03 2.1592E-03  $ Bi-214 Bi-214 Bi-214 Bi-214 Bi-214
         4.3784E-03 1.6194E-03 2.0392E-03 1.1396E-04 4.4984E-04  $ Bi-214 Bi-214 Bi-214 Bi-214 Bi-214
         7.0176E-03 1.4395E-03 1.8593E-02 9.7162E-02 9.5966E-05  $ Bi-214 Bi-214 Bi-214 Bi-214 Bi-214
         7.1976E-05 2.3391E-03 1.2955E-02 1.3795E-03 5.4580E-04  $ Bi-214 Bi-214 Bi-214 Bi-214 Bi-214
         1.0796E-03 3.8386E-04 3.1189E-04 3.2988E-05 1.7993E-05  $ Bi-214 Bi-214 Bi-214 Bi-214 Bi-214
         2.9989E-04 1.1396E-04 4.2585E-04 5.9978E-05 3.4188E-04  $ Bi-214 Bi-214 Bi-214 Bi-214 Bi-214
         5.3380E-04 7.3770E-03 9.5966E-05 2.3991E-05 3.7187E-04  $ Bi-214 Bi-214 Bi-214 Bi-214 Bi-214
         3.0469E-02 4.1985E-05 5.3980E-05 1.0796E-04 1.7993E-05  $ Bi-214 Bi-214 Bi-214 Bi-214 Bi-214
         3.1189E-05 1.9793E-03 7.1976E-05 1.1396E-05 1.3195E-04  $ Bi-214 Bi-214 Bi-214 Bi-214 Bi-214
         1.1396E-05 1.7993E-05 7.1976E-05 1.1996E-05 3.5987E-05  $ Bi-214 Bi-214 Bi-214 Bi-214 Bi-214
         9.4764E-03 1.2596E-05 3.5987E-05 2.3991E-06 2.7590E-06  $ Bi-214 Bi-214 Bi-214 Bi-214 Bi-214
         5.3980E-06 1.7993E-06 1.9793E-04 1.6794E-05 1.0796E-05  $ Bi-214 Bi-214 Bi-214 Bi-214 Bi-214
         1.5594E-04 3.5987E-05 1.4995E-05 2.0992E-06 5.6379E-05  $ Bi-214 Bi-214 Bi-214 Bi-214 Bi-214
         3.8986E-05 9.5966E-05 7.1976E-06 3.4787E-06 1.0197E-05  $ Bi-214 Bi-214 Bi-214 Bi-214 Bi-214
         8.9967E-05 6.5977E-06 5.3980E-05 1.3795E-04 2.6390E-05  $ Bi-214 Bi-214 Bi-214 Bi-214 Bi-214
         3.1189E-06 2.0992E-06 9.5966E-06 3.1189E-06 8.9967E-06  $ Bi-214 Bi-214 Bi-214 Bi-214 Bi-214
         1.1996E-06 5.9978E-07                                   $ Bi-214 Bi-214
c
c   -- Material Specifications --
c
c   -- Concrete --
c
m1    06000 -0.167900  $ Carbon in Concrete
      08000 -0.484500  $ Oxygen in Concrete
      11000 -0.000260  $ Sodium in Concrete
      12000 -0.011900  $ Magnesium in Concrete
      13000 -0.004440  $ Aluminum in Concrete
      14000 -0.015100  $ Silicon in Concrete
      19000 -0.001087  $ Potassium in Concrete
      20000 -0.310100  $ Calcium in Concrete
      25000 -0.000304  $ Manganese in Concrete
      26000 -0.004366  $ Iron in Concrete
c
c   -- Aluminum, Structural 6061 --
c
m2    13000 -0.9685    $ Aluminum
      26000 -0.0070    $ Iron
      29000 -0.0025    $ Copper
      14000 -0.0060    $ Silicon
      12000 -0.0110    $ Magnesium
      24000 -0.0035    $ Chromium
      25000 -0.0015    $ Manganese
c
c   -- Air (suitable for breathing!) --
c
m3    06000 -0.000124  $ Carbon in Air
      07000 -0.755268  $ Nitrogen in Air
      08000 -0.231781  $ Oxygen in Air
      18000 -0.012827  $ Argon in Air
c
c   -- PVT Scintillator --
c
m4    01000 -0.085000   $ Hydrogen in PVT
      06000 -0.915000   $ Carbon in PVT
c
c   -- Germanium Detector --
c m4    32000 -1.000000   $ Germanium Detector
c
c   -- Steel, Stainless 304 --
c
m5    24000 -0.190000   $ Chromium in Steel
```

```
      25000 -0.020000   $ Manganese in Steel
      26000 -0.695000   $ Iron in Steel
      28000 -0.095000   $ Nickel in Steel
c
c   -- Lead --
c
m6    82000 -1.000000   $ Pure lead
c
c   -- PMMA (Light Pipe Lucite) --
c
m7    01000 -0.080538   $ Hydrogen in PMMA
      06000 -0.599848   $ Carbon in PMMA
      08000 -0.319614   $ Oxygen in PMMA
c
c   -- Tallies --
c
F18:P 11                      $ Pulse height tally in RIGHT LOWER detector
E18 0.0 0.00001 0.040 1.0 3.0  $ Energy bins
F28:P 12                      $ Pulse height tally in RIGHT UPPER detector
E28 0.0 0.00001 0.040 1.0 3.0  $ Energy bins
F38:P 21                      $ Pulse height tally in LEFT LOWER detector
E38 0.0 0.00001 0.040 1.0 3.0  $ Energy bins
F48:P 22                      $ Pulse height tally in LEFT UPPER detector
E48 0.0 0.00001 0.040 1.0 3.0  $ Energy bins
c
c * END OF FILE *
```

APPENDIX O

MCNP SIMULATION OF SOURCE WITHIN 2.79M RADIUS OF CENTER OF RPM

```
c Portal Monitor Environmental Gamma Background Study
c Created by Alexander Solodov, GNSTD, Oak Ridge National Laboratory
c Modified by Christopher Ryan, NSSPI, Texas A&M University
c Further Modified by Stephen Revis, NSSPI, Texas A&M University
c
c * CELL CARDS *
1  1  -2.301    -100 101 -99    imp:p=1 $ Concrete Slab
11 4  -1.032    -112            imp:p=1 $ PVT (Right Lower Detector)
12 4  -1.032    -113            imp:p=1 $ PVT (Right Upper Detector)
14 6  -11.34    -114 112 116    imp:p=1 $ Shielding, Lead (Right Lower Detector)
15 6  -11.34    -115 113 117    imp:p=1 $ Shielding, Lead (Right Upper Detector)
16 7  -1.19     -116            imp:p=1 $ PMMA (Right Lower Detector)
17 7  -1.19     -117            imp:p=1 $ PMMA (Right Upper Detector)
21 4  -1.032    -122            imp:p=1 $ PVT (Left Lower Detector)
22 4  -1.032    -123            imp:p=1 $ PVT (Left Upper Detector)
24 6  -11.34    -124 122 126    imp:p=1 $ Shielding, Lead (Left Lower Detector)
25 6  -11.34    -125 123 127    imp:p=1 $ Shielding, Lead (Left Upper Detector)
26 7  -1.19     -126            imp:p=1 $ PMMA (Left Lower Detector)
27 7  -1.19     -127            imp:p=1 $ PMMA (Left Upper Detector)
c begin new stuff
c right
c 100 1 -2.301  -200 -100 101   imp:p=1 $ concrete under portal (no source here)
110 2 -2.700    -200 100 -210   imp:p=1 $ right portal inner face (Aluminum)
111 5  -7.920  (-220:221:-290:291:211)
               -200 210 100     imp:p=1 $ SS304 (Right Portal, Back & Sides)
112 3 -1.205E-3 210 -211 220 -221
               290 -291 112 113
               114 115          imp:p=1 $ Interior Air (Right Portal Arm)
c left
c 200 1 -2.301   -201 -100 101  imp:p=1 $ concrete under portal (no source here)
210 2 -2.700   -201 100  213    imp:p=1 $ left portal inner face (Aluminum)
211 5  -7.920  (-220:221:-290:291:-212)
               -201 -213 100    imp:p=1 $ SS304 (Left Portal, Back & Sides)
212 3 -1.205E-3 212 -213 220 -221
               290 -291 122 123
               124 125          imp:p=1 $ Interior Air (Left Portal Arm)
c other
998 3 -1.205E-3 100 200 201
                -99             imp:p=1 $ Universe Sphere
999 0           +99:-101        imp:p=0 $ The edge of the universe...
1000 0          903 904         imp:p=1 $ Cookie Cutter Cell
c end new stuff
c * END CELL CARDS *

c * SURFACE CARDS *
100 pz  0      $ top of concrete slab
101 pz  -30.48 $ bottom of concrete slab
112 RPP 269.5 273.5 -24.5 -9.5 23 99 $ right lower detector surf
113 RPP 269.5 273.5 -24.5 -9.5 214 290 $ right upper detertor surf
114 RPP 269.5 274.4525 -25.4525 -8.5475 22.0475 112 $ lead around right lower det surf
115 RPP 269.5 274.4525 -25.4525 -8.5475 201 290.9525 $ lead around right upper det surf
```

```
116 RPP 269.5 273.5 -24.5 -9.5 99 112 $ lucite right lower
117 RPP 269.5 273.5 -24.5 -9.5 201 214 $ lucite right upper
122 RPP -273.5 -269.5 -24.5 -9.5 23 99 $ left lower detector surf
123 RPP -273.5 -269.5 -24.5 -9.5 214 290 $ left upper detector surf
124 RPP -274.4525 -269.5 -25.4525 -8.5475 22.0475 112 $ lead around left lower det surf
125 RPP -274.4525 -269.5 -25.4525 -8.5475 201 290.9525 $ lead around left upper det surf
126 RPP -273.5 -269.5 -24.5 -9.5 99 112 $ lucite left lower
127 RPP -273.5 -269.5 -24.5 -9.5 201 214 $ lucite left upper
c new stuff
200 RPP 254 277 -33 33 -40 304 $ right portal outer
201 RPP -277 -254 -33 33 -40 304 $ left portal outer
210 px 254.3175 $right portal inner face
211 px 276.6825 $right portal outer face
212 px -276.6825 $left portal outer face
213 px -254.3175 $left portal inner face
220 py -32.6825 $ right portal side
221 py  32.6825 $ right portal side
290 pz  0.3175  $ portal bottom
291 pz 303.6825 $ portal top
99 so 4000 $ universe sphere
903 RPP 253.99 277.01 -33.01 33.01 -40.01 304.01 $ right portal ccc
904 RPP -277.01 -253.99 -33.01 33.01 -40.01 304.01 $ left portal ccc
c * END SURFACE CARDS *

c * DATA CARDS *
NPS 1.00E9
c   -- Source Specifications --
c Source
c Located +/- 1mm from surface of concrete (surface 100)
c 3.742:1 initial ratio of Bi-214 to Pb-214
c This source represents the spectrum found 1s after rain ends.
c Source is isotropic
MODE p
SDEF  ERG D2 PAR 2 AXS 0 0 1 VEC 0 0 1 POS 0 0 -0.025 DIR D1 EXT D4 RAD D3
      CCC 1000
si1 -1   0    1 $Isotropic Source
sp1  0   0.5  1
sb1  0   0.1  1
si4  -0.075 0.125 $Pos is not 0 0 0
sp4  0 1          $to avoid placing pos on surface 100
si3  0 279
sp3  -21 1  $ power law distribution
C      ---------------------------------------------------------------
C      Photon Source Definition - generated from ORIGEN F71 file
C         total strength:  2.2668E11 gammas/second
C         discrete lines:  2.2668E11 gammas/second in 242 lines
C                          100.00% of energy
C         multigroup bins: 0.0000E00 gammas/second in 18 bins
C                          0.00% of energy
C         not counted:     0.0000E00 gammas/second
C      ---------------------------------------------------------------
C
C      discrete lines (in MeV) and their probabilities
si2    l 1.2213E-02 1.2614E-02 1.2614E-02 1.2614E-02 1.3024E-02  $ Bi-210 Tl-206 Po-210 Po-214 Pb-210
         1.3024E-02 1.3446E-02 4.6520E-02 5.3226E-02 7.0832E-02  $ Pb-214 Bi-214 Pb-210 Pb-214 Bi-210
         7.2805E-02 7.2805E-02 7.2805E-02 7.2873E-02 7.4815E-02  $ Tl-206 Po-210 Po-214 Bi-210 Pb-214
         7.4969E-02 7.4969E-02 7.4969E-02 7.6861E-02 7.7107E-02  $ Tl-206 Po-210 Po-214 Bi-214 Pb-214
         7.9291E-02 8.2344E-02 8.4685E-02 8.4694E-02 8.4694E-02  $ Bi-214 Bi-210 Bi-210 Tl-206 Po-210
         8.4694E-02 8.7089E-02 8.7111E-02 8.7111E-02 8.7111E-02  $ Po-214 Pb-214 Tl-206 Po-210 Po-214
         8.9527E-02 8.9588E-02 9.2110E-02 1.3745E-01 1.4130E-01  $ Bi-214 Pb-214 Bi-214 Pb-214 Pb-214
         1.9630E-01 2.4191E-01 2.5879E-01 2.6560E-01 2.7370E-01  $ Pb-214 Pb-214 Pb-214 Bi-210 Bi-214
         2.7453E-01 2.8094E-01 2.8690E-01 2.9517E-01 2.9800E-01  $ Pb-214 Bi-214 Bi-214 Pb-214 Po-214
         3.0443E-01 3.0460E-01 3.0560E-01 3.1420E-01 3.2430E-01  $ Bi-214 Bi-210 Pb-214 Pb-214 Pb-214
         3.3361E-01 3.3490E-01 3.3850E-01 3.4710E-01 3.5190E-01  $ Bi-214 Bi-214 Bi-214 Bi-214 Pb-214
```

```
          3.6420E-01 3.7660E-01 3.8700E-01 3.8910E-01 3.9400E-01  $ Bi-214 Bi-214 Bi-214 Bi-214 Bi-214
          3.9601E-01 4.0574E-01 4.2650E-01 4.4040E-01 4.5477E-01  $ Bi-214 Bi-214 Bi-214 Bi-214 Bi-214
          4.6210E-01 4.6969E-01 4.7060E-01 4.7438E-01 4.8042E-01  $ Pb-214 Bi-214 Pb-214 Bi-214 Pb-214
          4.8708E-01 4.9460E-01 5.0220E-01 5.1100E-01 5.2040E-01  $ Pb-214 Bi-214 Bi-214 Pb-214 Bi-214
          5.2500E-01 5.3369E-01 5.3694E-01 5.3870E-01 5.4340E-01  $ Bi-214 Pb-214 Bi-214 Pb-214 Bi-214
          5.4410E-01 5.4710E-01 5.7283E-01 5.8015E-01 5.9600E-01  $ Pb-214 Bi-214 Bi-214 Pb-214 Bi-214
          6.0932E-01 6.1578E-01 6.1710E-01 6.2640E-01 6.3120E-01  $ Bi-214 Bi-214 Bi-214 Bi-214 Bi-214
          6.3314E-01 6.3937E-01 6.4918E-01 6.6140E-01 6.6545E-01  $ Bi-214 Bi-214 Bi-214 Bi-214 Bi-214
          6.8322E-01 6.8770E-01 6.9330E-01 6.9790E-01 7.0311E-01  $ Bi-214 Bi-214 Bi-214 Bi-214 Bi-214
          7.1080E-01 7.1986E-01 7.2340E-01 7.2780E-01 7.3365E-01  $ Bi-214 Bi-214 Bi-214 Bi-214 Bi-214
          7.4150E-01 7.5284E-01 7.6600E-01 7.6836E-01 7.8591E-01  $ Bi-214 Bi-214 Pb-214 Bi-214 Pb-214
          7.8610E-01 7.9970E-01 7.9976E-01 8.0310E-01 8.0310E-01  $ Bi-214 Po-214 Bi-214 Tl-206 Po-210
          8.0617E-01 8.1508E-01 8.2118E-01 8.2620E-01 8.3235E-01  $ Bi-214 Bi-214 Bi-214 Bi-214 Bi-214
          8.3903E-01 8.4720E-01 9.0425E-01 9.1580E-01 9.3405E-01  $ Pb-214 Bi-214 Bi-214 Bi-214 Bi-214
          9.4330E-01 9.6408E-01 9.7620E-01 9.8920E-01 1.0134E00  $ Bi-214 Bi-214 Bi-214 Bi-214 Bi-214
          1.0205E00 1.0324E00 1.0380E00 1.0454E00 1.0520E00  $ Bi-214 Bi-214 Bi-214 Bi-214 Bi-214
          1.0669E00 1.0700E00 1.1037E00 1.1048E00 1.1203E00  $ Bi-214 Bi-214 Bi-214 Bi-214 Bi-214
          1.1308E00 1.1337E00 1.1552E00 1.1731E00 1.2077E00  $ Bi-214 Bi-214 Bi-214 Bi-214 Bi-214
          1.2268E00 1.2305E00 1.2381E00 1.2810E00 1.3038E00  $ Bi-214 Bi-214 Bi-214 Bi-214 Bi-214
          1.3170E00 1.3300E00 1.3415E00 1.3530E00 1.3777E00  $ Bi-214 Bi-214 Bi-214 Bi-214 Bi-214
          1.3853E00 1.3925E00 1.4015E00 1.4080E00 1.4197E00  $ Bi-214 Bi-214 Bi-214 Bi-214 Bi-214
          1.4711E00 1.4792E00 1.5092E00 1.5385E00 1.5433E00  $ Bi-214 Bi-214 Bi-214 Bi-214 Bi-214
          1.5832E00 1.5947E00 1.5993E00 1.6366E00 1.6574E00  $ Bi-214 Bi-214 Bi-214 Bi-214 Bi-214
          1.6613E00 1.6840E00 1.7296E00 1.7645E00 1.7821E00  $ Bi-214 Bi-214 Bi-214 Bi-214 Bi-214
          1.8137E00 1.8384E00 1.8474E00 1.8732E00 1.8903E00  $ Bi-214 Bi-214 Bi-214 Bi-214 Bi-214
          1.8963E00 1.8987E00 1.9358E00 1.9947E00 2.0045E00  $ Bi-214 Bi-214 Bi-214 Bi-214 Bi-214
          2.0107E00 2.0218E00 2.0529E00 2.0850E00 2.0895E00  $ Bi-214 Bi-214 Bi-214 Bi-214 Bi-214
          2.1099E00 2.1185E00 2.1478E00 2.1768E00 2.1926E00  $ Bi-214 Bi-214 Bi-214 Bi-214 Bi-214
          2.2041E00 2.2512E00 2.2597E00 2.2666E00 2.2700E00  $ Bi-214 Bi-214 Bi-214 Bi-214 Bi-214
          2.2844E00 2.2934E00 2.3122E00 2.3248E00 2.3313E00  $ Bi-214 Bi-214 Bi-214 Bi-214 Bi-214
          2.3609E00 2.3693E00 2.3770E00 2.3909E00 2.4235E00  $ Bi-214 Bi-214 Bi-214 Bi-214 Bi-214
          2.4477E00 2.4828E00 2.5056E00 2.5510E00 2.6045E00  $ Bi-214 Bi-214 Bi-214 Bi-214 Bi-214
          2.6309E00 2.6620E00 2.6948E00 2.6994E00 2.7194E00  $ Bi-214 Bi-214 Bi-214 Bi-214 Bi-214
          2.7700E00 2.7861E00 2.8270E00 2.8609E00 2.8804E00  $ Bi-214 Bi-214 Bi-214 Bi-214 Bi-214
          2.8936E00 2.9221E00 2.9287E00 2.9349E00 2.9400E00  $ Bi-214 Bi-214 Bi-214 Bi-214 Bi-214
          2.9788E00 2.9887E00 3.0000E00 3.0539E00 3.0817E00  $ Bi-214 Bi-214 Bi-214 Bi-214 Bi-214
          3.0939E00 3.1363E00 3.1426E00 3.1605E00 3.1836E00  $ Bi-214 Bi-214 Bi-214 Bi-214 Bi-214
          3.2333E00 3.2697E00                                $ Bi-214 Bi-214
sp2     d 4.4729E-23 3.6645E-28 3.3541E-31 2.3003E-07 1.4604E-10  $ Bi-210 Tl-206 Po-210 Po-214 Pb-210
          2.2506E-02 3.3687E-03 2.4340E-11 1.7956E-03 2.9819E-23  $ Pb-214 Bi-214 Pb-210 Pb-214 Bi-210
          1.2721E-28 2.2392E-31 1.5132E-07 5.0500E-23 1.0454E-02  $ Tl-206 Po-210 Po-214 Bi-210 Pb-214
          2.1254E-28 3.7815E-31 2.5627E-07 2.1421E-03 1.7613E-02  $ Tl-206 Po-210 Po-214 Bi-214 Pb-214
          3.5884E-03 1.7314E-23 4.9538E-24 7.6431E-29 1.3008E-31  $ Bi-214 Bi-210 Bi-210 Tl-206 Po-210
          8.7863E-08 6.0504E-03 1.8322E-29 3.8279E-32 2.5627E-08  $ Po-214 Pb-214 Tl-206 Po-210 Po-214
          1.2389E-03 1.8265E-03 3.8509E-04 9.6187E-05 6.4124E-05  $ Bi-214 Pb-214 Bi-214 Pb-214 Pb-214
          8.0156E-05 1.2168E-02 8.9774E-04 2.1585E-22 1.0796E-03  $ Pb-214 Pb-214 Pb-214 Bi-210 Bi-214
          5.2903E-04 4.9182E-04 1.9793E-04 3.1260E-02 3.0508E-07  $ Pb-214 Bi-214 Bi-214 Pb-214 Po-214
          2.0992E-04 2.7299E-22 3.6872E-05 1.2825E-04 3.2062E-05  $ Bi-214 Bi-210 Pb-214 Pb-214 Pb-214
          5.8179E-04 3.4787E-04 2.3991E-04 3.5987E-04 6.0437E-02  $ Bi-214 Bi-214 Bi-214 Bi-214 Pb-214
          3.8386E-05 2.9989E-05 2.2192E-03 2.5191E-03 5.3980E-05  $ Bi-214 Bi-214 Bi-214 Bi-214 Bi-214
          1.8593E-04 1.0197E-03 6.5977E-04 1.7993E-04 1.9433E-03  $ Bi-214 Bi-214 Bi-214 Bi-214 Bi-214
          2.7253E-04 8.0972E-04 1.6031E-05 7.1976E-04 5.5147E-04  $ Pb-214 Bi-214 Pb-214 Bi-214 Pb-214
          7.1659E-04 5.3980E-05 1.0796E-04 4.8093E-05 3.4787E-05  $ Pb-214 Bi-214 Bi-214 Pb-214 Bi-214
          9.5966E-05 3.0940E-04 4.3185E-04 8.0156E-06 5.1581E-04  $ Bi-214 Pb-214 Bi-214 Pb-214 Bi-214
          3.6872E-05 1.9793E-04 4.9782E-04 5.9315E-04 7.1976E-05  $ Pb-214 Bi-214 Bi-214 Pb-214 Bi-214
          2.8130E-01 4.1985E-04 2.0992E-04 2.9989E-05 1.0197E-04  $ Bi-214 Bi-214 Bi-214 Bi-214 Bi-214
          3.6587E-04 1.9193E-04 3.5987E-04 2.6390E-04 9.5368E-03  $ Bi-214 Bi-214 Bi-214 Bi-214 Bi-214
          4.7983E-04 3.5987E-05 3.5987E-05 2.2791E-04 2.8789E-03  $ Bi-214 Bi-214 Bi-214 Bi-214 Bi-214
          4.5584E-04 2.4591E-03 2.7590E-04 9.5966E-05 2.8789E-04  $ Bi-214 Bi-214 Bi-214 Bi-214 Bi-214
          2.3991E-04 8.0972E-04 1.2825E-04 2.9809E-02 1.7794E-03  $ Bi-214 Bi-214 Pb-214 Bi-214 Pb-214
          1.9193E-03 6.3456E-05 2.5191E-04 3.1992E-29 9.8486E-29  $ Bi-214 Po-214 Bi-214 Tl-206 Po-210
          7.4973E-03 2.4591E-04 9.1768E-04 5.6379E-04 1.3795E-04  $ Bi-214 Bi-214 Bi-214 Bi-214 Bi-214
          9.5706E-04 1.0197E-04 6.4177E-04 1.3795E-04 1.9313E-02  $ Pb-214 Bi-214 Bi-214 Bi-214 Bi-214
          1.0197E-04 2.3391E-03 1.3795E-04 7.1976E-05 5.9978E-05  $ Bi-214 Bi-214 Bi-214 Bi-214 Bi-214
```

```
         7.1976E-05 5.8778E-04 1.0197E-04 1.7394E-04 1.9253E-03  $ Bi-214 Bi-214 Bi-214 Bi-214 Bi-214
         1.7394E-04 1.7394E-03 5.9978E-04 4.8582E-04 9.1768E-02  $ Bi-214 Bi-214 Bi-214 Bi-214 Bi-214
         2.7590E-04 1.5535E-03 1.0316E-02 3.5387E-04 2.8070E-03  $ Bi-214 Bi-214 Bi-214 Bi-214 Bi-214
         1.6194E-04 1.3195E-04 3.6107E-02 8.9967E-03 7.3770E-04  $ Bi-214 Bi-214 Bi-214 Bi-214 Bi-214
         5.2181E-04 6.5977E-05 1.3795E-04 2.7590E-05 2.4531E-02  $ Bi-214 Bi-214 Bi-214 Bi-214 Bi-214
         4.7383E-03 1.1396E-04 8.4566E-03 1.5115E-02 3.1189E-05  $ Bi-214 Bi-214 Bi-214 Bi-214 Bi-214
         7.1976E-05 4.1985E-04 1.3375E-02 2.5191E-03 2.1592E-03  $ Bi-214 Bi-214 Bi-214 Bi-214 Bi-214
         4.3784E-03 1.6194E-03 2.0392E-03 1.1396E-04 4.4984E-04  $ Bi-214 Bi-214 Bi-214 Bi-214 Bi-214
         7.0176E-03 1.4395E-03 1.8593E-02 9.7162E-02 9.5966E-05  $ Bi-214 Bi-214 Bi-214 Bi-214 Bi-214
         7.1976E-05 2.3391E-03 1.2955E-02 1.3795E-03 5.4580E-04  $ Bi-214 Bi-214 Bi-214 Bi-214 Bi-214
         1.0796E-03 3.8386E-04 3.1189E-04 3.2988E-05 1.7993E-05  $ Bi-214 Bi-214 Bi-214 Bi-214 Bi-214
         2.9989E-04 1.1396E-04 4.2585E-04 5.9978E-05 3.4188E-04  $ Bi-214 Bi-214 Bi-214 Bi-214 Bi-214
         5.3380E-04 7.3770E-03 9.5966E-05 2.3991E-05 3.7187E-04  $ Bi-214 Bi-214 Bi-214 Bi-214 Bi-214
         3.0469E-02 4.1985E-05 5.3980E-05 1.0796E-04 1.7993E-05  $ Bi-214 Bi-214 Bi-214 Bi-214 Bi-214
         3.1189E-05 1.9793E-03 7.1976E-05 1.1396E-05 1.3195E-04  $ Bi-214 Bi-214 Bi-214 Bi-214 Bi-214
         1.1396E-05 1.7993E-05 7.1976E-05 1.1996E-05 3.5987E-05  $ Bi-214 Bi-214 Bi-214 Bi-214 Bi-214
         9.4764E-03 1.2596E-05 3.5987E-05 2.3991E-06 2.7590E-06  $ Bi-214 Bi-214 Bi-214 Bi-214 Bi-214
         5.3980E-06 1.7993E-06 1.9793E-04 1.6794E-05 1.0796E-05  $ Bi-214 Bi-214 Bi-214 Bi-214 Bi-214
         1.5594E-04 3.5987E-05 1.4995E-05 2.0992E-06 5.6379E-05  $ Bi-214 Bi-214 Bi-214 Bi-214 Bi-214
         3.8986E-05 9.5966E-05 7.1976E-06 3.4787E-06 1.0197E-05  $ Bi-214 Bi-214 Bi-214 Bi-214 Bi-214
         8.9967E-05 6.5977E-06 5.3980E-05 1.3795E-04 2.6390E-05  $ Bi-214 Bi-214 Bi-214 Bi-214 Bi-214
         3.1189E-06 2.0992E-06 9.5966E-06 3.1189E-06 8.9967E-06  $ Bi-214 Bi-214 Bi-214 Bi-214 Bi-214
         1.1996E-06 5.9978E-07                                   $ Bi-214 Bi-214
c
c   -- Material Specifications --
c
c   -- Concrete --
c
m1    06000 -0.167900  $ Carbon in Concrete
      08000 -0.484500  $ Oxygen in Concrete
      11000 -0.000260  $ Sodium in Concrete
      12000 -0.011900  $ Magnesium in Concrete
      13000 -0.004440  $ Aluminum in Concrete
      14000 -0.015100  $ Silicon in Concrete
      19000 -0.001087  $ Potassium in Concrete
      20000 -0.310100  $ Calcium in Concrete
      25000 -0.000304  $ Manganese in Concrete
      26000 -0.004366  $ Iron in Concrete
c
c   -- Aluminum, Structural 6061 --
c
m2    13000 -0.9685    $ Aluminum
      26000 -0.0070    $ Iron
      29000 -0.0025    $ Copper
      14000 -0.0060    $ Silicon
      12000 -0.0110    $ Magnesium
      24000 -0.0035    $ Chromium
      25000 -0.0015    $ Manganese
c
c   -- Air (suitable for breathing!) --
c
m3    06000 -0.000124  $ Carbon in Air
      07000 -0.755268  $ Nitrogen in Air
      08000 -0.231781  $ Oxygen in Air
      18000 -0.012827  $ Argon in Air
c
c   -- PVT Scintillator --
c
m4    01000 -0.085000   $ Hydrogen in PVT
      06000 -0.915000   $ Carbon in PVT
c
c   -- Germanium Detector --
c m4    32000 -1.000000   $ Germanium Detector
c
```

```
c   -- Steel, Stainless 304 --
c
m5    24000 -0.190000   $ Chromium in Steel
      25000 -0.020000   $ Manganese in Steel
      26000 -0.695000   $ Iron in Steel
      28000 -0.095000   $ Nickel in Steel
c
c   -- Lead --
c
m6    82000 -1.000000   $ Pure lead
c
c   -- PMMA (Light Pipe Lucite) --
c
m7    01000 -0.080538   $ Hydrogen in PMMA
      06000 -0.599848   $ Carbon in PMMA
      08000 -0.319614   $ Oxygen in PMMA
c
c   -- Tallies --
c
F18:P 11                      $ Pulse height tally in RIGHT LOWER detector
E18 0.0 0.00001 0.040 1.0 3.0  $ Energy bins
F28:P 12                      $ Pulse height tally in RIGHT UPPER detector
E28 0.0 0.00001 0.040 1.0 3.0  $ Energy bins
F38:P 21                      $ Pulse height tally in LEFT LOWER detector
E38 0.0 0.00001 0.040 1.0 3.0  $ Energy bins
F48:P 22                      $ Pulse height tally in LEFT UPPER detector
E48 0.0 0.00001 0.040 1.0 3.0  $ Energy bins
c
c * END OF FILE *
```

APPENDIX P

MCNP SIMULATION OF SOURCE OF RADIUS FROM 2.79 M TO 20 M FROM CENTER OF RPM

```
c Portal Monitor Environmental Gamma Background Study
c Created by Alexander Solodov, GNSTD, Oak Ridge National Laboratory
c Modified by Christopher Ryan, NSSPI, Texas A&M University
c Further Modified by Stephen Revis, NSSPI, Texas A&M University
c
c * CELL CARDS *
1  1  -2.301    -100 101 -99    imp:p=1 $ Concrete Slab
11 4  -1.032    -112            imp:p=1 $ PVT (Right Lower Detector)
12 4  -1.032    -113            imp:p=1 $ PVT (Right Upper Detector)
14 6  -11.34    -114 112 116    imp:p=1 $ Shielding, Lead (Right Lower Detector)
15 6  -11.34    -115 113 117    imp:p=1 $ Shielding, Lead (Right Upper Detector)
16 7  -1.19     -116            imp:p=1 $ PMMA (Right Lower Detector)
17 7  -1.19     -117            imp:p=1 $ PMMA (Right Upper Detector)
21 4  -1.032    -122            imp:p=1 $ PVT (Left Lower Detector)
22 4  -1.032    -123            imp:p=1 $ PVT (Left Upper Detector)
24 6  -11.34    -124 122 126    imp:p=1 $ Shielding, Lead (Left Lower Detector)
25 6  -11.34    -125 123 127    imp:p=1 $ Shielding, Lead (Left Upper Detector)
26 7  -1.19     -126            imp:p=1 $ PMMA (Left Lower Detector)
27 7  -1.19     -127            imp:p=1 $ PMMA (Left Upper Detector)
c begin new stuff
c right
c 100 1 -2.301  -200 -100 101   imp:p=1 $ concrete under portal (no source here)
110 2 -2.700    -200 100 -210   imp:p=1 $ right portal inner face (Aluminum)
111 5  -7.920  (-220:221:-290:291:211)
               -200 210 100     imp:p=1 $ SS304 (Right Portal, Back & Sides)
112 3 -1.205E-3 210 -211 220 -221
               290 -291 112 113
               114 115          imp:p=1 $ Interior Air (Right Portal Arm)
c left
c 200 1 -2.301   -201 -100 101  imp:p=1 $ concrete under portal (no source here)
210 2 -2.700   -201 100  213    imp:p=1 $ left portal inner face (Aluminum)
211 5  -7.920  (-220:221:-290:291:-212)
               -201 -213 100    imp:p=1 $ SS304 (Left Portal, Back & Sides)
212 3 -1.205E-3 212 -213 220 -221
               290 -291 122 123
               124 125          imp:p=1 $ Interior Air (Left Portal Arm)
c other
998 3 -1.205E-3 100 200 201
                -99         imp:p=1 $ Universe Sphere
999 0           +99:-101        imp:p=0 $ The edge of the universe...
c end new stuff
c * END CELL CARDS *

c * SURFACE CARDS *
100 pz  0      $ top of concrete slab
101 pz  -30.48 $ bottom of concrete slab
112 RPP 269.5 273.5 -24.5 -9.5 23 99 $ right lower detector surf
113 RPP 269.5 273.5 -24.5 -9.5 214 290 $ right upper detertor surf
114 RPP 269.5 274.4525 -25.4525 -8.5475 22.0475 112 $ lead around right lower det surf
115 RPP 269.5 274.4525 -25.4525 -8.5475 201 290.9525 $ lead around right upper det surf
116 RPP 269.5 273.5 -24.5 -9.5 99 112 $ lucite right lower
```

```
117 RPP 269.5 273.5 -24.5 -9.5 201 214 $ lucite right upper
122 RPP -273.5 -269.5 -24.5 -9.5 23 99 $ left lower detector surf
123 RPP -273.5 -269.5 -24.5 -9.5 214 290 $ left upper detector surf
124 RPP -274.4525 -269.5 -25.4525 -8.5475 22.0475 112 $ lead around left lower det surf
125 RPP -274.4525 -269.5 -25.4525 -8.5475 201 290.9525 $ lead around left upper det surf
126 RPP -273.5 -269.5 -24.5 -9.5 99 112 $ lucite left lower
127 RPP -273.5 -269.5 -24.5 -9.5 201 214 $ lucite left upper
c new stuff
200 RPP 254 277 -33 33 -40 304 $ right portal outer
201 RPP -277 -254 -33 33 -40 304 $ left portal outer
210 px 254.3175 $right portal inner face
211 px 276.6825 $right portal outer face
212 px -276.6825 $left portal outer face
213 px -254.3175 $left portal inner face
220 py -32.6825 $ right portal side
221 py  32.6825 $ right portal side
290 pz  0.3175  $ portal bottom
291 pz 303.6825 $ portal top
99 so 4000 $ universe sphere
903 RPP 253.99 277.01 -33.01 33.01 -40.01 304.01 $ right portal ccc
904 RPP -277.01 -253.99 -33.01 33.01 -40.01 304.01 $ left portal ccc
c * END SURFACE CARDS *

c * DATA CARDS *
NPS 1.00E9
c   -- Source Specifications --
c Source
c Located +/- 1mm from surface of concrete (surface 100)
c 3.742:1 initial ratio of Bi-214 to Pb-214
c This source represents the spectrum found 1s after rain ends.
c Source is isotropic
MODE p
SDEF  ERG D2 PAR 2 AXS 0 0 1 VEC 0 0 1 POS 0 0 -0.025 DIR D1 EXT D4 RAD D3
si1 -1   0    1 $Isotropic Source
sp1  0   0.5  1
sb1  0   0.1  1
si4  -0.075 0.125 $Pos is not 0 0 0
sp4  0 1          $to avoid placing pos on surface 100
si3  279 2000
sp3  -21 1  $ power law distribution
C      ---------------------------------------------------------------
C      Photon Source Definition - generated from ORIGEN F71 file
C         total strength:  2.2668E11 gammas/second
C         discrete lines:  2.2668E11 gammas/second in 242 lines
C                          100.00% of energy
C         multigroup bins: 0.0000E00 gammas/second in 18 bins
C                          0.00% of energy
C         not counted:     0.0000E00 gammas/second
C      ---------------------------------------------------------------
C
C      discrete lines (in MeV) and their probabilities
si2    l 1.2213E-02 1.2614E-02 1.2614E-02 1.2614E-02 1.3024E-02  $ Bi-210 Tl-206 Po-210 Po-214 Pb-210
         1.3024E-02 1.3446E-02 4.6520E-02 5.3226E-02 7.0832E-02  $ Pb-214 Bi-214 Pb-210 Pb-214 Bi-210
         7.2805E-02 7.2805E-02 7.2805E-02 7.2873E-02 7.4815E-02  $ Tl-206 Po-210 Po-214 Bi-210 Pb-214
         7.4969E-02 7.4969E-02 7.4969E-02 7.6861E-02 7.7107E-02  $ Tl-206 Po-210 Po-214 Bi-214 Pb-214
         7.9291E-02 8.2344E-02 8.4685E-02 8.4694E-02 8.4694E-02  $ Bi-214 Bi-210 Bi-210 Tl-206 Po-210
         8.4694E-02 8.7089E-02 8.7111E-02 8.7111E-02 8.7111E-02  $ Po-214 Pb-214 Tl-206 Po-210 Po-214
         8.9527E-02 8.9588E-02 9.2110E-02 1.3745E-01 1.4130E-01  $ Bi-214 Pb-214 Bi-214 Pb-214 Pb-214
         1.9630E-01 2.4191E-01 2.5879E-01 2.6560E-01 2.7370E-01  $ Pb-214 Pb-214 Pb-214 Bi-210 Bi-214
         2.7453E-01 2.8094E-01 2.8690E-01 2.9517E-01 2.9800E-01  $ Pb-214 Bi-214 Bi-214 Pb-214 Po-214
         3.0443E-01 3.0460E-01 3.0560E-01 3.1420E-01 3.2430E-01  $ Bi-214 Bi-210 Pb-214 Pb-214 Pb-214
         3.3361E-01 3.3490E-01 3.3850E-01 3.4710E-01 3.5190E-01  $ Bi-214 Bi-214 Bi-214 Bi-214 Pb-214
         3.6420E-01 3.7660E-01 3.8700E-01 3.8910E-01 3.9400E-01  $ Bi-214 Bi-214 Bi-214 Bi-214 Bi-214
         3.9601E-01 4.0574E-01 4.2650E-01 4.4040E-01 4.5477E-01  $ Bi-214 Bi-214 Bi-214 Bi-214 Bi-214
```

```
          4.6210E-01 4.6969E-01 4.7060E-01 4.7438E-01 4.8042E-01  $ Pb-214 Bi-214 Pb-214 Bi-214 Pb-214
          4.8708E-01 4.9460E-01 5.0220E-01 5.1100E-01 5.2040E-01  $ Pb-214 Bi-214 Bi-214 Pb-214 Bi-214
          5.2500E-01 5.3369E-01 5.3694E-01 5.3870E-01 5.4340E-01  $ Bi-214 Pb-214 Bi-214 Pb-214 Bi-214
          5.4410E-01 5.4710E-01 5.7283E-01 5.8015E-01 5.9600E-01  $ Pb-214 Bi-214 Bi-214 Pb-214 Bi-214
          6.0932E-01 6.1578E-01 6.1710E-01 6.2640E-01 6.3120E-01  $ Bi-214 Bi-214 Bi-214 Bi-214 Bi-214
          6.3314E-01 6.3937E-01 6.4918E-01 6.6140E-01 6.6545E-01  $ Bi-214 Bi-214 Bi-214 Bi-214 Bi-214
          6.8322E-01 6.8770E-01 6.9330E-01 6.9790E-01 7.0311E-01  $ Bi-214 Bi-214 Bi-214 Bi-214 Bi-214
          7.1080E-01 7.1986E-01 7.2340E-01 7.2780E-01 7.3365E-01  $ Bi-214 Bi-214 Bi-214 Bi-214 Bi-214
          7.4150E-01 7.5284E-01 7.6600E-01 7.6836E-01 7.8591E-01  $ Bi-214 Bi-214 Pb-214 Bi-214 Pb-214
          7.8610E-01 7.9970E-01 7.9976E-01 8.0310E-01 8.0310E-01  $ Bi-214 Po-214 Bi-214 Tl-206 Po-210
          8.0617E-01 8.1508E-01 8.2118E-01 8.2620E-01 8.3235E-01  $ Bi-214 Bi-214 Bi-214 Bi-214 Bi-214
          8.3903E-01 8.4720E-01 9.0425E-01 9.1580E-01 9.3405E-01  $ Pb-214 Bi-214 Bi-214 Bi-214 Bi-214
          9.4330E-01 9.6408E-01 9.7620E-01 9.8920E-01 1.0134E00  $ Bi-214 Bi-214 Bi-214 Bi-214 Bi-214
          1.0205E00 1.0324E00 1.0380E00 1.0454E00 1.0520E00  $ Bi-214 Bi-214 Bi-214 Bi-214 Bi-214
          1.0669E00 1.0700E00 1.1037E00 1.1048E00 1.1203E00  $ Bi-214 Bi-214 Bi-214 Bi-214 Bi-214
          1.1308E00 1.1337E00 1.1552E00 1.1731E00 1.2077E00  $ Bi-214 Bi-214 Bi-214 Bi-214 Bi-214
          1.2268E00 1.2305E00 1.2381E00 1.2810E00 1.3038E00  $ Bi-214 Bi-214 Bi-214 Bi-214 Bi-214
          1.3170E00 1.3300E00 1.3415E00 1.3530E00 1.3777E00  $ Bi-214 Bi-214 Bi-214 Bi-214 Bi-214
          1.3853E00 1.3925E00 1.4015E00 1.4080E00 1.4197E00  $ Bi-214 Bi-214 Bi-214 Bi-214 Bi-214
          1.4711E00 1.4792E00 1.5092E00 1.5385E00 1.5433E00  $ Bi-214 Bi-214 Bi-214 Bi-214 Bi-214
          1.5832E00 1.5947E00 1.5993E00 1.6366E00 1.6574E00  $ Bi-214 Bi-214 Bi-214 Bi-214 Bi-214
          1.6613E00 1.6840E00 1.7296E00 1.7645E00 1.7821E00  $ Bi-214 Bi-214 Bi-214 Bi-214 Bi-214
          1.8137E00 1.8384E00 1.8474E00 1.8732E00 1.8903E00  $ Bi-214 Bi-214 Bi-214 Bi-214 Bi-214
          1.8963E00 1.8987E00 1.9358E00 1.9947E00 2.0045E00  $ Bi-214 Bi-214 Bi-214 Bi-214 Bi-214
          2.0107E00 2.0218E00 2.0529E00 2.0850E00 2.0895E00  $ Bi-214 Bi-214 Bi-214 Bi-214 Bi-214
          2.1099E00 2.1185E00 2.1478E00 2.1768E00 2.1926E00  $ Bi-214 Bi-214 Bi-214 Bi-214 Bi-214
          2.2041E00 2.2512E00 2.2597E00 2.2666E00 2.2700E00  $ Bi-214 Bi-214 Bi-214 Bi-214 Bi-214
          2.2844E00 2.2934E00 2.3122E00 2.3248E00 2.3313E00  $ Bi-214 Bi-214 Bi-214 Bi-214 Bi-214
          2.3609E00 2.3693E00 2.3770E00 2.3909E00 2.4235E00  $ Bi-214 Bi-214 Bi-214 Bi-214 Bi-214
          2.4477E00 2.4828E00 2.5056E00 2.5510E00 2.6045E00  $ Bi-214 Bi-214 Bi-214 Bi-214 Bi-214
          2.6309E00 2.6620E00 2.6948E00 2.6994E00 2.7194E00  $ Bi-214 Bi-214 Bi-214 Bi-214 Bi-214
          2.7700E00 2.7861E00 2.8270E00 2.8609E00 2.8804E00  $ Bi-214 Bi-214 Bi-214 Bi-214 Bi-214
          2.8936E00 2.9221E00 2.9287E00 2.9349E00 2.9400E00  $ Bi-214 Bi-214 Bi-214 Bi-214 Bi-214
          2.9788E00 2.9887E00 3.0000E00 3.0539E00 3.0817E00  $ Bi-214 Bi-214 Bi-214 Bi-214 Bi-214
          3.0939E00 3.1363E00 3.1426E00 3.1605E00 3.1836E00  $ Bi-214 Bi-214 Bi-214 Bi-214 Bi-214
          3.2333E00 3.2697E00                                $ Bi-214 Bi-214
sp2     d 4.4729E-23 3.6645E-28 3.3541E-31 2.3003E-07 1.4604E-10  $ Bi-210 Tl-206 Po-210 Po-214 Pb-210
          2.2506E-02 3.3687E-03 2.4340E-11 1.7956E-03 2.9819E-23  $ Pb-214 Bi-214 Pb-210 Pb-214 Bi-210
          1.2721E-28 2.2392E-31 1.5132E-07 5.0500E-23 1.0454E-02  $ Tl-206 Po-210 Po-214 Bi-210 Pb-214
          2.1254E-28 3.7815E-31 2.5627E-07 2.1421E-03 1.7613E-02  $ Tl-206 Po-210 Po-214 Bi-214 Pb-214
          3.5884E-03 1.7314E-23 4.9538E-24 7.6431E-29 1.3008E-31  $ Bi-214 Bi-210 Bi-210 Tl-206 Po-210
          8.7863E-08 6.0504E-03 1.8322E-29 3.8279E-32 2.5627E-08  $ Po-214 Pb-214 Tl-206 Po-210 Po-214
          1.2389E-03 1.8265E-03 3.8509E-04 9.6187E-05 6.4124E-05  $ Bi-214 Pb-214 Bi-214 Pb-214 Pb-214
          8.0156E-05 1.2168E-02 8.9774E-04 2.1585E-22 1.0796E-03  $ Pb-214 Pb-214 Pb-214 Bi-210 Bi-214
          5.2903E-04 4.9182E-04 1.9793E-04 3.1260E-02 3.0508E-07  $ Pb-214 Bi-214 Bi-214 Pb-214 Po-214
          2.0992E-04 2.7299E-22 3.6872E-05 1.2825E-04 3.2062E-05  $ Bi-214 Bi-210 Pb-214 Pb-214 Pb-214
          5.8179E-04 3.4787E-04 2.3991E-04 3.5987E-04 6.0437E-02  $ Bi-214 Bi-214 Bi-214 Bi-214 Pb-214
          3.8386E-05 2.9989E-05 2.2192E-03 2.5191E-03 5.3980E-05  $ Bi-214 Bi-214 Bi-214 Bi-214 Bi-214
          1.8593E-04 1.0197E-03 6.5977E-04 1.7993E-04 1.9433E-03  $ Bi-214 Bi-214 Bi-214 Bi-214 Bi-214
          2.7253E-04 8.0972E-04 1.6031E-05 7.1976E-04 5.5147E-04  $ Pb-214 Bi-214 Pb-214 Bi-214 Pb-214
          7.1659E-04 5.3980E-05 1.0796E-04 4.8093E-05 3.4787E-05  $ Pb-214 Bi-214 Bi-214 Pb-214 Bi-214
          9.5966E-05 3.0940E-04 4.3185E-04 8.0156E-06 5.1581E-04  $ Bi-214 Pb-214 Bi-214 Pb-214 Bi-214
          3.6872E-05 1.9793E-04 4.9782E-04 5.9315E-04 7.1976E-05  $ Pb-214 Bi-214 Bi-214 Pb-214 Bi-214
          2.8130E-01 4.1985E-04 2.0992E-04 2.9989E-05 1.0197E-04  $ Bi-214 Bi-214 Bi-214 Bi-214 Bi-214
          3.6587E-04 1.9193E-04 3.5987E-04 2.6390E-04 9.5368E-03  $ Bi-214 Bi-214 Bi-214 Bi-214 Bi-214
          4.7983E-04 3.5987E-05 3.5987E-05 2.2791E-04 2.8789E-03  $ Bi-214 Bi-214 Bi-214 Bi-214 Bi-214
          4.5584E-04 2.4591E-03 2.7590E-04 9.5966E-05 2.8789E-04  $ Bi-214 Bi-214 Bi-214 Bi-214 Bi-214
          2.3991E-04 8.0972E-04 1.2825E-04 2.9809E-02 1.7794E-03  $ Bi-214 Bi-214 Pb-214 Bi-214 Pb-214
          1.9193E-03 6.3456E-05 2.5191E-04 3.1992E-29 9.8486E-29  $ Bi-214 Po-214 Bi-214 Tl-206 Po-210
          7.4973E-03 2.4591E-04 9.1768E-04 5.6379E-04 1.3795E-04  $ Bi-214 Bi-214 Bi-214 Bi-214 Bi-214
          9.5706E-04 1.0197E-04 6.4177E-04 1.3795E-04 1.9313E-02  $ Pb-214 Bi-214 Bi-214 Bi-214 Bi-214
          1.0197E-04 2.3391E-03 1.3795E-04 7.1976E-05 5.9978E-05  $ Bi-214 Bi-214 Bi-214 Bi-214 Bi-214
          7.1976E-05 5.8778E-04 1.0197E-04 1.7394E-04 1.9253E-03  $ Bi-214 Bi-214 Bi-214 Bi-214 Bi-214
          1.7394E-04 1.7394E-03 5.9978E-04 4.8582E-04 9.1768E-02  $ Bi-214 Bi-214 Bi-214 Bi-214 Bi-214
```

```
         2.7590E-04 1.5535E-03 1.0316E-02 3.5387E-04 2.8070E-03  $ Bi-214 Bi-214 Bi-214 Bi-214 Bi-214
         1.6194E-04 1.3195E-04 3.6107E-02 8.9967E-03 7.3770E-04  $ Bi-214 Bi-214 Bi-214 Bi-214 Bi-214
         5.2181E-04 6.5977E-05 1.3795E-04 2.7590E-05 2.4531E-02  $ Bi-214 Bi-214 Bi-214 Bi-214 Bi-214
         4.7383E-03 1.1396E-04 8.4566E-03 1.5115E-02 3.1189E-05  $ Bi-214 Bi-214 Bi-214 Bi-214 Bi-214
         7.1976E-05 4.1985E-04 1.3375E-02 2.5191E-03 2.1592E-03  $ Bi-214 Bi-214 Bi-214 Bi-214 Bi-214
         4.3784E-03 1.6194E-03 2.0392E-03 1.1396E-04 4.4984E-04  $ Bi-214 Bi-214 Bi-214 Bi-214 Bi-214
         7.0176E-03 1.4395E-03 1.8593E-02 9.7162E-02 9.5966E-05  $ Bi-214 Bi-214 Bi-214 Bi-214 Bi-214
         7.1976E-05 2.3391E-03 1.2955E-02 1.3795E-03 5.4580E-04  $ Bi-214 Bi-214 Bi-214 Bi-214 Bi-214
         1.0796E-03 3.8386E-04 3.1189E-04 3.2988E-05 1.7993E-05  $ Bi-214 Bi-214 Bi-214 Bi-214 Bi-214
         2.9989E-04 1.1396E-04 4.2585E-04 5.9978E-05 3.4188E-04  $ Bi-214 Bi-214 Bi-214 Bi-214 Bi-214
         5.3380E-04 7.3770E-03 9.5966E-05 2.3991E-05 3.7187E-04  $ Bi-214 Bi-214 Bi-214 Bi-214 Bi-214
         3.0469E-02 4.1985E-05 5.3980E-05 1.0796E-04 1.7993E-05  $ Bi-214 Bi-214 Bi-214 Bi-214 Bi-214
         3.1189E-05 1.9793E-03 7.1976E-05 1.1396E-05 1.3195E-04  $ Bi-214 Bi-214 Bi-214 Bi-214 Bi-214
         1.1396E-05 1.7993E-05 7.1976E-05 1.1996E-05 3.5987E-05  $ Bi-214 Bi-214 Bi-214 Bi-214 Bi-214
         9.4764E-03 1.2596E-05 3.5987E-05 2.3991E-06 2.7590E-06  $ Bi-214 Bi-214 Bi-214 Bi-214 Bi-214
         5.3980E-06 1.7993E-06 1.9793E-04 1.6794E-05 1.0796E-05  $ Bi-214 Bi-214 Bi-214 Bi-214 Bi-214
         1.5594E-04 3.5987E-05 1.4995E-05 2.0992E-06 5.6379E-05  $ Bi-214 Bi-214 Bi-214 Bi-214 Bi-214
         3.8986E-05 9.5966E-05 7.1976E-06 3.4787E-06 1.0197E-05  $ Bi-214 Bi-214 Bi-214 Bi-214 Bi-214
         8.9967E-05 6.5977E-06 5.3980E-05 1.3795E-04 2.6390E-05  $ Bi-214 Bi-214 Bi-214 Bi-214 Bi-214
         3.1189E-06 2.0992E-06 9.5966E-06 3.1189E-06 8.9967E-06  $ Bi-214 Bi-214 Bi-214 Bi-214 Bi-214
         1.1996E-06 5.9978E-07                                   $ Bi-214 Bi-214
c
c   -- Material Specifications --
c
c   -- Concrete --
c
m1    06000 -0.167900  $ Carbon in Concrete
      08000 -0.484500  $ Oxygen in Concrete
      11000 -0.000260  $ Sodium in Concrete
      12000 -0.011900  $ Magnesium in Concrete
      13000 -0.004440  $ Aluminum in Concrete
      14000 -0.015100  $ Silicon in Concrete
      19000 -0.001087  $ Potassium in Concrete
      20000 -0.310100  $ Calcium in Concrete
      25000 -0.000304  $ Manganese in Concrete
      26000 -0.004366  $ Iron in Concrete
c
c   -- Aluminum, Structural 6061 --
c
m2    13000 -0.9685    $ Aluminum
      26000 -0.0070    $ Iron
      29000 -0.0025    $ Copper
      14000 -0.0060    $ Silicon
      12000 -0.0110    $ Magnesium
      24000 -0.0035    $ Chromium
      25000 -0.0015    $ Manganese
c
c   -- Air (suitable for breathing!) --
c
m3    06000 -0.000124  $ Carbon in Air
      07000 -0.755268  $ Nitrogen in Air
      08000 -0.231781  $ Oxygen in Air
      18000 -0.012827  $ Argon in Air
c
c   -- PVT Scintillator --
c
m4    01000 -0.085000   $ Hydrogen in PVT
      06000 -0.915000   $ Carbon in PVT
c
c   -- Germanium Detector --
c m4    32000 -1.000000   $ Germanium Detector
c
c   -- Steel, Stainless 304 --
c
```

```
m5    24000 -0.190000   $ Chromium in Steel
      25000 -0.020000   $ Manganese in Steel
      26000 -0.695000   $ Iron in Steel
      28000 -0.095000   $ Nickel in Steel
c
c   -- Lead --
c
m6    82000 -1.000000   $ Pure lead
c
c   -- PMMA (Light Pipe Lucite) --
c
m7    01000 -0.080538   $ Hydrogen in PMMA
      06000 -0.599848   $ Carbon in PMMA
      08000 -0.319614   $ Oxygen in PMMA
c
c  -- ASTM A366 Steel (7.85 g/cc)
c
m8    26000 -0.990000   $ Iron in sheet steel
      29000 -0.004500   $ Copper in sheet steel
      06000 -0.001000   $ Carbon in sheet steel
      25000 -0.004500   $ Manganese in sheet steel
c
c   -- Tallies --
c
F18:P 11                      $ Pulse height tally in RIGHT LOWER detector
E18 0.0 0.00001 0.040 1.0 3.0  $ Energy bins
F28:P 12                      $ Pulse height tally in RIGHT UPPER detector
E28 0.0 0.00001 0.040 1.0 3.0  $ Energy bins
F38:P 21                      $ Pulse height tally in LEFT LOWER detector
E38 0.0 0.00001 0.040 1.0 3.0  $ Energy bins
F48:P 22                      $ Pulse height tally in LEFT UPPER detector
E48 0.0 0.00001 0.040 1.0 3.0  $ Energy bins
c
c * END OF FILE *
```

APPENDIX Q

MCNP SIMULATION OF SOURCE OF RADIATION SOURCE ON SURFACE OF 20 M DIAMETER STEEL DOME SHIELD

```
c Portal Monitor Environmental Gamma Background Study
c Created by Alexander Solodov, GNSTD, Oak Ridge National Laboratory
c Modified by Christopher Ryan, NSSPI, Texas A&M University
c Further Modified by Stephen Revis, NSSPI, Texas A&M University
c
c * CELL CARDS *
1  1  -2.301    -100 101 -99    imp:p=1 $ Concrete Slab
11 4  -1.032    -112            imp:p=1 $ PVT (Right Lower Detector)
12 4  -1.032    -113            imp:p=1 $ PVT (Right Upper Detector)
14 6  -11.34    -114 112 116    imp:p=1 $ Shielding, Lead (Right Lower Detector)
15 6  -11.34    -115 113 117    imp:p=1 $ Shielding, Lead (Right Upper Detector)
16 7  -1.19     -116            imp:p=1 $ PMMA (Right Lower Detector)
17 7  -1.19     -117            imp:p=1 $ PMMA (Right Upper Detector)
21 4  -1.032    -122            imp:p=1 $ PVT (Left Lower Detector)
22 4  -1.032    -123            imp:p=1 $ PVT (Left Upper Detector)
24 6  -11.34    -124 122 126    imp:p=1 $ Shielding, Lead (Left Lower Detector)
25 6  -11.34    -125 123 127    imp:p=1 $ Shielding, Lead (Left Upper Detector)
26 7  -1.19     -126            imp:p=1 $ PMMA (Left Lower Detector)
27 7  -1.19     -127            imp:p=1 $ PMMA (Left Upper Detector)
c begin new stuff
c right
c 100 1 -2.301  -200 -100 101   imp:p=1 $ concrete under portal (no source here)
110 2 -2.700    -200 100 -210   imp:p=1 $ right portal inner face (Aluminum)
111 5  -7.920  (-220:221:-290:291:211)
               -200 210 100     imp:p=1 $ SS304 (Right Portal, Back & Sides)
112 3 -1.205E-3 210 -211 220 -221
               290 -291 112 113
               114 115          imp:p=1 $ Interior Air (Right Portal Arm)
c left
c 200 1 -2.301   -201 -100 101  imp:p=1 $ concrete under portal (no source here)
210 2 -2.700   -201 100  213    imp:p=1 $ left portal inner face (Aluminum)
211 5  -7.920  (-220:221:-290:291:-212)
               -201 -213 100    imp:p=1 $ SS304 (Left Portal, Back & Sides)
212 3 -1.205E-3 212 -213 220 -221
               290 -291 122 123
               124 125          imp:p=1 $ Interior Air (Left Portal Arm)
c dome
300 8  -7.850 301 -300 310 100  imp:p=1          $steel dome
c other
998 3 -1.205E-3 100 200 201
                -99 #300        imp:p=1 $ Universe Sphere
999 0           +99:-101        imp:p=0 $ The edge of the universe...
c end new stuff
c * END CELL CARDS *

c * SURFACE CARDS *
100 pz  0      $ top of concrete slab
101 pz  -30.48 $ bottom of concrete slab
112 RPP 269.5 273.5 -24.5 -9.5 23 99 $ right lower detector surf
113 RPP 269.5 273.5 -24.5 -9.5 214 290 $ right upper detertor surf
114 RPP 269.5 274.4525 -25.4525 -8.5475 22.0475 112 $ lead around right lower det surf
```

```
115 RPP 269.5 274.4525 -25.4525 -8.5475 201 290.9525 $ lead around right upper det surf
116 RPP 269.5 273.5 -24.5 -9.5 99 112 $ lucite right lower
117 RPP 269.5 273.5 -24.5 -9.5 201 214 $ lucite right upper
122 RPP -273.5 -269.5 -24.5 -9.5 23 99 $ left lower detector surf
123 RPP -273.5 -269.5 -24.5 -9.5 214 290 $ left upper detector surf
124 RPP -274.4525 -269.5 -25.4525 -8.5475 22.0475 112 $ lead around left lower det surf
125 RPP -274.4525 -269.5 -25.4525 -8.5475 201 290.9525 $ lead around left upper det surf
126 RPP -273.5 -269.5 -24.5 -9.5 99 112 $ lucite left lower
127 RPP -273.5 -269.5 -24.5 -9.5 201 214 $ lucite left upper
c new stuff
200 RPP 254 277 -33 33 -40 304 $ right portal outer
201 RPP -277 -254 -33 33 -40 304 $ left portal outer
210 px 254.3175 $right portal inner face
211 px 276.6825 $right portal outer face
212 px -276.6825 $left portal outer face
213 px -254.3175 $left portal inner face
220 py -32.6825 $ right portal side
221 py  32.6825 $ right portal side
290 pz  0.3175  $ portal bottom
291 pz 303.6825 $ portal top
300 so 1000 $ outer aluminum sphere
301 so 999.6825 $inner aluminum sphere (0.125 in thickness)
310 rpp -200 200 -1001 1001 1 450
99 so 4000 $ universe sphere
903 RPP 253.99 277.01 -33.01 33.01 -40.01 304.01 $ right portal ccc
904 RPP -277.01 -253.99 -33.01 33.01 -40.01 304.01 $ left portal ccc
c * END SURFACE CARDS *

c * DATA CARDS *
NPS 1.00E9
c   -- Source Specifications --
c Source
c Located +/- 1mm from surface of concrete (surface 100)
c 3.742:1 initial ratio of Bi-214 to Pb-214
c This source represents the spectrum found 1s after rain ends.
c Source is isotropic
MODE p
SDEF  ERG D2 PAR 2 SUR=300 AXS 0 0 1 DIR D1 EXT D3
si1 -1 1 $Isotropic Source
sp1  0 1
si3  0 1 $stay on sphere
sp3  -21 1
C      ---------------------------------------------------------------
C      Photon Source Definition - generated from ORIGEN F71 file
C         total strength:  2.2668E11 gammas/second
C         discrete lines:  2.2668E11 gammas/second in 242 lines
C                          100.00% of energy
C         multigroup bins: 0.0000E00 gammas/second in 18 bins
C                          0.00% of energy
C         not counted:     0.0000E00 gammas/second
C      ---------------------------------------------------------------
C
C      discrete lines (in MeV) and their probabilities
si2    l 1.2213E-02 1.2614E-02 1.2614E-02 1.2614E-02 1.3024E-02  $ Bi-210 Tl-206 Po-210 Po-214 Pb-210
         1.3024E-02 1.3446E-02 4.6520E-02 5.3226E-02 7.0832E-02  $ Pb-214 Bi-214 Pb-210 Pb-214 Bi-210
         7.2805E-02 7.2805E-02 7.2805E-02 7.2873E-02 7.4815E-02  $ Tl-206 Po-210 Po-214 Bi-210 Pb-214
         7.4969E-02 7.4969E-02 7.4969E-02 7.6861E-02 7.7107E-02  $ Tl-206 Po-210 Po-214 Bi-214 Pb-214
         7.9291E-02 8.2344E-02 8.4685E-02 8.4694E-02 8.4694E-02  $ Bi-214 Bi-210 Bi-210 Tl-206 Po-210
         8.4694E-02 8.7089E-02 8.7111E-02 8.7111E-02 8.7111E-02  $ Po-214 Pb-214 Tl-206 Po-210 Po-214
         8.9527E-02 8.9588E-02 9.2110E-02 1.3745E-01 1.4130E-01  $ Bi-214 Pb-214 Bi-214 Pb-214 Pb-214
         1.9630E-01 2.4191E-01 2.5879E-01 2.6560E-01 2.7370E-01  $ Pb-214 Pb-214 Pb-214 Bi-210 Bi-214
         2.7453E-01 2.8094E-01 2.8690E-01 2.9517E-01 2.9800E-01  $ Pb-214 Bi-214 Bi-214 Pb-214 Po-214
         3.0443E-01 3.0460E-01 3.0560E-01 3.1420E-01 3.2430E-01  $ Bi-214 Bi-210 Pb-214 Pb-214 Pb-214
         3.3361E-01 3.3490E-01 3.3850E-01 3.4710E-01 3.5190E-01  $ Bi-214 Bi-214 Bi-214 Bi-214 Pb-214
```

```
          3.6420E-01 3.7660E-01 3.8700E-01 3.8910E-01 3.9400E-01  $ Bi-214 Bi-214 Bi-214 Bi-214 Bi-214
          3.9601E-01 4.0574E-01 4.2650E-01 4.4040E-01 4.5477E-01  $ Bi-214 Bi-214 Bi-214 Bi-214 Bi-214
          4.6210E-01 4.6969E-01 4.7060E-01 4.7438E-01 4.8042E-01  $ Pb-214 Bi-214 Pb-214 Bi-214 Pb-214
          4.8708E-01 4.9460E-01 5.0220E-01 5.1100E-01 5.2040E-01  $ Pb-214 Bi-214 Bi-214 Pb-214 Bi-214
          5.2500E-01 5.3369E-01 5.3694E-01 5.3870E-01 5.4340E-01  $ Bi-214 Pb-214 Bi-214 Pb-214 Bi-214
          5.4410E-01 5.4710E-01 5.7283E-01 5.8015E-01 5.9600E-01  $ Pb-214 Bi-214 Bi-214 Pb-214 Bi-214
          6.0932E-01 6.1578E-01 6.1710E-01 6.2640E-01 6.3120E-01  $ Bi-214 Bi-214 Bi-214 Bi-214 Bi-214
          6.3314E-01 6.3937E-01 6.4918E-01 6.6140E-01 6.6545E-01  $ Bi-214 Bi-214 Bi-214 Bi-214 Bi-214
          6.8322E-01 6.8770E-01 6.9330E-01 6.9790E-01 7.0311E-01  $ Bi-214 Bi-214 Bi-214 Bi-214 Bi-214
          7.1080E-01 7.1986E-01 7.2340E-01 7.2780E-01 7.3365E-01  $ Bi-214 Bi-214 Bi-214 Bi-214 Bi-214
          7.4150E-01 7.5284E-01 7.6600E-01 7.6836E-01 7.8591E-01  $ Bi-214 Bi-214 Pb-214 Bi-214 Pb-214
          7.8610E-01 7.9970E-01 7.9976E-01 8.0310E-01 8.0310E-01  $ Bi-214 Po-214 Bi-214 Tl-206 Po-210
          8.0617E-01 8.1508E-01 8.2118E-01 8.2620E-01 8.3235E-01  $ Bi-214 Bi-214 Bi-214 Bi-214 Bi-214
          8.3903E-01 8.4720E-01 9.0425E-01 9.1580E-01 9.3405E-01  $ Pb-214 Bi-214 Bi-214 Bi-214 Bi-214
          9.4330E-01 9.6408E-01 9.7620E-01 9.8920E-01 1.0134E00  $ Bi-214 Bi-214 Bi-214 Bi-214 Bi-214
          1.0205E00 1.0324E00 1.0380E00 1.0454E00 1.0520E00  $ Bi-214 Bi-214 Bi-214 Bi-214 Bi-214
          1.0669E00 1.0700E00 1.1037E00 1.1048E00 1.1203E00  $ Bi-214 Bi-214 Bi-214 Bi-214 Bi-214
          1.1308E00 1.1337E00 1.1552E00 1.1731E00 1.2077E00  $ Bi-214 Bi-214 Bi-214 Bi-214 Bi-214
          1.2268E00 1.2305E00 1.2381E00 1.2810E00 1.3038E00  $ Bi-214 Bi-214 Bi-214 Bi-214 Bi-214
          1.3170E00 1.3300E00 1.3415E00 1.3530E00 1.3777E00  $ Bi-214 Bi-214 Bi-214 Bi-214 Bi-214
          1.3853E00 1.3925E00 1.4015E00 1.4080E00 1.4197E00  $ Bi-214 Bi-214 Bi-214 Bi-214 Bi-214
          1.4711E00 1.4792E00 1.5092E00 1.5385E00 1.5433E00  $ Bi-214 Bi-214 Bi-214 Bi-214 Bi-214
          1.5832E00 1.5947E00 1.5993E00 1.6366E00 1.6574E00  $ Bi-214 Bi-214 Bi-214 Bi-214 Bi-214
          1.6613E00 1.6840E00 1.7296E00 1.7645E00 1.7821E00  $ Bi-214 Bi-214 Bi-214 Bi-214 Bi-214
          1.8137E00 1.8384E00 1.8474E00 1.8732E00 1.8903E00  $ Bi-214 Bi-214 Bi-214 Bi-214 Bi-214
          1.8963E00 1.8987E00 1.9358E00 1.9947E00 2.0045E00  $ Bi-214 Bi-214 Bi-214 Bi-214 Bi-214
          2.0107E00 2.0218E00 2.0529E00 2.0850E00 2.0895E00  $ Bi-214 Bi-214 Bi-214 Bi-214 Bi-214
          2.1099E00 2.1185E00 2.1478E00 2.1768E00 2.1926E00  $ Bi-214 Bi-214 Bi-214 Bi-214 Bi-214
          2.2041E00 2.2512E00 2.2597E00 2.2666E00 2.2700E00  $ Bi-214 Bi-214 Bi-214 Bi-214 Bi-214
          2.2844E00 2.2934E00 2.3122E00 2.3248E00 2.3313E00  $ Bi-214 Bi-214 Bi-214 Bi-214 Bi-214
          2.3609E00 2.3693E00 2.3770E00 2.3909E00 2.4235E00  $ Bi-214 Bi-214 Bi-214 Bi-214 Bi-214
          2.4477E00 2.4828E00 2.5056E00 2.5510E00 2.6045E00  $ Bi-214 Bi-214 Bi-214 Bi-214 Bi-214
          2.6309E00 2.6620E00 2.6948E00 2.6994E00 2.7194E00  $ Bi-214 Bi-214 Bi-214 Bi-214 Bi-214
          2.7700E00 2.7861E00 2.8270E00 2.8609E00 2.8804E00  $ Bi-214 Bi-214 Bi-214 Bi-214 Bi-214
          2.8936E00 2.9221E00 2.9287E00 2.9349E00 2.9400E00  $ Bi-214 Bi-214 Bi-214 Bi-214 Bi-214
          2.9788E00 2.9887E00 3.0000E00 3.0539E00 3.0817E00  $ Bi-214 Bi-214 Bi-214 Bi-214 Bi-214
          3.0939E00 3.1363E00 3.1426E00 3.1605E00 3.1836E00  $ Bi-214 Bi-214 Bi-214 Bi-214 Bi-214
          3.2333E00 3.2697E00                                $ Bi-214 Bi-214
sp2     d 4.4729E-23 3.6645E-28 3.3541E-31 2.3003E-07 1.4604E-10  $ Bi-210 Tl-206 Po-210 Po-214 Pb-210
          2.2506E-02 3.3687E-03 2.4340E-11 1.7956E-03 2.9819E-23  $ Pb-214 Bi-214 Pb-210 Pb-214 Bi-210
          1.2721E-28 2.2392E-31 1.5132E-07 5.0500E-23 1.0454E-02  $ Tl-206 Po-210 Po-214 Bi-210 Pb-214
          2.1254E-28 3.7815E-31 2.5627E-07 2.1421E-03 1.7613E-02  $ Tl-206 Po-210 Po-214 Bi-214 Pb-214
          3.5884E-03 1.7314E-23 4.9538E-24 7.6431E-29 1.3008E-31  $ Bi-214 Bi-210 Bi-210 Tl-206 Po-210
          8.7863E-08 6.0504E-03 1.8322E-29 3.8279E-32 2.5627E-08  $ Po-214 Pb-214 Tl-206 Po-210 Po-214
          1.2389E-03 1.8265E-03 3.8509E-04 9.6187E-05 6.4124E-05  $ Bi-214 Pb-214 Bi-214 Pb-214 Pb-214
          8.0156E-05 1.2168E-02 8.9774E-04 2.1585E-22 1.0796E-03  $ Pb-214 Pb-214 Pb-214 Bi-210 Bi-214
          5.2903E-04 4.9182E-04 1.9793E-04 3.1260E-02 3.0508E-07  $ Pb-214 Bi-214 Bi-214 Pb-214 Po-214
          2.0992E-04 2.7299E-22 3.6872E-05 1.2825E-04 3.2062E-05  $ Bi-214 Bi-210 Pb-214 Pb-214 Pb-214
          5.8179E-04 3.4787E-04 2.3991E-04 3.5987E-04 6.0437E-02  $ Bi-214 Bi-214 Bi-214 Bi-214 Pb-214
          3.8386E-05 2.9989E-05 2.2192E-03 2.5191E-03 5.3980E-05  $ Bi-214 Bi-214 Bi-214 Bi-214 Bi-214
          1.8593E-04 1.0197E-03 6.5977E-04 1.7993E-04 1.9433E-03  $ Bi-214 Bi-214 Bi-214 Bi-214 Bi-214
          2.7253E-04 8.0972E-04 1.6031E-05 7.1976E-04 5.5147E-04  $ Pb-214 Bi-214 Pb-214 Bi-214 Pb-214
          7.1659E-04 5.3980E-05 1.0796E-04 4.8093E-05 3.4787E-05  $ Pb-214 Bi-214 Bi-214 Pb-214 Bi-214
          9.5966E-05 3.0940E-04 4.3185E-04 8.0156E-06 5.1581E-04  $ Bi-214 Pb-214 Bi-214 Pb-214 Bi-214
          3.6872E-05 1.9793E-04 4.9782E-04 5.9315E-04 7.1976E-05  $ Pb-214 Bi-214 Bi-214 Pb-214 Bi-214
          2.8130E-01 4.1985E-04 2.0992E-04 2.9989E-05 1.0197E-04  $ Bi-214 Bi-214 Bi-214 Bi-214 Bi-214
          3.6587E-04 1.9193E-04 3.5987E-04 2.6390E-04 9.5368E-03  $ Bi-214 Bi-214 Bi-214 Bi-214 Bi-214
          4.7983E-04 3.5987E-05 3.5987E-05 2.2791E-04 2.8789E-03  $ Bi-214 Bi-214 Bi-214 Bi-214 Bi-214
          4.5584E-04 2.4591E-03 2.7590E-04 9.5966E-05 2.8789E-04  $ Bi-214 Bi-214 Bi-214 Bi-214 Bi-214
          2.3991E-04 8.0972E-04 1.2825E-04 2.9809E-02 1.7794E-03  $ Bi-214 Bi-214 Pb-214 Bi-214 Pb-214
          1.9193E-03 6.3456E-05 2.5191E-04 3.1992E-29 9.8486E-29  $ Bi-214 Po-214 Bi-214 Tl-206 Po-210
          7.4973E-03 2.4591E-04 9.1768E-04 5.6379E-04 1.3795E-04  $ Bi-214 Bi-214 Bi-214 Bi-214 Bi-214
          9.5706E-04 1.0197E-04 6.4177E-04 1.3795E-04 1.9313E-02  $ Pb-214 Bi-214 Bi-214 Bi-214 Bi-214
          1.0197E-04 2.3391E-03 1.3795E-04 7.1976E-05 5.9978E-05  $ Bi-214 Bi-214 Bi-214 Bi-214 Bi-214
```

```
         7.1976E-05 5.8778E-04 1.0197E-04 1.7394E-04 1.9253E-03  $ Bi-214 Bi-214 Bi-214 Bi-214 Bi-214
         1.7394E-04 1.7394E-03 5.9978E-04 4.8582E-04 9.1768E-02  $ Bi-214 Bi-214 Bi-214 Bi-214 Bi-214
         2.7590E-04 1.5535E-03 1.0316E-02 3.5387E-04 2.8070E-03  $ Bi-214 Bi-214 Bi-214 Bi-214 Bi-214
         1.6194E-04 1.3195E-04 3.6107E-02 8.9967E-03 7.3770E-04  $ Bi-214 Bi-214 Bi-214 Bi-214 Bi-214
         5.2181E-04 6.5977E-05 1.3795E-04 2.7590E-05 2.4531E-02  $ Bi-214 Bi-214 Bi-214 Bi-214 Bi-214
         4.7383E-03 1.1396E-04 8.4566E-03 1.5115E-02 3.1189E-05  $ Bi-214 Bi-214 Bi-214 Bi-214 Bi-214
         7.1976E-05 4.1985E-04 1.3375E-02 2.5191E-03 2.1592E-03  $ Bi-214 Bi-214 Bi-214 Bi-214 Bi-214
         4.3784E-03 1.6194E-03 2.0392E-03 1.1396E-04 4.4984E-04  $ Bi-214 Bi-214 Bi-214 Bi-214 Bi-214
         7.0176E-03 1.4395E-03 1.8593E-02 9.7162E-02 9.5966E-05  $ Bi-214 Bi-214 Bi-214 Bi-214 Bi-214
         7.1976E-05 2.3391E-03 1.2955E-02 1.3795E-03 5.4580E-04  $ Bi-214 Bi-214 Bi-214 Bi-214 Bi-214
         1.0796E-03 3.8386E-04 3.1189E-04 3.2988E-05 1.7993E-05  $ Bi-214 Bi-214 Bi-214 Bi-214 Bi-214
         2.9989E-04 1.1396E-04 4.2585E-04 5.9978E-05 3.4188E-04  $ Bi-214 Bi-214 Bi-214 Bi-214 Bi-214
         5.3380E-04 7.3770E-03 9.5966E-05 2.3991E-05 3.7187E-04  $ Bi-214 Bi-214 Bi-214 Bi-214 Bi-214
         3.0469E-02 4.1985E-05 5.3980E-05 1.0796E-04 1.7993E-05  $ Bi-214 Bi-214 Bi-214 Bi-214 Bi-214
         3.1189E-05 1.9793E-03 7.1976E-05 1.1396E-05 1.3195E-04  $ Bi-214 Bi-214 Bi-214 Bi-214 Bi-214
         1.1396E-05 1.7993E-05 7.1976E-05 1.1996E-05 3.5987E-05  $ Bi-214 Bi-214 Bi-214 Bi-214 Bi-214
         9.4764E-03 1.2596E-05 3.5987E-05 2.3991E-06 2.7590E-06  $ Bi-214 Bi-214 Bi-214 Bi-214 Bi-214
         5.3980E-06 1.7993E-06 1.9793E-04 1.6794E-05 1.0796E-05  $ Bi-214 Bi-214 Bi-214 Bi-214 Bi-214
         1.5594E-04 3.5987E-05 1.4995E-05 2.0992E-06 5.6379E-05  $ Bi-214 Bi-214 Bi-214 Bi-214 Bi-214
         3.8986E-05 9.5966E-05 7.1976E-06 3.4787E-06 1.0197E-05  $ Bi-214 Bi-214 Bi-214 Bi-214 Bi-214
         8.9967E-05 6.5977E-06 5.3980E-05 1.3795E-04 2.6390E-05  $ Bi-214 Bi-214 Bi-214 Bi-214 Bi-214
         3.1189E-06 2.0992E-06 9.5966E-06 3.1189E-06 8.9967E-06  $ Bi-214 Bi-214 Bi-214 Bi-214 Bi-214
         1.1996E-06 5.9978E-07                                   $ Bi-214 Bi-214
c
c   -- Material Specifications --
c
c   -- Concrete --
c
m1    06000 -0.167900  $ Carbon in Concrete
      08000 -0.484500  $ Oxygen in Concrete
      11000 -0.000260  $ Sodium in Concrete
      12000 -0.011900  $ Magnesium in Concrete
      13000 -0.004440  $ Aluminum in Concrete
      14000 -0.015100  $ Silicon in Concrete
      19000 -0.001087  $ Potassium in Concrete
      20000 -0.310100  $ Calcium in Concrete
      25000 -0.000304  $ Manganese in Concrete
      26000 -0.004366  $ Iron in Concrete
c
c   -- Aluminum, Structural 6061 --
c
m2    13000 -0.9685    $ Aluminum
      26000 -0.0070    $ Iron
      29000 -0.0025    $ Copper
      14000 -0.0060    $ Silicon
      12000 -0.0110    $ Magnesium
      24000 -0.0035    $ Chromium
      25000 -0.0015    $ Manganese
c
c   -- Air (suitable for breathing!) --
c
m3    06000 -0.000124  $ Carbon in Air
      07000 -0.755268  $ Nitrogen in Air
      08000 -0.231781  $ Oxygen in Air
      18000 -0.012827  $ Argon in Air
c
c   -- PVT Scintillator --
c
m4    01000 -0.085000   $ Hydrogen in PVT
      06000 -0.915000   $ Carbon in PVT
c
c   -- Germanium Detector --
c m4    32000 -1.000000   $ Germanium Detector
c
```

```
c   -- Steel, Stainless 304 --
c
m5    24000 -0.190000   $ Chromium in Steel
      25000 -0.020000   $ Manganese in Steel
      26000 -0.695000   $ Iron in Steel
      28000 -0.095000   $ Nickel in Steel
c
c   -- Lead --
c
m6    82000 -1.000000   $ Pure lead
c
c   -- PMMA (Light Pipe Lucite) --
c
m7    01000 -0.080538   $ Hydrogen in PMMA
      06000 -0.599848   $ Carbon in PMMA
      08000 -0.319614   $ Oxygen in PMMA
c
c  -- ASTM A366 Steel (7.85 g/cc)
c
m8    26000 -0.990000   $ Iron in sheet steel
      29000 -0.004500   $ Copper in sheet steel
       06000 -0.001000   $ Carbon in sheet steel
       25000 -0.004500   $ Manganese in sheet steel
c
c   -- Tallies --
c
F18:P 11                      $ Pulse height tally in RIGHT LOWER detector
E18 0.0 0.00001 0.040 1.0 3.0  $ Energy bins
F28:P 12                      $ Pulse height tally in RIGHT UPPER detector
E28 0.0 0.00001 0.040 1.0 3.0  $ Energy bins
F38:P 21                      $ Pulse height tally in LEFT LOWER detector
E38 0.0 0.00001 0.040 1.0 3.0  $ Energy bins
F48:P 22                      $ Pulse height tally in LEFT UPPER detector
E48 0.0 0.00001 0.040 1.0 3.0  $ Energy bins
c
c * END OF FILE *
```

APPENDIX R

MCNP SIMULATION OF SOURCE OF RADIATION SOURCE OUTSIDE OF 20 M DIAMETER STEEL DOME SHIELD

```
c Portal Monitor Environmental Gamma Background Study
c Created by Alexander Solodov, GNSTD, Oak Ridge National Laboratory
c Modified by Christopher Ryan, NSSPI, Texas A&M University
c Further Modified by Stephen Revis, NSSPI, Texas A&M University
c
c * CELL CARDS *
1  1  -2.301    -100 101 -99    imp:p=1 $ Concrete Slab
11 4  -1.032    -112            imp:p=1 $ PVT (Right Lower Detector)
12 4  -1.032    -113            imp:p=1 $ PVT (Right Upper Detector)
14 6  -11.34    -114 112 116    imp:p=1 $ Shielding, Lead (Right Lower Detector)
15 6  -11.34    -115 113 117    imp:p=1 $ Shielding, Lead (Right Upper Detector)
16 7  -1.19     -116            imp:p=1 $ PMMA (Right Lower Detector)
17 7  -1.19     -117            imp:p=1 $ PMMA (Right Upper Detector)
21 4  -1.032    -122            imp:p=1 $ PVT (Left Lower Detector)
22 4  -1.032    -123            imp:p=1 $ PVT (Left Upper Detector)
24 6  -11.34    -124 122 126    imp:p=1 $ Shielding, Lead (Left Lower Detector)
25 6  -11.34    -125 123 127    imp:p=1 $ Shielding, Lead (Left Upper Detector)
26 7  -1.19     -126            imp:p=1 $ PMMA (Left Lower Detector)
27 7  -1.19     -127            imp:p=1 $ PMMA (Left Upper Detector)
c begin new stuff
c right
c 100 1 -2.301  -200 -100 101   imp:p=1 $ concrete under portal (no source here)
110 2 -2.700    -200 100 -210   imp:p=1 $ right portal inner face (Aluminum)
111 5  -7.920  (-220:221:-290:291:211)
               -200 210 100     imp:p=1 $ SS304 (Right Portal, Back & Sides)
112 3 -1.205E-3 210 -211 220 -221
               290 -291 112 113
               114 115          imp:p=1 $ Interior Air (Right Portal Arm)
c left
c 200 1 -2.301   -201 -100 101  imp:p=1 $ concrete under portal (no source here)
210 2 -2.700   -201 100  213    imp:p=1 $ left portal inner face (Aluminum)
211 5  -7.920  (-220:221:-290:291:-212)
               -201 -213 100    imp:p=1 $ SS304 (Left Portal, Back & Sides)
212 3 -1.205E-3 212 -213 220 -221
               290 -291 122 123
               124 125          imp:p=1 $ Interior Air (Left Portal Arm)
c dome
300 8  -7.850 301 -300 310 100  imp:p=1           $steel dome
c other
998 3 -1.205E-3 100 200 201
                -99 #300        imp:p=1 $ Universe Sphere
999 0           +99:-101        imp:p=0 $ The edge of the universe...
c end new stuff
c * END CELL CARDS *

c * SURFACE CARDS *
100 pz  0      $ top of concrete slab
101 pz  -30.48 $ bottom of concrete slab
112 RPP 269.5 273.5 -24.5 -9.5 23 99 $ right lower detector surf
113 RPP 269.5 273.5 -24.5 -9.5 214 290 $ right upper detertor surf
114 RPP 269.5 274.4525 -25.4525 -8.5475 22.0475 112 $ lead around right lower det surf
```

```
115 RPP 269.5 274.4525 -25.4525 -8.5475 201 290.9525 $ lead around right upper det surf
116 RPP 269.5 273.5 -24.5 -9.5 99 112 $ lucite right lower
117 RPP 269.5 273.5 -24.5 -9.5 201 214 $ lucite right upper
122 RPP -273.5 -269.5 -24.5 -9.5 23 99 $ left lower detector surf
123 RPP -273.5 -269.5 -24.5 -9.5 214 290 $ left upper detector surf
124 RPP -274.4525 -269.5 -25.4525 -8.5475 22.0475 112 $ lead around left lower det surf
125 RPP -274.4525 -269.5 -25.4525 -8.5475 201 290.9525 $ lead around left upper det surf
126 RPP -273.5 -269.5 -24.5 -9.5 99 112 $ lucite left lower
127 RPP -273.5 -269.5 -24.5 -9.5 201 214 $ lucite left upper
c new stuff
200 RPP 254 277 -33 33 -40 304 $ right portal outer
201 RPP -277 -254 -33 33 -40 304 $ left portal outer
210 px 254.3175 $right portal inner face
211 px 276.6825 $right portal outer face
212 px -276.6825 $left portal outer face
213 px -254.3175 $left portal inner face
220 py -32.6825 $ right portal side
221 py  32.6825 $ right portal side
290 pz  0.3175  $ portal bottom
291 pz 303.6825 $ portal top
300 so 1000 $ outer aluminum sphere
301 so 999.6825 $inner aluminum sphere (0.125 in thickness)
310 rpp -200 200 -1001 1001 1 450
99 so 4000 $ universe sphere
903 RPP 253.99 277.01 -33.01 33.01 -40.01 304.01 $ right portal ccc
904 RPP -277.01 -253.99 -33.01 33.01 -40.01 304.01 $ left portal ccc
c * END SURFACE CARDS *

c * DATA CARDS *
NPS 1.00E9
c   -- Source Specifications --
c Source
c Located +/- 1mm from surface of concrete (surface 100)
c 3.742:1 initial ratio of Bi-214 to Pb-214
c This source represents the spectrum found 1s after rain ends.
c Source is isotropic
MODE p
SDEF  ERG D2 PAR 2 AXS 0 0 1 VEC 0 0 1 POS 0 0 -0.025 DIR D1 EXT D4 RAD D3
si1 -1   0    1 $Isotropic Source
sp1  0   0.5  1
sb1  0   0.1  1
si4  -0.075 0.125 $Pos is not 0 0 0
sp4  0 1          $to avoid placing pos on surface 100
si3  1000 2000
sp3  -21 1  $ power law distribution
C      ---------------------------------------------------------------
C      Photon Source Definition - generated from ORIGEN F71 file
C         total strength:  2.2668E11 gammas/second
C         discrete lines:  2.2668E11 gammas/second in 242 lines
C                          100.00% of energy
C         multigroup bins: 0.0000E00 gammas/second in 18 bins
C                          0.00% of energy
C         not counted:     0.0000E00 gammas/second
C      ---------------------------------------------------------------
C
C      discrete lines (in MeV) and their probabilities
si2    l 1.2213E-02 1.2614E-02 1.2614E-02 1.2614E-02 1.3024E-02  $ Bi-210 Tl-206 Po-210 Po-214 Pb-210
         1.3024E-02 1.3446E-02 4.6520E-02 5.3226E-02 7.0832E-02  $ Pb-214 Bi-214 Pb-210 Pb-214 Bi-210
         7.2805E-02 7.2805E-02 7.2805E-02 7.2873E-02 7.4815E-02  $ Tl-206 Po-210 Po-214 Bi-210 Pb-214
         7.4969E-02 7.4969E-02 7.4969E-02 7.6861E-02 7.7107E-02  $ Tl-206 Po-210 Po-214 Bi-214 Pb-214
         7.9291E-02 8.2344E-02 8.4685E-02 8.4694E-02 8.4694E-02  $ Bi-214 Bi-210 Bi-210 Tl-206 Po-210
         8.4694E-02 8.7089E-02 8.7111E-02 8.7111E-02 8.7111E-02  $ Po-214 Pb-214 Tl-206 Po-210 Po-214
         8.9527E-02 8.9588E-02 9.2110E-02 1.3745E-01 1.4130E-01  $ Bi-214 Pb-214 Bi-214 Pb-214 Pb-214
         1.9630E-01 2.4191E-01 2.5879E-01 2.6560E-01 2.7370E-01  $ Pb-214 Pb-214 Pb-214 Bi-210 Bi-214
```

```
          2.7453E-01 2.8094E-01 2.8690E-01 2.9517E-01 2.9800E-01  $ Pb-214 Bi-214 Bi-214 Pb-214 Po-214
          3.0443E-01 3.0460E-01 3.0560E-01 3.1420E-01 3.2430E-01  $ Bi-214 Bi-210 Pb-214 Pb-214 Pb-214
          3.3361E-01 3.3490E-01 3.3850E-01 3.4710E-01 3.5190E-01  $ Bi-214 Bi-214 Bi-214 Bi-214 Pb-214
          3.6420E-01 3.7660E-01 3.8700E-01 3.8910E-01 3.9400E-01  $ Bi-214 Bi-214 Bi-214 Bi-214 Bi-214
          3.9601E-01 4.0574E-01 4.2650E-01 4.4040E-01 4.5477E-01  $ Bi-214 Bi-214 Bi-214 Bi-214 Bi-214
          4.6210E-01 4.6969E-01 4.7060E-01 4.7438E-01 4.8042E-01  $ Pb-214 Bi-214 Pb-214 Bi-214 Pb-214
          4.8708E-01 4.9460E-01 5.0220E-01 5.1100E-01 5.2040E-01  $ Pb-214 Bi-214 Bi-214 Pb-214 Bi-214
          5.2500E-01 5.3369E-01 5.3694E-01 5.3870E-01 5.4340E-01  $ Bi-214 Pb-214 Bi-214 Pb-214 Bi-214
          5.4410E-01 5.4710E-01 5.7283E-01 5.8015E-01 5.9600E-01  $ Pb-214 Bi-214 Bi-214 Pb-214 Bi-214
          6.0932E-01 6.1578E-01 6.1710E-01 6.2640E-01 6.3120E-01  $ Bi-214 Bi-214 Bi-214 Bi-214 Bi-214
          6.3314E-01 6.3937E-01 6.4918E-01 6.6140E-01 6.6545E-01  $ Bi-214 Bi-214 Bi-214 Bi-214 Bi-214
          6.8322E-01 6.8770E-01 6.9330E-01 6.9790E-01 7.0311E-01  $ Bi-214 Bi-214 Bi-214 Bi-214 Bi-214
          7.1080E-01 7.1986E-01 7.2340E-01 7.2780E-01 7.3365E-01  $ Bi-214 Bi-214 Bi-214 Bi-214 Bi-214
          7.4150E-01 7.5284E-01 7.6600E-01 7.6836E-01 7.8591E-01  $ Bi-214 Bi-214 Pb-214 Bi-214 Pb-214
          7.8610E-01 7.9970E-01 7.9976E-01 8.0310E-01 8.0310E-01  $ Bi-214 Po-214 Bi-214 Tl-206 Po-210
          8.0617E-01 8.1508E-01 8.2118E-01 8.2620E-01 8.3235E-01  $ Bi-214 Bi-214 Bi-214 Bi-214 Bi-214
          8.3903E-01 8.4720E-01 9.0425E-01 9.1580E-01 9.3405E-01  $ Pb-214 Bi-214 Bi-214 Bi-214 Bi-214
          9.4330E-01 9.6408E-01 9.7620E-01 9.8920E-01 1.0134E00  $ Bi-214 Bi-214 Bi-214 Bi-214 Bi-214
          1.0205E00 1.0324E00 1.0380E00 1.0454E00 1.0520E00  $ Bi-214 Bi-214 Bi-214 Bi-214 Bi-214
          1.0669E00 1.0700E00 1.1037E00 1.1048E00 1.1203E00  $ Bi-214 Bi-214 Bi-214 Bi-214 Bi-214
          1.1308E00 1.1337E00 1.1552E00 1.1731E00 1.2077E00  $ Bi-214 Bi-214 Bi-214 Bi-214 Bi-214
          1.2268E00 1.2305E00 1.2381E00 1.2810E00 1.3038E00  $ Bi-214 Bi-214 Bi-214 Bi-214 Bi-214
          1.3170E00 1.3300E00 1.3415E00 1.3530E00 1.3777E00  $ Bi-214 Bi-214 Bi-214 Bi-214 Bi-214
          1.3853E00 1.3925E00 1.4015E00 1.4080E00 1.4197E00  $ Bi-214 Bi-214 Bi-214 Bi-214 Bi-214
          1.4711E00 1.4792E00 1.5092E00 1.5385E00 1.5433E00  $ Bi-214 Bi-214 Bi-214 Bi-214 Bi-214
          1.5832E00 1.5947E00 1.5993E00 1.6366E00 1.6574E00  $ Bi-214 Bi-214 Bi-214 Bi-214 Bi-214
          1.6613E00 1.6840E00 1.7296E00 1.7645E00 1.7821E00  $ Bi-214 Bi-214 Bi-214 Bi-214 Bi-214
          1.8137E00 1.8384E00 1.8474E00 1.8732E00 1.8903E00  $ Bi-214 Bi-214 Bi-214 Bi-214 Bi-214
          1.8963E00 1.8987E00 1.9358E00 1.9947E00 2.0045E00  $ Bi-214 Bi-214 Bi-214 Bi-214 Bi-214
          2.0107E00 2.0218E00 2.0529E00 2.0850E00 2.0895E00  $ Bi-214 Bi-214 Bi-214 Bi-214 Bi-214
          2.1099E00 2.1185E00 2.1478E00 2.1768E00 2.1926E00  $ Bi-214 Bi-214 Bi-214 Bi-214 Bi-214
          2.2041E00 2.2512E00 2.2597E00 2.2666E00 2.2700E00  $ Bi-214 Bi-214 Bi-214 Bi-214 Bi-214
          2.2844E00 2.2934E00 2.3122E00 2.3248E00 2.3313E00  $ Bi-214 Bi-214 Bi-214 Bi-214 Bi-214
          2.3609E00 2.3693E00 2.3770E00 2.3909E00 2.4235E00  $ Bi-214 Bi-214 Bi-214 Bi-214 Bi-214
          2.4477E00 2.4828E00 2.5056E00 2.5510E00 2.6045E00  $ Bi-214 Bi-214 Bi-214 Bi-214 Bi-214
          2.6309E00 2.6620E00 2.6948E00 2.6994E00 2.7194E00  $ Bi-214 Bi-214 Bi-214 Bi-214 Bi-214
          2.7700E00 2.7861E00 2.8270E00 2.8609E00 2.8804E00  $ Bi-214 Bi-214 Bi-214 Bi-214 Bi-214
          2.8936E00 2.9221E00 2.9287E00 2.9349E00 2.9400E00  $ Bi-214 Bi-214 Bi-214 Bi-214 Bi-214
          2.9788E00 2.9887E00 3.0000E00 3.0539E00 3.0817E00  $ Bi-214 Bi-214 Bi-214 Bi-214 Bi-214
          3.0939E00 3.1363E00 3.1426E00 3.1605E00 3.1836E00  $ Bi-214 Bi-214 Bi-214 Bi-214 Bi-214
          3.2333E00 3.2697E00                                $ Bi-214 Bi-214
sp2     d 4.4729E-23 3.6645E-28 3.3541E-31 2.3003E-07 1.4604E-10  $ Bi-210 Tl-206 Po-210 Po-214 Pb-210
          2.2506E-02 3.3687E-03 2.4340E-11 1.7956E-03 2.9819E-23  $ Pb-214 Bi-214 Pb-210 Pb-214 Bi-210
          1.2721E-28 2.2392E-31 1.5132E-07 5.0500E-23 1.0454E-02  $ Tl-206 Po-210 Po-214 Bi-210 Pb-214
          2.1254E-28 3.7815E-31 2.5627E-07 2.1421E-03 1.7613E-02  $ Tl-206 Po-210 Po-214 Bi-214 Pb-214
          3.5884E-03 1.7314E-23 4.9538E-24 7.6431E-29 1.3008E-31  $ Bi-214 Bi-210 Bi-210 Tl-206 Po-210
          8.7863E-08 6.0504E-03 1.8322E-29 3.8279E-32 2.5627E-08  $ Po-214 Pb-214 Tl-206 Po-210 Po-214
          1.2389E-03 1.8265E-03 3.8509E-04 9.6187E-05 6.4124E-05  $ Bi-214 Pb-214 Bi-214 Pb-214 Pb-214
          8.0156E-05 1.2168E-02 8.9774E-04 2.1585E-22 1.0796E-03  $ Pb-214 Pb-214 Pb-214 Bi-210 Bi-214
          5.2903E-04 4.9182E-04 1.9793E-04 3.1260E-02 3.0508E-07  $ Pb-214 Bi-214 Bi-214 Pb-214 Po-214
          2.0992E-04 2.7299E-22 3.6872E-05 1.2825E-04 3.2062E-05  $ Bi-214 Bi-210 Pb-214 Pb-214 Pb-214
          5.8179E-04 3.4787E-04 2.3991E-04 3.5987E-04 6.0437E-02  $ Bi-214 Bi-214 Bi-214 Bi-214 Pb-214
          3.8386E-05 2.9989E-05 2.2192E-03 2.5191E-03 5.3980E-05  $ Bi-214 Bi-214 Bi-214 Bi-214 Bi-214
          1.8593E-04 1.0197E-03 6.5977E-04 1.7993E-04 1.9433E-03  $ Bi-214 Bi-214 Bi-214 Bi-214 Bi-214
          2.7253E-04 8.0972E-04 1.6031E-05 7.1976E-04 5.5147E-04  $ Pb-214 Bi-214 Pb-214 Bi-214 Pb-214
          7.1659E-04 5.3980E-05 1.0796E-04 4.8093E-05 3.4787E-05  $ Pb-214 Bi-214 Bi-214 Pb-214 Bi-214
          9.5966E-05 3.0940E-04 4.3185E-04 8.0156E-06 5.1581E-04  $ Bi-214 Pb-214 Bi-214 Pb-214 Bi-214
          3.6872E-05 1.9793E-04 4.9782E-04 5.9315E-04 7.1976E-05  $ Pb-214 Bi-214 Bi-214 Pb-214 Bi-214
          2.8130E-01 4.1985E-04 2.0992E-04 2.9989E-05 1.0197E-04  $ Bi-214 Bi-214 Bi-214 Bi-214 Bi-214
          3.6587E-04 1.9193E-04 3.5987E-04 2.6390E-04 9.5368E-03  $ Bi-214 Bi-214 Bi-214 Bi-214 Bi-214
          4.7983E-04 3.5987E-05 3.5987E-05 2.2791E-04 2.8789E-03  $ Bi-214 Bi-214 Bi-214 Bi-214 Bi-214
          4.5584E-04 2.4591E-03 2.7590E-04 9.5966E-05 2.8789E-04  $ Bi-214 Bi-214 Bi-214 Bi-214 Bi-214
          2.3991E-04 8.0972E-04 1.2825E-04 2.9809E-02 1.7794E-03  $ Bi-214 Bi-214 Pb-214 Bi-214 Pb-214
          1.9193E-03 6.3456E-05 2.5191E-04 3.1992E-29 9.8486E-29  $ Bi-214 Po-214 Bi-214 Tl-206 Po-210
```

```
         7.4973E-03 2.4591E-04 9.1768E-04 5.6379E-04 1.3795E-04  $ Bi-214 Bi-214 Bi-214 Bi-214 Bi-214
         9.5706E-04 1.0197E-04 6.4177E-04 1.3795E-04 1.9313E-02  $ Pb-214 Bi-214 Bi-214 Bi-214 Bi-214
         1.0197E-04 2.3391E-03 1.3795E-04 7.1976E-05 5.9978E-05  $ Bi-214 Bi-214 Bi-214 Bi-214 Bi-214
         7.1976E-05 5.8778E-04 1.0197E-04 1.7394E-04 1.9253E-03  $ Bi-214 Bi-214 Bi-214 Bi-214 Bi-214
         1.7394E-04 1.7394E-03 5.9978E-04 4.8582E-04 9.1768E-02  $ Bi-214 Bi-214 Bi-214 Bi-214 Bi-214
         2.7590E-04 1.5535E-03 1.0316E-02 3.5387E-04 2.8070E-03  $ Bi-214 Bi-214 Bi-214 Bi-214 Bi-214
         1.6194E-04 1.3195E-04 3.6107E-02 8.9967E-03 7.3770E-04  $ Bi-214 Bi-214 Bi-214 Bi-214 Bi-214
         5.2181E-04 6.5977E-05 1.3795E-04 2.7590E-05 2.4531E-02  $ Bi-214 Bi-214 Bi-214 Bi-214 Bi-214
         4.7383E-03 1.1396E-04 8.4566E-03 1.5115E-02 3.1189E-05  $ Bi-214 Bi-214 Bi-214 Bi-214 Bi-214
         7.1976E-05 4.1985E-04 1.3375E-02 2.5191E-03 2.1592E-03  $ Bi-214 Bi-214 Bi-214 Bi-214 Bi-214
         4.3784E-03 1.6194E-03 2.0392E-03 1.1396E-04 4.4984E-04  $ Bi-214 Bi-214 Bi-214 Bi-214 Bi-214
         7.0176E-03 1.4395E-03 1.8593E-02 9.7162E-02 9.5966E-05  $ Bi-214 Bi-214 Bi-214 Bi-214 Bi-214
         7.1976E-05 2.3391E-03 1.2955E-02 1.3795E-03 5.4580E-04  $ Bi-214 Bi-214 Bi-214 Bi-214 Bi-214
         1.0796E-03 3.8386E-04 3.1189E-04 3.2988E-05 1.7993E-05  $ Bi-214 Bi-214 Bi-214 Bi-214 Bi-214
         2.9989E-04 1.1396E-04 4.2585E-04 5.9978E-05 3.4188E-04  $ Bi-214 Bi-214 Bi-214 Bi-214 Bi-214
         5.3380E-04 7.3770E-03 9.5966E-05 2.3991E-05 3.7187E-04  $ Bi-214 Bi-214 Bi-214 Bi-214 Bi-214
         3.0469E-02 4.1985E-05 5.3980E-05 1.0796E-04 1.7993E-05  $ Bi-214 Bi-214 Bi-214 Bi-214 Bi-214
         3.1189E-05 1.9793E-03 7.1976E-05 1.1396E-05 1.3195E-04  $ Bi-214 Bi-214 Bi-214 Bi-214 Bi-214
         1.1396E-05 1.7993E-05 7.1976E-05 1.1996E-05 3.5987E-05  $ Bi-214 Bi-214 Bi-214 Bi-214 Bi-214
         9.4764E-03 1.2596E-05 3.5987E-05 2.3991E-06 2.7590E-06  $ Bi-214 Bi-214 Bi-214 Bi-214 Bi-214
         5.3980E-06 1.7993E-06 1.9793E-04 1.6794E-05 1.0796E-05  $ Bi-214 Bi-214 Bi-214 Bi-214 Bi-214
         1.5594E-04 3.5987E-05 1.4995E-05 2.0992E-06 5.6379E-05  $ Bi-214 Bi-214 Bi-214 Bi-214 Bi-214
         3.8986E-05 9.5966E-05 7.1976E-06 3.4787E-06 1.0197E-05  $ Bi-214 Bi-214 Bi-214 Bi-214 Bi-214
         8.9967E-05 6.5977E-06 5.3980E-05 1.3795E-04 2.6390E-05  $ Bi-214 Bi-214 Bi-214 Bi-214 Bi-214
         3.1189E-06 2.0992E-06 9.5966E-06 3.1189E-06 8.9967E-06  $ Bi-214 Bi-214 Bi-214 Bi-214 Bi-214
         1.1996E-06 5.9978E-07                                  $ Bi-214 Bi-214
c
c   -- Material Specifications --
c
c   -- Concrete --
c
m1    06000 -0.167900  $ Carbon in Concrete
      08000 -0.484500  $ Oxygen in Concrete
      11000 -0.000260  $ Sodium in Concrete
      12000 -0.011900  $ Magnesium in Concrete
      13000 -0.004440  $ Aluminum in Concrete
      14000 -0.015100  $ Silicon in Concrete
      19000 -0.001087  $ Potassium in Concrete
      20000 -0.310100  $ Calcium in Concrete
      25000 -0.000304  $ Manganese in Concrete
      26000 -0.004366  $ Iron in Concrete
c
c   -- Aluminum, Structural 6061 --
c
m2    13000 -0.9685    $ Aluminum
      26000 -0.0070    $ Iron
      29000 -0.0025    $ Copper
      14000 -0.0060    $ Silicon
      12000 -0.0110    $ Magnesium
      24000 -0.0035    $ Chromium
      25000 -0.0015    $ Manganese
c
c   -- Air (suitable for breathing!) --
c
m3    06000 -0.000124  $ Carbon in Air
      07000 -0.755268  $ Nitrogen in Air
      08000 -0.231781  $ Oxygen in Air
      18000 -0.012827  $ Argon in Air
c
c   -- PVT Scintillator --
c
m4    01000 -0.085000   $ Hydrogen in PVT
      06000 -0.915000   $ Carbon in PVT
c
```

```
c   -- Germanium Detector --
c m4    32000 -1.000000   $ Germanium Detector
c
c   -- Steel, Stainless 304 --
c
m5    24000 -0.190000   $ Chromium in Steel
      25000 -0.020000   $ Manganese in Steel
      26000 -0.695000   $ Iron in Steel
      28000 -0.095000   $ Nickel in Steel
c
c   -- Lead --
c
m6    82000 -1.000000   $ Pure lead
c
c   -- PMMA (Light Pipe Lucite) --
c
m7    01000 -0.080538   $ Hydrogen in PMMA
      06000 -0.599848   $ Carbon in PMMA
      08000 -0.319614   $ Oxygen in PMMA
c
c  -- ASTM A366 Steel (7.85 g/cc)
c
m8    26000 -0.990000   $ Iron in sheet steel
      29000 -0.004500   $ Copper in sheet steel
       06000 -0.001000   $ Carbon in sheet steel
       25000 -0.004500   $ Manganese in sheet steel
c
c   -- Tallies --
c
F18:P 11                      $ Pulse height tally in RIGHT LOWER detector
E18 0.0 0.00001 0.040 1.0 3.0  $ Energy bins
F28:P 12                      $ Pulse height tally in RIGHT UPPER detector
E28 0.0 0.00001 0.040 1.0 3.0  $ Energy bins
F38:P 21                      $ Pulse height tally in LEFT LOWER detector
E38 0.0 0.00001 0.040 1.0 3.0  $ Energy bins
F48:P 22                      $ Pulse height tally in LEFT UPPER detector
E48 0.0 0.00001 0.040 1.0 3.0  $ Energy bins
c
c * END OF FILE *
```

APPENDIX S

MCNP SIMULATION OF SOURCE OF RADIATION SOURCE ON SURFACE OF CONCRETE SHIELD WITH 30 CM WALL THICKNESS

```
c Portal Monitor Environmental Gamma Background Study
c Created by Alexander Solodov, GNSTD, Oak Ridge National Laboratory
c Modified by Christopher Ryan, NSSPI, Texas A&M University
c Further Modified by Stephen Revis, NSSPI, Texas A&M University
c
c * CELL CARDS *
1  1  -2.301    -100 101 -99    imp:p=1 $ Concrete Slab
11 4  -1.032    -112            imp:p=1 $ PVT (Right Lower Detector)
12 4  -1.032    -113            imp:p=1 $ PVT (Right Upper Detector)
14 6  -11.34    -114 112 116    imp:p=1 $ Shielding, Lead (Right Lower Detector)
15 6  -11.34    -115 113 117    imp:p=1 $ Shielding, Lead (Right Upper Detector)
16 7  -1.19     -116            imp:p=1 $ PMMA (Right Lower Detector)
17 7  -1.19     -117            imp:p=1 $ PMMA (Right Upper Detector)
21 4  -1.032    -122            imp:p=1 $ PVT (Left Lower Detector)
22 4  -1.032    -123            imp:p=1 $ PVT (Left Upper Detector)
24 6  -11.34    -124 122 126    imp:p=1 $ Shielding, Lead (Left Lower Detector)
25 6  -11.34    -125 123 127    imp:p=1 $ Shielding, Lead (Left Upper Detector)
26 7  -1.19     -126            imp:p=1 $ PMMA (Left Lower Detector)
27 7  -1.19     -127            imp:p=1 $ PMMA (Left Upper Detector)
c begin new stuff
c right
c 100 1 -2.301  -200 -100 101   imp:p=1 $ concrete under portal (no source here)
110 2 -2.700    -200 100 -210   imp:p=1 $ right portal inner face (Aluminum)
111 5  -7.920  (-220:221:-290:291:211)
               -200 210 100     imp:p=1 $ SS304 (Right Portal, Back & Sides)
112 3 -1.205E-3 210 -211 220 -221
               290 -291 112 113
               114 115          imp:p=1 $ Interior Air (Right Portal Arm)
c left
c 200 1 -2.301   -201 -100 101  imp:p=1 $ concrete under portal (no source here)
210 2 -2.700   -201 100  213    imp:p=1 $ left portal inner face (Aluminum)
211 5  -7.920  (-220:221:-290:291:-212)
               -201 -213 100    imp:p=1 $ SS304 (Left Portal, Back & Sides)
212 3 -1.205E-3 212 -213 220 -221
               290 -291 122 123
               124 125          imp:p=1 $ Interior Air (Left Portal Arm)
c concrete
300 1  -2.301 320 -321 310 100  imp:p=1           $steel dome
c other
998 3 -1.205E-3 100 200 201
                -99 #300        imp:p=1 $ Universe Sphere
999 0           +99:-101        imp:p=0 $ The edge of the universe...
c end new stuff
c * END CELL CARDS *

c * SURFACE CARDS *
100 pz  0      $ top of concrete slab
101 pz  -30.48 $ bottom of concrete slab
112 RPP 269.5 273.5 -24.5 -9.5 23 99 $ right lower detector surf
113 RPP 269.5 273.5 -24.5 -9.5 214 290 $ right upper detertor surf
114 RPP 269.5 274.4525 -25.4525 -8.5475 22.0475 112 $ lead around right lower det surf
```

```
115 RPP 269.5 274.4525 -25.4525 -8.5475 201 290.9525 $ lead around right upper det surf
116 RPP 269.5 273.5 -24.5 -9.5 99 112 $ lucite right lower
117 RPP 269.5 273.5 -24.5 -9.5 201 214 $ lucite right upper
122 RPP -273.5 -269.5 -24.5 -9.5 23 99 $ left lower detector surf
123 RPP -273.5 -269.5 -24.5 -9.5 214 290 $ left upper detector surf
124 RPP -274.4525 -269.5 -25.4525 -8.5475 22.0475 112 $ lead around left lower det surf
125 RPP -274.4525 -269.5 -25.4525 -8.5475 201 290.9525 $ lead around left upper det surf
126 RPP -273.5 -269.5 -24.5 -9.5 99 112 $ lucite left lower
127 RPP -273.5 -269.5 -24.5 -9.5 201 214 $ lucite left upper
c new stuff
200 RPP 254 277 -33 33 -40 304 $ right portal outer
201 RPP -277 -254 -33 33 -40 304 $ left portal outer
210 px 254.3175 $right portal inner face
211 px 276.6825 $right portal outer face
212 px -276.6825 $left portal outer face
213 px -254.3175 $left portal inner face
220 py -32.6825 $ right portal side
221 py  32.6825 $ right portal side
290 pz  0.3175  $ portal bottom
291 pz 303.6825 $ portal top
300 so 1000 $ outer aluminum sphere
c 301 so 999.6825 $inner aluminum sphere (0.125 in thickness)
310 rpp -200 200 -1001 1001 1 450
320 rpp  -500 500 -500 500 -10 500
321 rpp  -530 530 -530 530 -11 510
99 so 4000 $ universe sphere
903 RPP 253.99 277.01 -33.01 33.01 -40.01 304.01 $ right portal ccc
904 RPP -277.01 -253.99 -33.01 33.01 -40.01 304.01 $ left portal ccc
c * END SURFACE CARDS *

c * DATA CARDS *
NPS 1.00E9
c   -- Source Specifications --
c Source
c Located +/- 1mm from surface of concrete (surface 100)
c 3.742:1 initial ratio of Bi-214 to Pb-214
c This source represents the spectrum found 1s after rain ends.
c Source is isotropic
MODE p
SDEF  ERG D2 PAR 2 X=D3 Y=D4 Z=510.1 VEC=0 0 1 DIR=D1
si1 -1 1 $Isotropic Source
sp1  0 1
si3  -530 530 $ xmin and xmax of cell 321
sp3   0   1
si4  -530 530 $ ymin and ymax of cell 321
sp4   0   1
C      ---------------------------------------------------------------
C      Photon Source Definition - generated from ORIGEN F71 file
C         total strength:  2.2668E11 gammas/second
C         discrete lines:  2.2668E11 gammas/second in 242 lines
C                          100.00% of energy
C         multigroup bins: 0.0000E00 gammas/second in 18 bins
C                          0.00% of energy
C         not counted:     0.0000E00 gammas/second
C      ---------------------------------------------------------------
C
C      discrete lines (in MeV) and their probabilities
si2    l 1.2213E-02 1.2614E-02 1.2614E-02 1.2614E-02 1.3024E-02  $ Bi-210 Tl-206 Po-210 Po-214 Pb-210
         1.3024E-02 1.3446E-02 4.6520E-02 5.3226E-02 7.0832E-02  $ Pb-214 Bi-214 Pb-210 Pb-214 Bi-210
         7.2805E-02 7.2805E-02 7.2805E-02 7.2873E-02 7.4815E-02  $ Tl-206 Po-210 Po-214 Bi-210 Pb-214
         7.4969E-02 7.4969E-02 7.4969E-02 7.6861E-02 7.7107E-02  $ Tl-206 Po-210 Po-214 Bi-214 Pb-214
         7.9291E-02 8.2344E-02 8.4685E-02 8.4694E-02 8.4694E-02  $ Bi-214 Bi-210 Bi-210 Tl-206 Po-210
         8.4694E-02 8.7089E-02 8.7111E-02 8.7111E-02 8.7111E-02  $ Po-214 Pb-214 Tl-206 Po-210 Po-214
         8.9527E-02 8.9588E-02 9.2110E-02 1.3745E-01 1.4130E-01  $ Bi-214 Pb-214 Bi-214 Pb-214 Pb-214
```

```
          1.9630E-01 2.4191E-01 2.5879E-01 2.6560E-01 2.7370E-01  $ Pb-214 Pb-214 Pb-214 Bi-210 Bi-214
          2.7453E-01 2.8094E-01 2.8690E-01 2.9517E-01 2.9800E-01  $ Pb-214 Bi-214 Bi-214 Pb-214 Po-214
          3.0443E-01 3.0460E-01 3.0560E-01 3.1420E-01 3.2430E-01  $ Bi-214 Bi-210 Pb-214 Pb-214 Pb-214
          3.3361E-01 3.3490E-01 3.3850E-01 3.4710E-01 3.5190E-01  $ Bi-214 Bi-214 Bi-214 Bi-214 Pb-214
          3.6420E-01 3.7660E-01 3.8700E-01 3.8910E-01 3.9400E-01  $ Bi-214 Bi-214 Bi-214 Bi-214 Bi-214
          3.9601E-01 4.0574E-01 4.2650E-01 4.4040E-01 4.5477E-01  $ Bi-214 Bi-214 Bi-214 Bi-214 Bi-214
          4.6210E-01 4.6969E-01 4.7060E-01 4.7438E-01 4.8042E-01  $ Pb-214 Bi-214 Pb-214 Bi-214 Pb-214
          4.8708E-01 4.9460E-01 5.0220E-01 5.1100E-01 5.2040E-01  $ Pb-214 Bi-214 Bi-214 Pb-214 Bi-214
          5.2500E-01 5.3369E-01 5.3694E-01 5.3870E-01 5.4340E-01  $ Bi-214 Pb-214 Bi-214 Pb-214 Bi-214
          5.4410E-01 5.4710E-01 5.7283E-01 5.8015E-01 5.9600E-01  $ Pb-214 Bi-214 Bi-214 Pb-214 Bi-214
          6.0932E-01 6.1578E-01 6.1710E-01 6.2640E-01 6.3120E-01  $ Bi-214 Bi-214 Bi-214 Bi-214 Bi-214
          6.3314E-01 6.3937E-01 6.4918E-01 6.6140E-01 6.6545E-01  $ Bi-214 Bi-214 Bi-214 Bi-214 Bi-214
          6.8322E-01 6.8770E-01 6.9330E-01 6.9790E-01 7.0311E-01  $ Bi-214 Bi-214 Bi-214 Bi-214 Bi-214
          7.1080E-01 7.1986E-01 7.2340E-01 7.2780E-01 7.3365E-01  $ Bi-214 Bi-214 Bi-214 Bi-214 Bi-214
          7.4150E-01 7.5284E-01 7.6600E-01 7.6836E-01 7.8591E-01  $ Bi-214 Bi-214 Pb-214 Bi-214 Pb-214
          7.8610E-01 7.9970E-01 7.9976E-01 8.0310E-01 8.0310E-01  $ Bi-214 Po-214 Bi-214 Tl-206 Po-210
          8.0617E-01 8.1508E-01 8.2118E-01 8.2620E-01 8.3235E-01  $ Bi-214 Bi-214 Bi-214 Bi-214 Bi-214
          8.3903E-01 8.4720E-01 9.0425E-01 9.1580E-01 9.3405E-01  $ Pb-214 Bi-214 Bi-214 Bi-214 Bi-214
          9.4330E-01 9.6408E-01 9.7620E-01 9.8920E-01 1.0134E00  $ Bi-214 Bi-214 Bi-214 Bi-214 Bi-214
          1.0205E00 1.0324E00 1.0380E00 1.0454E00 1.0520E00  $ Bi-214 Bi-214 Bi-214 Bi-214 Bi-214
          1.0669E00 1.0700E00 1.1037E00 1.1048E00 1.1203E00  $ Bi-214 Bi-214 Bi-214 Bi-214 Bi-214
          1.1308E00 1.1337E00 1.1552E00 1.1731E00 1.2077E00  $ Bi-214 Bi-214 Bi-214 Bi-214 Bi-214
          1.2268E00 1.2305E00 1.2381E00 1.2810E00 1.3038E00  $ Bi-214 Bi-214 Bi-214 Bi-214 Bi-214
          1.3170E00 1.3300E00 1.3415E00 1.3530E00 1.3777E00  $ Bi-214 Bi-214 Bi-214 Bi-214 Bi-214
          1.3853E00 1.3925E00 1.4015E00 1.4080E00 1.4197E00  $ Bi-214 Bi-214 Bi-214 Bi-214 Bi-214
          1.4711E00 1.4792E00 1.5092E00 1.5385E00 1.5433E00  $ Bi-214 Bi-214 Bi-214 Bi-214 Bi-214
          1.5832E00 1.5947E00 1.5993E00 1.6366E00 1.6574E00  $ Bi-214 Bi-214 Bi-214 Bi-214 Bi-214
          1.6613E00 1.6840E00 1.7296E00 1.7645E00 1.7821E00  $ Bi-214 Bi-214 Bi-214 Bi-214 Bi-214
          1.8137E00 1.8384E00 1.8474E00 1.8732E00 1.8903E00  $ Bi-214 Bi-214 Bi-214 Bi-214 Bi-214
          1.8963E00 1.8987E00 1.9358E00 1.9947E00 2.0045E00  $ Bi-214 Bi-214 Bi-214 Bi-214 Bi-214
          2.0107E00 2.0218E00 2.0529E00 2.0850E00 2.0895E00  $ Bi-214 Bi-214 Bi-214 Bi-214 Bi-214
          2.1099E00 2.1185E00 2.1478E00 2.1768E00 2.1926E00  $ Bi-214 Bi-214 Bi-214 Bi-214 Bi-214
          2.2041E00 2.2512E00 2.2597E00 2.2666E00 2.2700E00  $ Bi-214 Bi-214 Bi-214 Bi-214 Bi-214
          2.2844E00 2.2934E00 2.3122E00 2.3248E00 2.3313E00  $ Bi-214 Bi-214 Bi-214 Bi-214 Bi-214
          2.3609E00 2.3693E00 2.3770E00 2.3909E00 2.4235E00  $ Bi-214 Bi-214 Bi-214 Bi-214 Bi-214
          2.4477E00 2.4828E00 2.5056E00 2.5510E00 2.6045E00  $ Bi-214 Bi-214 Bi-214 Bi-214 Bi-214
          2.6309E00 2.6620E00 2.6948E00 2.6994E00 2.7194E00  $ Bi-214 Bi-214 Bi-214 Bi-214 Bi-214
          2.7700E00 2.7861E00 2.8270E00 2.8609E00 2.8804E00  $ Bi-214 Bi-214 Bi-214 Bi-214 Bi-214
          2.8936E00 2.9221E00 2.9287E00 2.9349E00 2.9400E00  $ Bi-214 Bi-214 Bi-214 Bi-214 Bi-214
          2.9788E00 2.9887E00 3.0000E00 3.0539E00 3.0817E00  $ Bi-214 Bi-214 Bi-214 Bi-214 Bi-214
          3.0939E00 3.1363E00 3.1426E00 3.1605E00 3.1836E00  $ Bi-214 Bi-214 Bi-214 Bi-214 Bi-214
          3.2333E00 3.2697E00                                $ Bi-214 Bi-214
sp2     d 4.4729E-23 3.6645E-28 3.3541E-31 2.3003E-07 1.4604E-10  $ Bi-210 Tl-206 Po-210 Po-214 Pb-210
          2.2506E-02 3.3687E-03 2.4340E-11 1.7956E-03 2.9819E-23  $ Pb-214 Bi-214 Pb-210 Pb-214 Bi-210
          1.2721E-28 2.2392E-31 1.5132E-07 5.0500E-23 1.0454E-02  $ Tl-206 Po-210 Po-214 Bi-210 Pb-214
          2.1254E-28 3.7815E-31 2.5627E-07 2.1421E-03 1.7613E-02  $ Tl-206 Po-210 Po-214 Bi-214 Pb-214
          3.5884E-03 1.7314E-23 4.9538E-24 7.6431E-29 1.3008E-31  $ Bi-214 Bi-210 Bi-210 Tl-206 Po-210
          8.7863E-08 6.0504E-03 1.8322E-29 3.8279E-32 2.5627E-08  $ Po-214 Pb-214 Tl-206 Po-210 Po-214
          1.2389E-03 1.8265E-03 3.8509E-04 9.6187E-05 6.4124E-05  $ Bi-214 Pb-214 Bi-214 Pb-214 Pb-214
          8.0156E-05 1.2168E-02 8.9774E-04 2.1585E-22 1.0796E-03  $ Pb-214 Pb-214 Pb-214 Bi-210 Bi-214
          5.2903E-04 4.9182E-04 1.9793E-04 3.1260E-02 3.0508E-07  $ Pb-214 Bi-214 Bi-214 Pb-214 Po-214
          2.0992E-04 2.7299E-22 3.6872E-05 1.2825E-04 3.2062E-05  $ Bi-214 Bi-210 Pb-214 Pb-214 Pb-214
          5.8179E-04 3.4787E-04 2.3991E-04 3.5987E-04 6.0437E-02  $ Bi-214 Bi-214 Bi-214 Bi-214 Pb-214
          3.8386E-05 2.9989E-05 2.2192E-03 2.5191E-03 5.3980E-05  $ Bi-214 Bi-214 Bi-214 Bi-214 Bi-214
          1.8593E-04 1.0197E-03 6.5977E-04 1.7993E-04 1.9433E-03  $ Bi-214 Bi-214 Bi-214 Bi-214 Bi-214
          2.7253E-04 8.0972E-04 1.6031E-05 7.1976E-04 5.5147E-04  $ Pb-214 Bi-214 Pb-214 Bi-214 Pb-214
          7.1659E-04 5.3980E-05 1.0796E-04 4.8093E-05 3.4787E-05  $ Pb-214 Bi-214 Bi-214 Pb-214 Bi-214
          9.5966E-05 3.0940E-04 4.3185E-04 8.0156E-06 5.1581E-04  $ Bi-214 Pb-214 Bi-214 Pb-214 Bi-214
          3.6872E-05 1.9793E-04 4.9782E-04 5.9315E-04 7.1976E-05  $ Pb-214 Bi-214 Bi-214 Pb-214 Bi-214
          2.8130E-01 4.1985E-04 2.0992E-04 2.9989E-05 1.0197E-04  $ Bi-214 Bi-214 Bi-214 Bi-214 Bi-214
          3.6587E-04 1.9193E-04 3.5987E-04 2.6390E-04 9.5368E-03  $ Bi-214 Bi-214 Bi-214 Bi-214 Bi-214
          4.7983E-04 3.5987E-05 3.5987E-05 2.2791E-04 2.8789E-03  $ Bi-214 Bi-214 Bi-214 Bi-214 Bi-214
          4.5584E-04 2.4591E-03 2.7590E-04 9.5966E-05 2.8789E-04  $ Bi-214 Bi-214 Bi-214 Bi-214 Bi-214
          2.3991E-04 8.0972E-04 1.2825E-04 2.9809E-02 1.7794E-03  $ Bi-214 Bi-214 Pb-214 Bi-214 Pb-214
```

```
         1.9193E-03 6.3456E-05 2.5191E-04 3.1992E-29 9.8486E-29  $ Bi-214 Po-214 Bi-214 Tl-206 Po-210
         7.4973E-03 2.4591E-04 9.1768E-04 5.6379E-04 1.3795E-04  $ Bi-214 Bi-214 Bi-214 Bi-214 Bi-214
         9.5706E-04 1.0197E-04 6.4177E-04 1.3795E-04 1.9313E-02  $ Pb-214 Bi-214 Bi-214 Bi-214 Bi-214
         1.0197E-04 2.3391E-03 1.3795E-04 7.1976E-05 5.9978E-05  $ Bi-214 Bi-214 Bi-214 Bi-214 Bi-214
         7.1976E-05 5.8778E-04 1.0197E-04 1.7394E-04 1.9253E-03  $ Bi-214 Bi-214 Bi-214 Bi-214 Bi-214
         1.7394E-04 1.7394E-03 5.9978E-04 4.8582E-04 9.1768E-02  $ Bi-214 Bi-214 Bi-214 Bi-214 Bi-214
         2.7590E-04 1.5535E-03 1.0316E-02 3.5387E-04 2.8070E-03  $ Bi-214 Bi-214 Bi-214 Bi-214 Bi-214
         1.6194E-04 1.3195E-04 3.6107E-02 8.9967E-03 7.3770E-04  $ Bi-214 Bi-214 Bi-214 Bi-214 Bi-214
         5.2181E-04 6.5977E-05 1.3795E-04 2.7590E-05 2.4531E-02  $ Bi-214 Bi-214 Bi-214 Bi-214 Bi-214
         4.7383E-03 1.1396E-04 8.4566E-03 1.5115E-02 3.1189E-05  $ Bi-214 Bi-214 Bi-214 Bi-214 Bi-214
         7.1976E-05 4.1985E-04 1.3375E-02 2.5191E-03 2.1592E-03  $ Bi-214 Bi-214 Bi-214 Bi-214 Bi-214
         4.3784E-03 1.6194E-03 2.0392E-03 1.1396E-04 4.4984E-04  $ Bi-214 Bi-214 Bi-214 Bi-214 Bi-214
         7.0176E-03 1.4395E-03 1.8593E-02 9.7162E-02 9.5966E-05  $ Bi-214 Bi-214 Bi-214 Bi-214 Bi-214
         7.1976E-05 2.3391E-03 1.2955E-02 1.3795E-03 5.4580E-04  $ Bi-214 Bi-214 Bi-214 Bi-214 Bi-214
         1.0796E-03 3.8386E-04 3.1189E-04 3.2988E-05 1.7993E-05  $ Bi-214 Bi-214 Bi-214 Bi-214 Bi-214
         2.9989E-04 1.1396E-04 4.2585E-04 5.9978E-05 3.4188E-04  $ Bi-214 Bi-214 Bi-214 Bi-214 Bi-214
         5.3380E-04 7.3770E-03 9.5966E-05 2.3991E-05 3.7187E-04  $ Bi-214 Bi-214 Bi-214 Bi-214 Bi-214
         3.0469E-02 4.1985E-05 5.3980E-05 1.0796E-04 1.7993E-05  $ Bi-214 Bi-214 Bi-214 Bi-214 Bi-214
         3.1189E-05 1.9793E-03 7.1976E-05 1.1396E-05 1.3195E-04  $ Bi-214 Bi-214 Bi-214 Bi-214 Bi-214
         1.1396E-05 1.7993E-05 7.1976E-05 1.1996E-05 3.5987E-05  $ Bi-214 Bi-214 Bi-214 Bi-214 Bi-214
         9.4764E-03 1.2596E-05 3.5987E-05 2.3991E-06 2.7590E-06  $ Bi-214 Bi-214 Bi-214 Bi-214 Bi-214
         5.3980E-06 1.7993E-06 1.9793E-04 1.6794E-05 1.0796E-05  $ Bi-214 Bi-214 Bi-214 Bi-214 Bi-214
         1.5594E-04 3.5987E-05 1.4995E-05 2.0992E-06 5.6379E-05  $ Bi-214 Bi-214 Bi-214 Bi-214 Bi-214
         3.8986E-05 9.5966E-05 7.1976E-06 3.4787E-06 1.0197E-05  $ Bi-214 Bi-214 Bi-214 Bi-214 Bi-214
         8.9967E-05 6.5977E-06 5.3980E-05 1.3795E-04 2.6390E-05  $ Bi-214 Bi-214 Bi-214 Bi-214 Bi-214
         3.1189E-06 2.0992E-06 9.5966E-06 3.1189E-06 8.9967E-06  $ Bi-214 Bi-214 Bi-214 Bi-214 Bi-214
         1.1996E-06 5.9978E-07                                  $ Bi-214 Bi-214
c
c   -- Material Specifications --
c
c   -- Concrete --
c
m1    06000 -0.167900  $ Carbon in Concrete
      08000 -0.484500  $ Oxygen in Concrete
      11000 -0.000260  $ Sodium in Concrete
      12000 -0.011900  $ Magnesium in Concrete
      13000 -0.004440  $ Aluminum in Concrete
      14000 -0.015100  $ Silicon in Concrete
      19000 -0.001087  $ Potassium in Concrete
      20000 -0.310100  $ Calcium in Concrete
      25000 -0.000304  $ Manganese in Concrete
      26000 -0.004366  $ Iron in Concrete
c
c   -- Aluminum, Structural 6061 --
c
m2    13000 -0.9685    $ Aluminum
      26000 -0.0070    $ Iron
      29000 -0.0025    $ Copper
      14000 -0.0060    $ Silicon
      12000 -0.0110    $ Magnesium
      24000 -0.0035    $ Chromium
      25000 -0.0015    $ Manganese
c
c   -- Air (suitable for breathing!) --
c
m3    06000 -0.000124  $ Carbon in Air
      07000 -0.755268  $ Nitrogen in Air
      08000 -0.231781  $ Oxygen in Air
      18000 -0.012827  $ Argon in Air
c
c   -- PVT Scintillator --
c
m4    01000 -0.085000   $ Hydrogen in PVT
      06000 -0.915000   $ Carbon in PVT
```

```
c
c   -- Germanium Detector --
c m4    32000 -1.000000   $ Germanium Detector
c
c   -- Steel, Stainless 304 --
c
m5    24000 -0.190000   $ Chromium in Steel
      25000 -0.020000   $ Manganese in Steel
      26000 -0.695000   $ Iron in Steel
      28000 -0.095000   $ Nickel in Steel
c
c   -- Lead --
c
m6    82000 -1.000000   $ Pure lead
c
c   -- PMMA (Light Pipe Lucite) --
c
m7    01000 -0.080538   $ Hydrogen in PMMA
      06000 -0.599848   $ Carbon in PMMA
      08000 -0.319614   $ Oxygen in PMMA
c
c  -- ASTM A366 Steel (7.85 g/cc)
c
m8    26000 -0.990000   $ Iron in sheet steel
      29000 -0.004500   $ Copper in sheet steel
       06000 -0.001000   $ Carbon in sheet steel
       25000 -0.004500   $ Manganese in sheet steel
c
c   -- Tallies --
c
F18:P 11                       $ Pulse height tally in RIGHT LOWER detector
E18 0.0 0.00001 0.040 1.0 3.0  $ Energy bins
F28:P 12                       $ Pulse height tally in RIGHT UPPER detector
E28 0.0 0.00001 0.040 1.0 3.0  $ Energy bins
F38:P 21                       $ Pulse height tally in LEFT LOWER detector
E38 0.0 0.00001 0.040 1.0 3.0  $ Energy bins
F48:P 22                       $ Pulse height tally in LEFT UPPER detector
E48 0.0 0.00001 0.040 1.0 3.0  $ Energy bins
c
c * END OF FILE *
```

APPENDIX T

MCNP SIMULATION OF SOURCE OF RADIATION SOURCE OUTSIDE OF CONCRETE SHIELD WITH 30 CM WALL THICKNESS

```
c Portal Monitor Environmental Gamma Background Study
c Created by Alexander Solodov, GNSTD, Oak Ridge National Laboratory
c Modified by Christopher Ryan, NSSPI, Texas A&M University
c Further Modified by Stephen Revis, NSSPI, Texas A&M University
c
c * CELL CARDS *
1  1  -2.301    -100 101 -99    imp:p=1 $ Concrete Slab
11 4  -1.032    -112            imp:p=1 $ PVT (Right Lower Detector)
12 4  -1.032    -113            imp:p=1 $ PVT (Right Upper Detector)
14 6  -11.34    -114 112 116    imp:p=1 $ Shielding, Lead (Right Lower Detector)
15 6  -11.34    -115 113 117    imp:p=1 $ Shielding, Lead (Right Upper Detector)
16 7  -1.19     -116            imp:p=1 $ PMMA (Right Lower Detector)
17 7  -1.19     -117            imp:p=1 $ PMMA (Right Upper Detector)
21 4  -1.032    -122            imp:p=1 $ PVT (Left Lower Detector)
22 4  -1.032    -123            imp:p=1 $ PVT (Left Upper Detector)
24 6  -11.34    -124 122 126    imp:p=1 $ Shielding, Lead (Left Lower Detector)
25 6  -11.34    -125 123 127    imp:p=1 $ Shielding, Lead (Left Upper Detector)
26 7  -1.19     -126            imp:p=1 $ PMMA (Left Lower Detector)
27 7  -1.19     -127            imp:p=1 $ PMMA (Left Upper Detector)
c begin new stuff
c right
c 100 1 -2.301  -200 -100 101   imp:p=1 $ concrete under portal (no source here)
110 2 -2.700    -200 100 -210   imp:p=1 $ right portal inner face (Aluminum)
111 5  -7.920  (-220:221:-290:291:211)
               -200 210 100     imp:p=1 $ SS304 (Right Portal, Back & Sides)
112 3 -1.205E-3 210 -211 220 -221
               290 -291 112 113
               114 115          imp:p=1 $ Interior Air (Right Portal Arm)
c left
c 200 1 -2.301   -201 -100 101  imp:p=1 $ concrete under portal (no source here)
210 2 -2.700   -201 100  213    imp:p=1 $ left portal inner face (Aluminum)
211 5  -7.920  (-220:221:-290:291:-212)
               -201 -213 100    imp:p=1 $ SS304 (Left Portal, Back & Sides)
212 3 -1.205E-3 212 -213 220 -221
               290 -291 122 123
               124 125          imp:p=1 $ Interior Air (Left Portal Arm)
c concrete
300 1  -2.301 320 -321 310 100  imp:p=1           $steel dome
c other
998 3 -1.205E-3 100 200 201
                -99 #300        imp:p=1 $ Universe Sphere
999 0           +99:-101        imp:p=0 $ The edge of the universe...
c end new stuff
c * END CELL CARDS *

c * SURFACE CARDS *
100 pz  0      $ top of concrete slab
101 pz  -30.48 $ bottom of concrete slab
112 RPP 269.5 273.5 -24.5 -9.5 23 99 $ right lower detector surf
113 RPP 269.5 273.5 -24.5 -9.5 214 290 $ right upper detertor surf
114 RPP 269.5 274.4525 -25.4525 -8.5475 22.0475 112 $ lead around right lower det surf
```

```
115 RPP 269.5 274.4525 -25.4525 -8.5475 201 290.9525 $ lead around right upper det surf
116 RPP 269.5 273.5 -24.5 -9.5 99 112 $ lucite right lower
117 RPP 269.5 273.5 -24.5 -9.5 201 214 $ lucite right upper
122 RPP -273.5 -269.5 -24.5 -9.5 23 99 $ left lower detector surf
123 RPP -273.5 -269.5 -24.5 -9.5 214 290 $ left upper detector surf
124 RPP -274.4525 -269.5 -25.4525 -8.5475 22.0475 112 $ lead around left lower det surf
125 RPP -274.4525 -269.5 -25.4525 -8.5475 201 290.9525 $ lead around left upper det surf
126 RPP -273.5 -269.5 -24.5 -9.5 99 112 $ lucite left lower
127 RPP -273.5 -269.5 -24.5 -9.5 201 214 $ lucite left upper
c new stuff
200 RPP 254 277 -33 33 -40 304 $ right portal outer
201 RPP -277 -254 -33 33 -40 304 $ left portal outer
210 px 254.3175 $right portal inner face
211 px 276.6825 $right portal outer face
212 px -276.6825 $left portal outer face
213 px -254.3175 $left portal inner face
220 py -32.6825 $ right portal side
221 py  32.6825 $ right portal side
290 pz  0.3175  $ portal bottom
291 pz 303.6825 $ portal top
300 so 1000 $ outer aluminum sphere
c 301 so 999.6825 $inner aluminum sphere (0.125 in thickness)
310 rpp -200 200 -1001 1001 1 450
320 rpp  -500 500 -500 500 -10 500
321 rpp  -530 530 -530 530 -11 510
99 so 4000 $ universe sphere
903 RPP 253.99 277.01 -33.01 33.01 -40.01 304.01 $ right portal ccc
904 RPP -277.01 -253.99 -33.01 33.01 -40.01 304.01 $ left portal ccc
c * END SURFACE CARDS *

c * DATA CARDS *
NPS 1.00E9
c   -- Source Specifications --
c Source
c Located +/- 1mm from surface of concrete (surface 100)
c 3.742:1 initial ratio of Bi-214 to Pb-214
c This source represents the spectrum found 1s after rain ends.
c Source is isotropic
MODE p
SDEF  ERG D2 PAR 2 X=D3 Y=fx d4 Z=0.1 VEC=0 0 1 DIR=D1
si1 -1 1 $Isotropic Source
sp1  0 1
si3 s 5        6         7        $ choose between left, center, right
sp3   0.39526  0.20949   0.39526
DS4 s 8        9         10
si5  -2000 -530.1  $-x outside of building
sp5   0     1
si6  -529.9 529.9 $ x above and below building
sp6  0     1
si7  530.1 2000 $ +x ouside of building
sp7  0     1
si8  -2000 2000  $y for -x outside of building
sp8  0     1
si9 s 11   12  $y for -x outside of building
sp9   0.5  0.5
si10  -2000 2000  $y for +x outside of building
sp10  0     1
si11  530.1 2000
sp11  0     1
si12  -2000 -530.1
sp12  0     1
C      ---------------------------------------------------------------
C      Photon Source Definition - generated from ORIGEN F71 file
C         total strength:  2.2668E11 gammas/second
```

```
C         discrete lines:  2.2668E11 gammas/second in 242 lines
C                          100.00% of energy
C         multigroup bins: 0.0000E00 gammas/second in 18 bins
C                          0.00% of energy
C         not counted:     0.0000E00 gammas/second
C       ------------------------------------------------------------
C
C       discrete lines (in MeV) and their probabilities
si2     l 1.2213E-02 1.2614E-02 1.2614E-02 1.2614E-02 1.3024E-02  $ Bi-210 Tl-206 Po-210 Po-214 Pb-210
          1.3024E-02 1.3446E-02 4.6520E-02 5.3226E-02 7.0832E-02  $ Pb-214 Bi-214 Pb-210 Pb-214 Bi-210
          7.2805E-02 7.2805E-02 7.2805E-02 7.2873E-02 7.4815E-02  $ Tl-206 Po-210 Po-214 Bi-210 Pb-214
          7.4969E-02 7.4969E-02 7.4969E-02 7.6861E-02 7.7107E-02  $ Tl-206 Po-210 Po-214 Bi-214 Pb-214
          7.9291E-02 8.2344E-02 8.4685E-02 8.4694E-02 8.4694E-02  $ Bi-214 Bi-210 Bi-210 Tl-206 Po-210
          8.4694E-02 8.7089E-02 8.7111E-02 8.7111E-02 8.7111E-02  $ Po-214 Pb-214 Tl-206 Po-210 Po-214
          8.9527E-02 8.9588E-02 9.2110E-02 1.3745E-01 1.4130E-01  $ Bi-214 Pb-214 Bi-214 Pb-214 Pb-214
          1.9630E-01 2.4191E-01 2.5879E-01 2.6560E-01 2.7370E-01  $ Pb-214 Pb-214 Pb-214 Bi-210 Bi-214
          2.7453E-01 2.8094E-01 2.8690E-01 2.9517E-01 2.9800E-01  $ Pb-214 Bi-214 Bi-214 Pb-214 Po-214
          3.0443E-01 3.0460E-01 3.0560E-01 3.1420E-01 3.2430E-01  $ Bi-214 Bi-210 Pb-214 Pb-214 Pb-214
          3.3361E-01 3.3490E-01 3.3850E-01 3.4710E-01 3.5190E-01  $ Bi-214 Bi-214 Bi-214 Bi-214 Pb-214
          3.6420E-01 3.7660E-01 3.8700E-01 3.8910E-01 3.9400E-01  $ Bi-214 Bi-214 Bi-214 Bi-214 Bi-214
          3.9601E-01 4.0574E-01 4.2650E-01 4.4040E-01 4.5477E-01  $ Bi-214 Bi-214 Bi-214 Bi-214 Bi-214
          4.6210E-01 4.6969E-01 4.7060E-01 4.7438E-01 4.8042E-01  $ Pb-214 Bi-214 Pb-214 Bi-214 Pb-214
          4.8708E-01 4.9460E-01 5.0220E-01 5.1100E-01 5.2040E-01  $ Pb-214 Bi-214 Bi-214 Pb-214 Bi-214
          5.2500E-01 5.3369E-01 5.3694E-01 5.3870E-01 5.4340E-01  $ Bi-214 Pb-214 Bi-214 Pb-214 Bi-214
          5.4410E-01 5.4710E-01 5.7283E-01 5.8015E-01 5.9600E-01  $ Pb-214 Bi-214 Bi-214 Pb-214 Bi-214
          6.0932E-01 6.1578E-01 6.1710E-01 6.2640E-01 6.3120E-01  $ Bi-214 Bi-214 Bi-214 Bi-214 Bi-214
          6.3314E-01 6.3937E-01 6.4918E-01 6.6140E-01 6.6545E-01  $ Bi-214 Bi-214 Bi-214 Bi-214 Bi-214
          6.8322E-01 6.8770E-01 6.9330E-01 6.9790E-01 7.0311E-01  $ Bi-214 Bi-214 Bi-214 Bi-214 Bi-214
          7.1080E-01 7.1986E-01 7.2340E-01 7.2780E-01 7.3365E-01  $ Bi-214 Bi-214 Bi-214 Bi-214 Bi-214
          7.4150E-01 7.5284E-01 7.6600E-01 7.6836E-01 7.8591E-01  $ Bi-214 Bi-214 Pb-214 Bi-214 Pb-214
          7.8610E-01 7.9970E-01 7.9976E-01 8.0310E-01 8.0310E-01  $ Bi-214 Po-214 Bi-214 Tl-206 Po-210
          8.0617E-01 8.1508E-01 8.2118E-01 8.2620E-01 8.3235E-01  $ Bi-214 Bi-214 Bi-214 Bi-214 Bi-214
          8.3903E-01 8.4720E-01 9.0425E-01 9.1580E-01 9.3405E-01  $ Pb-214 Bi-214 Bi-214 Bi-214 Bi-214
          9.4330E-01 9.6408E-01 9.7620E-01 9.8920E-01 1.0134E00  $ Bi-214 Bi-214 Bi-214 Bi-214 Bi-214
          1.0205E00 1.0324E00 1.0380E00 1.0454E00 1.0520E00  $ Bi-214 Bi-214 Bi-214 Bi-214 Bi-214
          1.0669E00 1.0700E00 1.1037E00 1.1048E00 1.1203E00  $ Bi-214 Bi-214 Bi-214 Bi-214 Bi-214
          1.1308E00 1.1337E00 1.1552E00 1.1731E00 1.2077E00  $ Bi-214 Bi-214 Bi-214 Bi-214 Bi-214
          1.2268E00 1.2305E00 1.2381E00 1.2810E00 1.3038E00  $ Bi-214 Bi-214 Bi-214 Bi-214 Bi-214
          1.3170E00 1.3300E00 1.3415E00 1.3530E00 1.3777E00  $ Bi-214 Bi-214 Bi-214 Bi-214 Bi-214
          1.3853E00 1.3925E00 1.4015E00 1.4080E00 1.4197E00  $ Bi-214 Bi-214 Bi-214 Bi-214 Bi-214
          1.4711E00 1.4792E00 1.5092E00 1.5385E00 1.5433E00  $ Bi-214 Bi-214 Bi-214 Bi-214 Bi-214
          1.5832E00 1.5947E00 1.5993E00 1.6366E00 1.6574E00  $ Bi-214 Bi-214 Bi-214 Bi-214 Bi-214
          1.6613E00 1.6840E00 1.7296E00 1.7645E00 1.7821E00  $ Bi-214 Bi-214 Bi-214 Bi-214 Bi-214
          1.8137E00 1.8384E00 1.8474E00 1.8732E00 1.8903E00  $ Bi-214 Bi-214 Bi-214 Bi-214 Bi-214
          1.8963E00 1.8987E00 1.9358E00 1.9947E00 2.0045E00  $ Bi-214 Bi-214 Bi-214 Bi-214 Bi-214
          2.0107E00 2.0218E00 2.0529E00 2.0850E00 2.0895E00  $ Bi-214 Bi-214 Bi-214 Bi-214 Bi-214
          2.1099E00 2.1185E00 2.1478E00 2.1768E00 2.1926E00  $ Bi-214 Bi-214 Bi-214 Bi-214 Bi-214
          2.2041E00 2.2512E00 2.2597E00 2.2666E00 2.2700E00  $ Bi-214 Bi-214 Bi-214 Bi-214 Bi-214
          2.2844E00 2.2934E00 2.3122E00 2.3248E00 2.3313E00  $ Bi-214 Bi-214 Bi-214 Bi-214 Bi-214
          2.3609E00 2.3693E00 2.3770E00 2.3909E00 2.4235E00  $ Bi-214 Bi-214 Bi-214 Bi-214 Bi-214
          2.4477E00 2.4828E00 2.5056E00 2.5510E00 2.6045E00  $ Bi-214 Bi-214 Bi-214 Bi-214 Bi-214
          2.6309E00 2.6620E00 2.6948E00 2.6994E00 2.7194E00  $ Bi-214 Bi-214 Bi-214 Bi-214 Bi-214
          2.7700E00 2.7861E00 2.8270E00 2.8609E00 2.8804E00  $ Bi-214 Bi-214 Bi-214 Bi-214 Bi-214
          2.8936E00 2.9221E00 2.9287E00 2.9349E00 2.9400E00  $ Bi-214 Bi-214 Bi-214 Bi-214 Bi-214
          2.9788E00 2.9887E00 3.0000E00 3.0539E00 3.0817E00  $ Bi-214 Bi-214 Bi-214 Bi-214 Bi-214
          3.0939E00 3.1363E00 3.1426E00 3.1605E00 3.1836E00  $ Bi-214 Bi-214 Bi-214 Bi-214 Bi-214
          3.2333E00 3.2697E00                                $ Bi-214 Bi-214
sp2     d 4.4729E-23 3.6645E-28 3.3541E-31 2.3003E-07 1.4604E-10  $ Bi-210 Tl-206 Po-210 Po-214 Pb-210
          2.2506E-02 3.3687E-03 2.4340E-11 1.7956E-03 2.9819E-23  $ Pb-214 Bi-214 Pb-210 Pb-214 Bi-210
          1.2721E-28 2.2392E-31 1.5132E-07 5.0500E-23 1.0454E-02  $ Tl-206 Po-210 Po-214 Bi-210 Pb-214
          2.1254E-28 3.7815E-31 2.5627E-07 2.1421E-03 1.7613E-02  $ Tl-206 Po-210 Po-214 Bi-214 Pb-214
          3.5884E-03 1.7314E-23 4.9538E-24 7.6431E-29 1.3008E-31  $ Bi-214 Bi-210 Bi-210 Tl-206 Po-210
          8.7863E-08 6.0504E-03 1.8322E-29 3.8279E-32 2.5627E-08  $ Po-214 Pb-214 Tl-206 Po-210 Po-214
          1.2389E-03 1.8265E-03 3.8509E-04 9.6187E-05 6.4124E-05  $ Bi-214 Pb-214 Bi-214 Pb-214 Pb-214
```

```
        8.0156E-05 1.2168E-02 8.9774E-04 2.1585E-22 1.0796E-03  $ Pb-214 Pb-214 Pb-214 Bi-210 Bi-214
        5.2903E-04 4.9182E-04 1.9793E-04 3.1260E-02 3.0508E-07  $ Pb-214 Bi-214 Bi-214 Pb-214 Po-214
        2.0992E-04 2.7299E-22 3.6872E-05 1.2825E-04 3.2062E-05  $ Bi-214 Bi-210 Pb-214 Pb-214 Pb-214
        5.8179E-04 3.4787E-04 2.3991E-04 3.5987E-04 6.0437E-02  $ Bi-214 Bi-214 Bi-214 Bi-214 Pb-214
        3.8386E-05 2.9989E-05 2.2192E-03 2.5191E-03 5.3980E-05  $ Bi-214 Bi-214 Bi-214 Bi-214 Bi-214
        1.8593E-04 1.0197E-03 6.5977E-04 1.7993E-04 1.9433E-03  $ Bi-214 Bi-214 Bi-214 Bi-214 Bi-214
        2.7253E-04 8.0972E-04 1.6031E-05 7.1976E-04 5.5147E-04  $ Pb-214 Bi-214 Pb-214 Bi-214 Pb-214
        7.1659E-04 5.3980E-05 1.0796E-04 4.8093E-05 3.4787E-05  $ Pb-214 Bi-214 Bi-214 Pb-214 Bi-214
        9.5966E-05 3.0940E-04 4.3185E-04 8.0156E-06 5.1581E-04  $ Bi-214 Pb-214 Bi-214 Pb-214 Bi-214
        3.6872E-05 1.9793E-04 4.9782E-04 5.9315E-04 7.1976E-05  $ Pb-214 Bi-214 Bi-214 Pb-214 Bi-214
        2.8130E-01 4.1985E-04 2.0992E-04 2.9989E-05 1.0197E-04  $ Bi-214 Bi-214 Bi-214 Bi-214 Bi-214
        3.6587E-04 1.9193E-04 3.5987E-04 2.6390E-04 9.5368E-03  $ Bi-214 Bi-214 Bi-214 Bi-214 Bi-214
        4.7983E-04 3.5987E-05 3.5987E-05 2.2791E-04 2.8789E-03  $ Bi-214 Bi-214 Bi-214 Bi-214 Bi-214
        4.5584E-04 2.4591E-03 2.7590E-04 9.5966E-05 2.8789E-04  $ Bi-214 Bi-214 Bi-214 Bi-214 Bi-214
        2.3991E-04 8.0972E-04 1.2825E-04 2.9809E-02 1.7794E-03  $ Bi-214 Bi-214 Pb-214 Bi-214 Pb-214
        1.9193E-03 6.3456E-05 2.5191E-04 3.1992E-29 9.8486E-29  $ Bi-214 Po-214 Bi-214 Tl-206 Po-210
        7.4973E-03 2.4591E-04 9.1768E-04 5.6379E-04 1.3795E-04  $ Bi-214 Bi-214 Bi-214 Bi-214 Bi-214
        9.5706E-04 1.0197E-04 6.4177E-04 1.3795E-04 1.9313E-02  $ Pb-214 Bi-214 Bi-214 Bi-214 Bi-214
        1.0197E-04 2.3391E-03 1.3795E-04 7.1976E-05 5.9978E-05  $ Bi-214 Bi-214 Bi-214 Bi-214 Bi-214
        7.1976E-05 5.8778E-04 1.0197E-04 1.7394E-04 1.9253E-03  $ Bi-214 Bi-214 Bi-214 Bi-214 Bi-214
        1.7394E-04 1.7394E-03 5.9978E-04 4.8582E-04 9.1768E-02  $ Bi-214 Bi-214 Bi-214 Bi-214 Bi-214
        2.7590E-04 1.5535E-03 1.0316E-02 3.5387E-04 2.8070E-03  $ Bi-214 Bi-214 Bi-214 Bi-214 Bi-214
        1.6194E-04 1.3195E-04 3.6107E-02 8.9967E-03 7.3770E-04  $ Bi-214 Bi-214 Bi-214 Bi-214 Bi-214
        5.2181E-04 6.5977E-05 1.3795E-04 2.7590E-05 2.4531E-02  $ Bi-214 Bi-214 Bi-214 Bi-214 Bi-214
        4.7383E-03 1.1396E-04 8.4566E-03 1.5115E-02 3.1189E-05  $ Bi-214 Bi-214 Bi-214 Bi-214 Bi-214
        7.1976E-05 4.1985E-04 1.3375E-02 2.5191E-03 2.1592E-03  $ Bi-214 Bi-214 Bi-214 Bi-214 Bi-214
        4.3784E-03 1.6194E-03 2.0392E-03 1.1396E-04 4.4984E-04  $ Bi-214 Bi-214 Bi-214 Bi-214 Bi-214
        7.0176E-03 1.4395E-03 1.8593E-02 9.7162E-02 9.5966E-05  $ Bi-214 Bi-214 Bi-214 Bi-214 Bi-214
        7.1976E-05 2.3391E-03 1.2955E-02 1.3795E-03 5.4580E-04  $ Bi-214 Bi-214 Bi-214 Bi-214 Bi-214
        1.0796E-03 3.8386E-04 3.1189E-04 3.2988E-05 1.7993E-05  $ Bi-214 Bi-214 Bi-214 Bi-214 Bi-214
        2.9989E-04 1.1396E-04 4.2585E-04 5.9978E-05 3.4188E-04  $ Bi-214 Bi-214 Bi-214 Bi-214 Bi-214
        5.3380E-04 7.3770E-03 9.5966E-05 2.3991E-05 3.7187E-04  $ Bi-214 Bi-214 Bi-214 Bi-214 Bi-214
        3.0469E-02 4.1985E-05 5.3980E-05 1.0796E-04 1.7993E-05  $ Bi-214 Bi-214 Bi-214 Bi-214 Bi-214
        3.1189E-05 1.9793E-03 7.1976E-05 1.1396E-05 1.3195E-04  $ Bi-214 Bi-214 Bi-214 Bi-214 Bi-214
        1.1396E-05 1.7993E-05 7.1976E-05 1.1996E-05 3.5987E-05  $ Bi-214 Bi-214 Bi-214 Bi-214 Bi-214
        9.4764E-03 1.2596E-05 3.5987E-05 2.3991E-06 2.7590E-06  $ Bi-214 Bi-214 Bi-214 Bi-214 Bi-214
        5.3980E-06 1.7993E-06 1.9793E-04 1.6794E-05 1.0796E-05  $ Bi-214 Bi-214 Bi-214 Bi-214 Bi-214
        1.5594E-04 3.5987E-05 1.4995E-05 2.0992E-06 5.6379E-05  $ Bi-214 Bi-214 Bi-214 Bi-214 Bi-214
        3.8986E-05 9.5966E-05 7.1976E-06 3.4787E-06 1.0197E-05  $ Bi-214 Bi-214 Bi-214 Bi-214 Bi-214
        8.9967E-05 6.5977E-06 5.3980E-05 1.3795E-04 2.6390E-05  $ Bi-214 Bi-214 Bi-214 Bi-214 Bi-214
        3.1189E-06 2.0992E-06 9.5966E-06 3.1189E-06 8.9967E-06  $ Bi-214 Bi-214 Bi-214 Bi-214 Bi-214
        1.1996E-06 5.9978E-07                                   $ Bi-214 Bi-214
c
c   -- Material Specifications --
c
c   -- Concrete --
c
m1    06000 -0.167900  $ Carbon in Concrete
      08000 -0.484500  $ Oxygen in Concrete
      11000 -0.000260  $ Sodium in Concrete
      12000 -0.011900  $ Magnesium in Concrete
      13000 -0.004440  $ Aluminum in Concrete
      14000 -0.015100  $ Silicon in Concrete
      19000 -0.001087  $ Potassium in Concrete
      20000 -0.310100  $ Calcium in Concrete
      25000 -0.000304  $ Manganese in Concrete
      26000 -0.004366  $ Iron in Concrete
c
c   -- Aluminum, Structural 6061 --
c
m2    13000 -0.9685    $ Aluminum
      26000 -0.0070    $ Iron
      29000 -0.0025    $ Copper
      14000 -0.0060    $ Silicon
```

```
      12000 -0.0110    $ Magnesium
      24000 -0.0035    $ Chromium
      25000 -0.0015    $ Manganese
c
c   -- Air (suitable for breathing!) --
c
m3    06000 -0.000124  $ Carbon in Air
      07000 -0.755268  $ Nitrogen in Air
      08000 -0.231781  $ Oxygen in Air
      18000 -0.012827  $ Argon in Air
c
c   -- PVT Scintillator --
c
m4    01000 -0.085000   $ Hydrogen in PVT
      06000 -0.915000   $ Carbon in PVT
c
c   -- Germanium Detector --
c m4    32000 -1.000000   $ Germanium Detector
c
c   -- Steel, Stainless 304 --
c
m5    24000 -0.190000   $ Chromium in Steel
      25000 -0.020000   $ Manganese in Steel
      26000 -0.695000   $ Iron in Steel
      28000 -0.095000   $ Nickel in Steel
c
c   -- Lead --
c
m6    82000 -1.000000   $ Pure lead
c
c   -- PMMA (Light Pipe Lucite) --
c
m7    01000 -0.080538   $ Hydrogen in PMMA
      06000 -0.599848   $ Carbon in PMMA
      08000 -0.319614   $ Oxygen in PMMA
c
c  -- ASTM A366 Steel (7.85 g/cc)
c
m8    26000 -0.990000   $ Iron in sheet steel
      29000 -0.004500   $ Copper in sheet steel
       06000 -0.001000   $ Carbon in sheet steel
       25000 -0.004500   $ Manganese in sheet steel
c
c   -- Tallies --
c
F18:P 11                      $ Pulse height tally in RIGHT LOWER detector
E18 0.0 0.00001 0.040 1.0 3.0  $ Energy bins
F28:P 12                      $ Pulse height tally in RIGHT UPPER detector
E28 0.0 0.00001 0.040 1.0 3.0  $ Energy bins
F38:P 21                      $ Pulse height tally in LEFT LOWER detector
E38 0.0 0.00001 0.040 1.0 3.0  $ Energy bins
F48:P 22                      $ Pulse height tally in LEFT UPPER detector
E48 0.0 0.00001 0.040 1.0 3.0  $ Energy bins
c
c * END OF FILE *
```

VITA

Name: Stephen Michael Revis

Address: Texas A&M University
Department of Nuclear Engineering
Nuclear Security Science and Policy Institute
3473 TAMU
College Station, TX 77843-3473

Email Address: s.revis1@gmail.com

Education: B.S., Nuclear Engineering, University of Wisconsin-Madison, 2009
M.S., Nuclear Engineering, Texas A&M University, 2012